Progress in host-guest macrocycle/pesticide research: recognition, detection, release and application

Pei hui Shan,[a] Jian hang Hu,[a] Ming Liu, [a] Zhu Tao,[a] Xin Xiao[a]* and Carl Redshaw[b]*

[a] *State Key Laboratory Breeding Base of Green Pesticide and Agricultural Bioengineering, Key Laboratory of Green Pesticide and Agricultural Bioengineering, Key Laboratory of Macrocyclic and Supramolecular Chemistry of Guizhou Province, Guizhou University, Guiyang 550025, China.*
[b] *Department of Chemistry, University of Hull, Hull HU6 7RX, U.K.*

Abstract: Macrocyclic compounds are formed via a series of cyclic oligomers possessing repeating units, and classical examples include cyclodextrins, calix[*n*]arenes, cucurbit[*n*]urils and pillar[*n*]arenes (n represents the number of repeat units). Given their unique host-guest binding ability, supramolecular polymers are often developed as hosts for specific guest molecular assembly systems, adsorption materials, drug delivery carriers, catalysts, and molecular recognition systems. For example, macrocyclic host molecules are widely used to encapsulate hydrophobic drug molecules to improve both the solubility and utilization efficiency of the drug. One type of potential host molecule that has seen increased agricultural use in recent years are pesticides. This includes herbicides, insecticides, and fungicides, and given the increased use, there is need to develop systems that can rapidly and effectively identify and detect such pesticides. In this review, we will discuss the use of cucurbit[*n*]urils, pillar[*n*]arenes, calix[*n*]arenes, cyclodextrins in this area, and their ability to form host-guest species with herbicides, insecticides and fungicides. Particular emphasis is given to the ability of such systems to improve the toxicity and release of the pesticide and the potential for practical application.

Contents

1.3. Interaction of macrocyclic compounds with pesticides

2. Supramolecular assemblies derived from pesticides and cucurbit[*n*]urils

    2.1. Use of cucurbit[6]urils

    2.1.1. Use of thiabendazole (TBZ)

    2.1.2 Use of carbendazim (CBZ)

    2.1.3 Use of fuberidazole (FBZ)

    2.1.4 Use of 6-benzyladenine (6-BA)

    2.2 Use of cucurbit[7]urils

    2.2.1 Use of paraquat

    2.2.2 Use of carbendazim (CBZ)

    2.2.3 Use of Cartap (CP)

    2.2.4 Use of nereistoxin (NTX)

    2.3 Use of cucurbit[8]urils

    2.3.1 Use of paraquat

    2.3.2 Use of carboxin

    2.3.3 Use of carbendazim (CBZ)

    2.4 Use of cucurbit[10]urils

3. Supramolecular assembly of pesticides with pillar[*n*]arenes

3.1. Host-guest complexes of pesticides with pillar[*n*]arenes

    3.1.1 Use of bora-, aza- or oxa pillar[n]arenes (n=4 to 6)

    3.1.2 Use of pillar[5]arenes

    3.1.3 Application of pillar[5]arenes and derivatives in pesticides recognition and detection

    3.1.4 Use of pillar[6]arene

    3.1.5 Use of pillar[7]arene

    3.1.6 Use of pillar[10]arene

4. Supramolecular assembly of pesticides with calix[*n*]arenes and derivatives

4.1. Detection of organophosphorus compounds with calix[*n*]arenes and derivatives

    4.1.1 Silica grafted systems

    4.1.2 Silver nanoparticle bound systems

    4.1.3 Systems grafted on titania nanorods

Abbreviations

AFM = Atomic force microscopy

AIE = Aggregation-induced emission

Bipy = Bipyridyl

BODIPY = 4,4-Difluoro-4-bora-3a,4a-diaza-s-indacene

CLD = Chlordecone

CLSM = Confocal laser scanning microscopy

COF = Covalent organic framework

DLS = Dynamic light scattering

DMSO = Dimethyl sulfoxide

EDS = Energy dispersive spectroscopy

EIS = Electrochemical impedance spectroscopy

ESI-MS = Electrospray ionisation mass spectrometry

EU = European Union

FL = Fluorescence

FRET = Fluorescence resonance energy transfer

FTIR = Fourier transform infrared spectroscopy

GCMS = Gas chromatography–mass spectrometry

GC-QTOF-MS = Gas chromatography with quadrupole time-of-flight mass spectrometry

H = Hour

HCH = Hexachlorocyclohexane

HMeQ[6] = *meta*-Hexamethyl-substituted cucurbit[6]uril

HPLC = High-performance liquid chromatography

i.d. = Inner diameter

ITC = Isothermal titration calorimetry

MCM41 = Mobil Composition of Matter No. 41

MIP = Molecularly imprinted polymer

MOF = Metal organic framework

MTT = 3-(4,5-Dimethylthiazol-2-yl)-2,5-diphenyltetrazolium bromide

NMR = Nuclear magnetic resonance

NOESY = Nuclear Overhauser Effect Spectroscopy

PEG = Polyethylene glycol

Q[*n*] = Cucurbit[*n*]uril

RSD = Relative standard deviation

SEM = Scanning electron microscopy

TEM = Transmission emission spectroscopy

TGA = Thermogravimetric analysis

TMeQ[6] = Tetramethylcucurbit[6]uril

UV = Ultra violet

VSM = Vibrating sample magnetometry

XPS = X-ray photoelectron spectroscopy

XRD = X-ray diffraction

1. Introduction

Over the years, pesticides, including includes herbicides, insecticides, and fungicides, have proved extremely useful, particularly for agricultural uses. However, their widespread use has taken its toll on the environment and many different types of pesticide have accumulated in soils, rivers etc. and have become a danger not only to wildlife but also to human health. [1, 2] Going forward, methods need to be employed which make the use and application of the required pesticides safer. Moreover, methods of contamination detection need to be improved. [3] One idea that has received attention over the last decade is to utilize the host-guest chemistry exhibited by a number of readily available macrocycles. [4, 5] The macrocycles that possess the requisite desirable properties include cucurbit[*n*]urils, pillar[*n*]arenes, calix[*n*]arenes and cyclodextrins, see chart 1, top.

Cucurbit[*n*]urils [6, 7] and pillar[*n*]arenes [8] are relatively new additions to the macrocyclic family and so their use to-date is somewhat less than that of the calixarenes [9]

and cyclodextrins. [10] In chart 1 below, the number of pesticides that have been investigated with each type of macrocycle is highlighted; the structures of each of these pesticides is provided in chart 2. By utilizing the host-guest properties of these macrocycles, it has proved possible to not only detect pesticides down to very low levels, but also to use the formed inclusion complex as a less toxic delivery agent without reducing the strength of the mode of action of the pesticide. The impact of this is that by employing such inclusion complexes, the more dangerous aspects associated with the use of pesticides can be either lowered and/or controlled, which will be of great benefit to the environment.

In the following review, we have organized the sections initially by macrocycle type, starting with cucurbit[n]urils and ending with cyclodextrins, and within each section, have broken it down into pesticide type, e.g. organophosphorus or organochlorine pesticide.
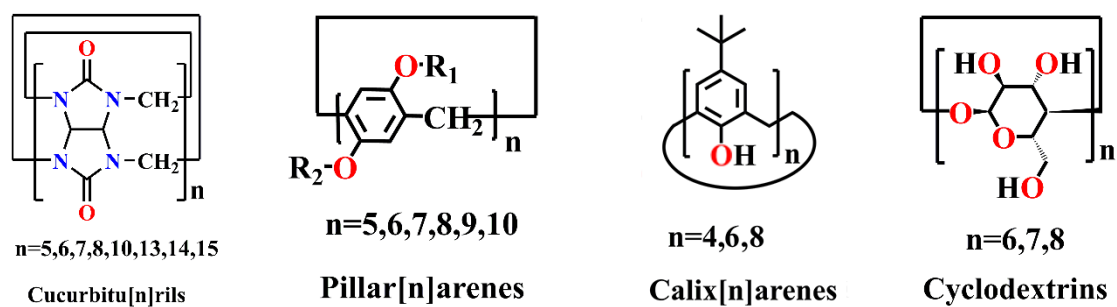
n=5,6,7,8,10,13,14,15	n=5,6,7,8,9,10	n=4,6,8	n=6,7,8
Cucurbitu[n]rils	Pillar[n]arenes	Calix[n]arenes	Cyclodextrins

Figure 1. Structures of the cucurbit[n]urils, pillar[n]arenes, calix[n]arenes and cyclodextrins. – to be combined with chart 1.
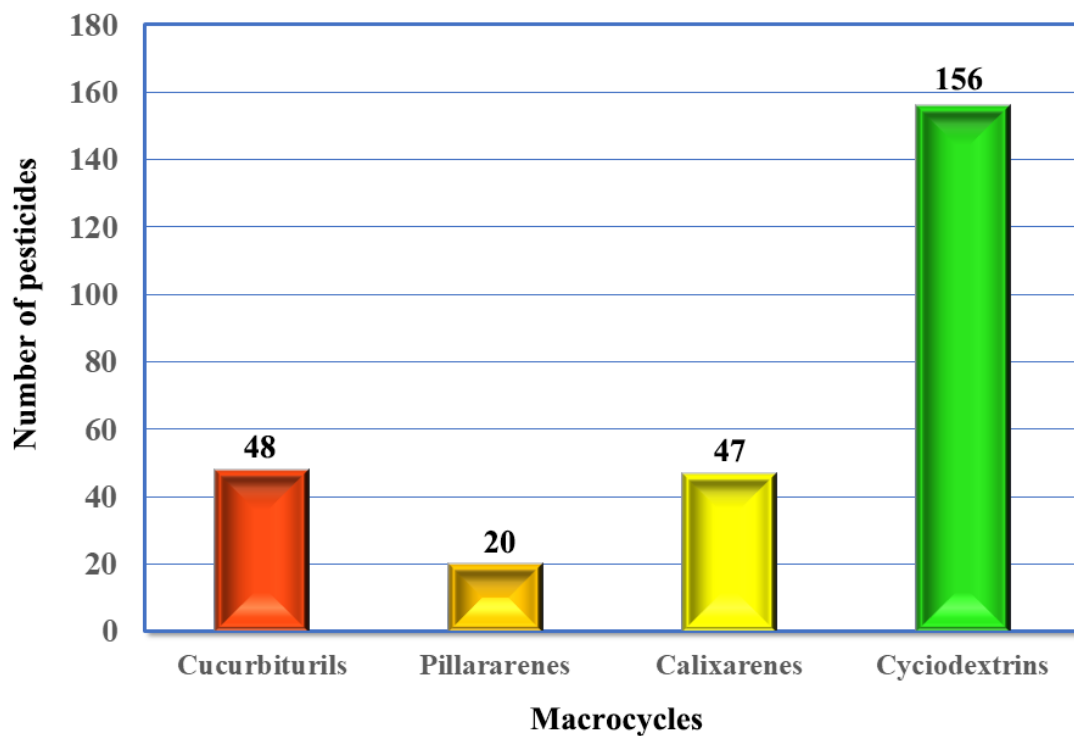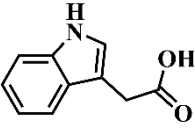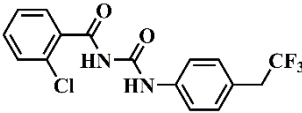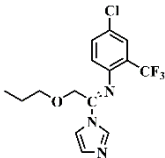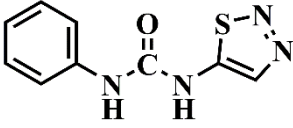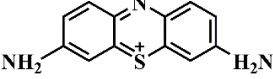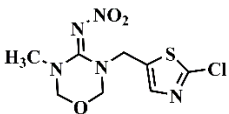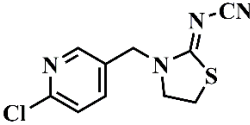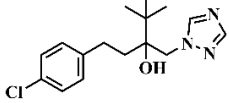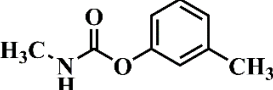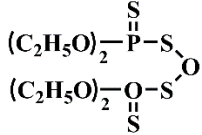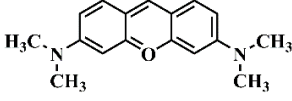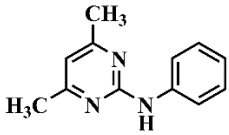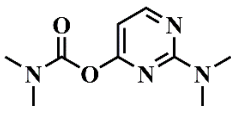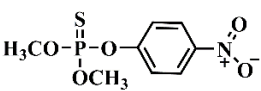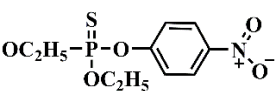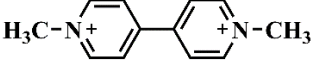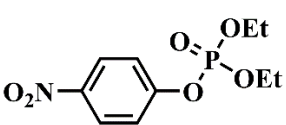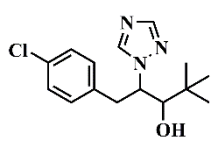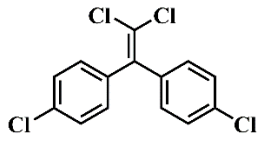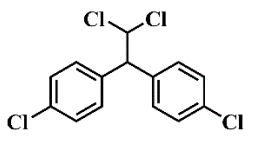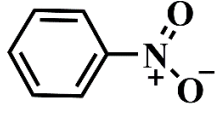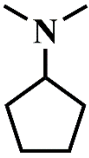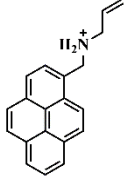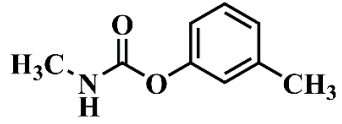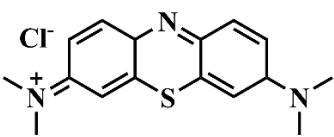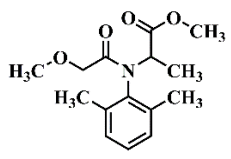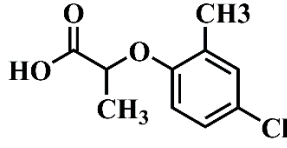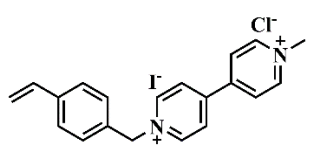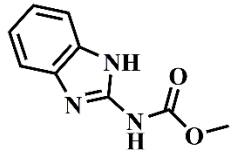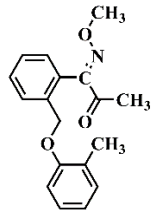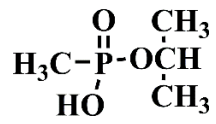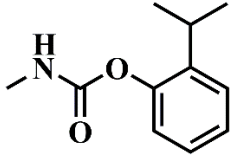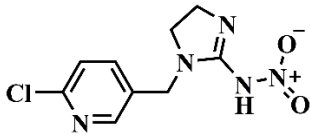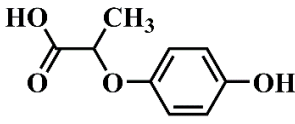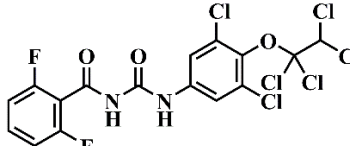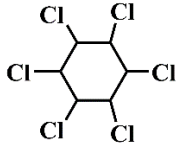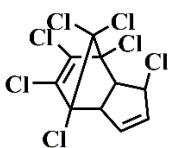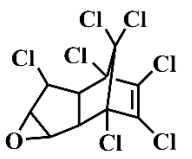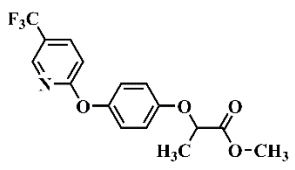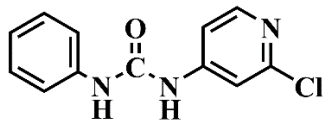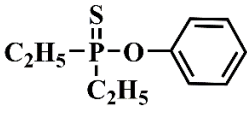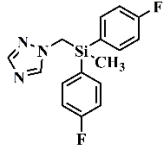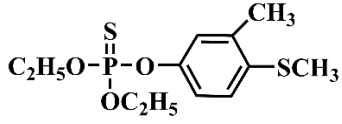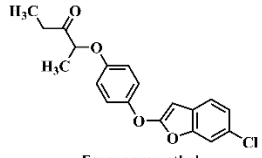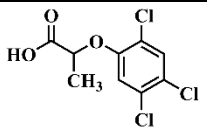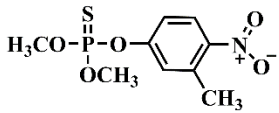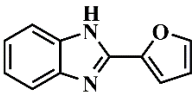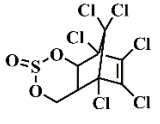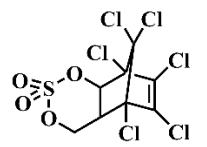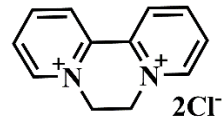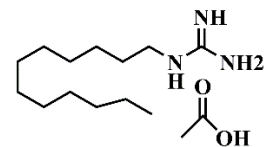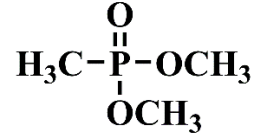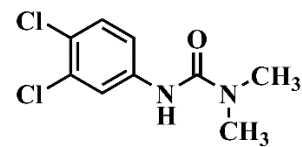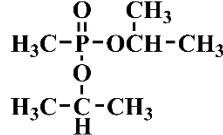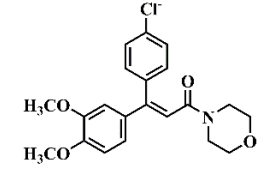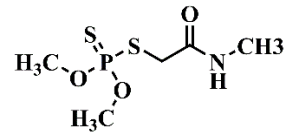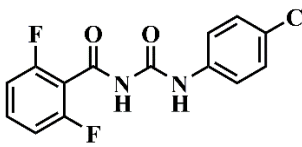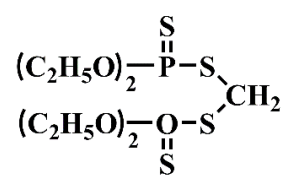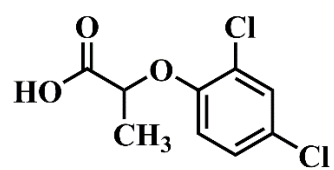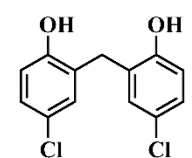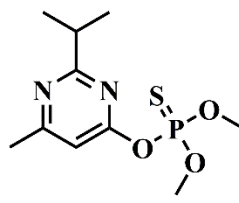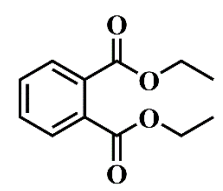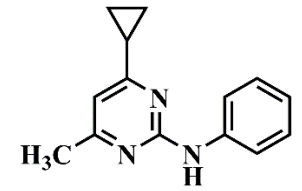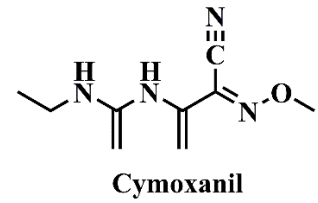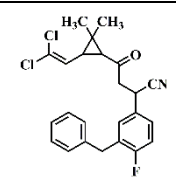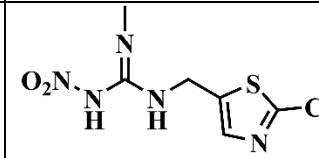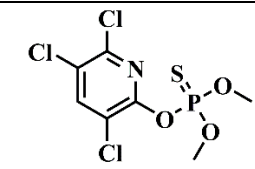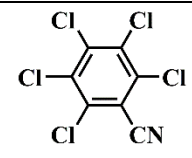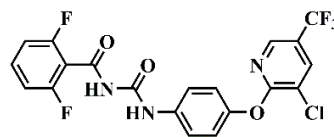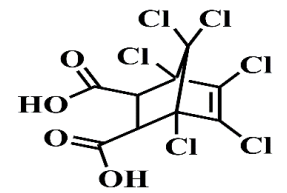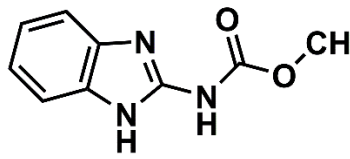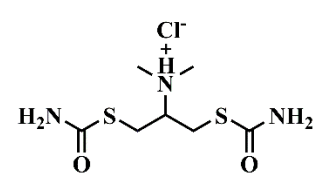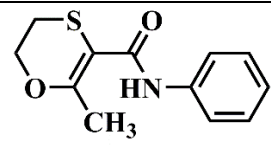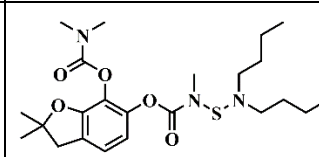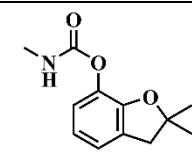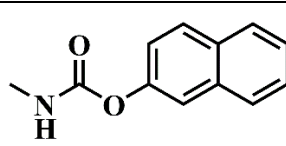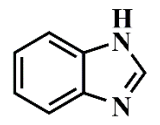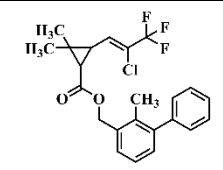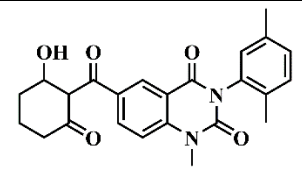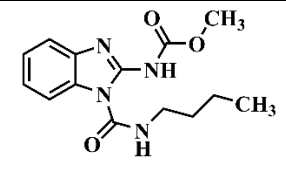
Chart 1. The number of different pesticides that have been investigated with each of the different types of macrocycle.

β–Indoleacetic Acid	Triflumuron	Triflumizole(TRI)	Thidiazuron
Thionine(TH)	Thiamethoxam	Thiacloprid	Tebuconazole
Metolcarb	Sulfotep	Pyronine(PyY)	Pyrimethanil(PYR)
Pirimicarb	Parathion-methyl	Parathion	paraquat

Paraoxon	**Paclobutrazol**	**p,p'-DDE**	**p,p'-DDD**
Nitrobenzene	**Nereistoxin(NTX)**	N-allyl-1-pyrenemethylammonium hydrochloride (APA⁺)	**Metolcarb**
Methylene blue (MB)	**Metalaxyl(MET)**	**Mecoprop**	**MC**
Carbendazim(methy-2-benzimidazole)(MBC)	**Kesoxim-methyl(KES)**	**Isopropyl hydrogen-methylphosphonate**	**Isoprocarb**
Imidacloprid	**Hydroprop**	**Hexaflumuron**	**Hexachlorocyclohexane**
Heptachlor	**Heptachlor epoxide**	**Haloxyfop methyl**	**Forchlorfenuron**
Fonofos	**Flusilazole(FLU)**	**Fenthion**	**Fenoxaprop ethyl**
Fenoprop	**Fenitrothion**	**Fuberidazole(FBZ)**	**Endosulfan**

Endosulfan sulfate	Diquat (DQ)	Dodine(DD)	DMMP
Diuron	DIMP	Dimethomorph(DIM)	Dimethoate
Diflubenzuron	Diethion	Dichlorprop	Dichlorophen
Diazinon	DEP	Cyprodinil(CYR)	Cymoxanil
Cyfluthrin	Clothianidin	Chlorpyrifos	Chlorothalonil
Chlorfluazuron	Chlorendic Acid	Carbendazim(CBZ)	Cartap(CP)
Carboxin	Carbosulfan	Carbofuran	Carbaryl
Benzimidazole(BZ)	Bifenthrin	Benquitrione	Benomyl
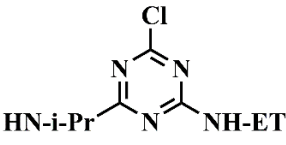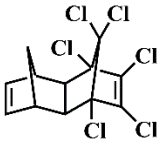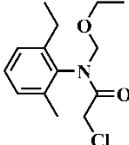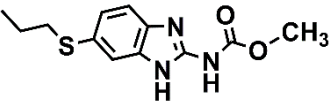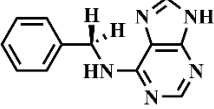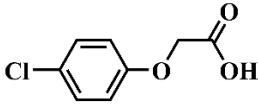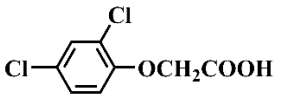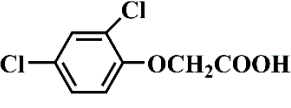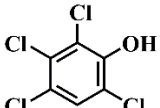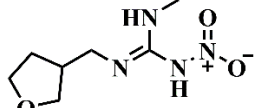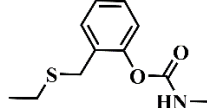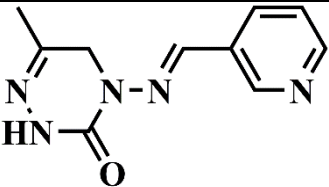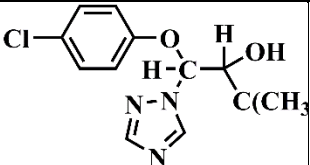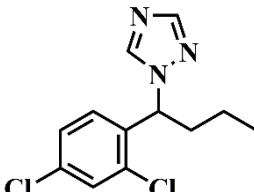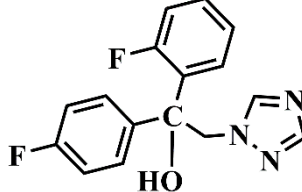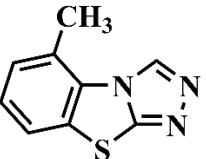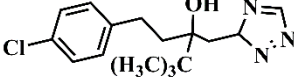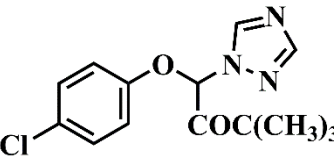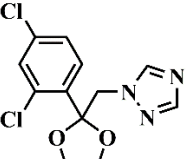
Atrazineacid	**Aldrin**	**Acetochlor**	**Acetamiprid**
Albendazole(ABZ)	**6-benzyladenine**	**4-chlorophenoxyacetic acid**	**2,4-dichlorophenoxyacetic acid**
2,4-D	**2,3,4,6tetrachlorophen**	**Dinotefuran**	**Ethiofencarb**
Pymetrozine	**Triadimenolisomer A**	**Penconazole**	**Flutriafol**
Tricclazole	**Tebuconzole**	**Triadimefon**	**Azaconazole**

Chart 2. Structures of the pesticides.

2. Supramolecular assemblies derived from pesticides and cucurbit[*n*]urils

Cucurbit[*n*]urils are a family of macrocycles derived from the acid catalyzed condensation of glycoluril and formaldehyde. The hydrophobic cavities associated with the Q[*n*]s play a central role in their host-guest complexation, a process associated with the release of water molecules from the cavity. As expected, the size of the cavity increases with the number of glycoluril units present, figure 1. Molecular structure determinations reveal that the internal cavity typically has a diameter in the range 4.4 – 12.6 Å, and calculated cavity volumes between 81 – 901 Å^3. [11] Cucurbit[*n*]urils can be abbreviated as either CB[*n*]s or Q[*n*]s, and in this review, we adopt the latter terminology. In this section, we discuss the use of Q[*n*]s by size, and note that the majority of the reports involve the use of either Q[6] or Q[7], whilst only a couple of reports discuss the use of Q[10] and none Q[5]. Where possible, further subsections are presented based on the pesticide
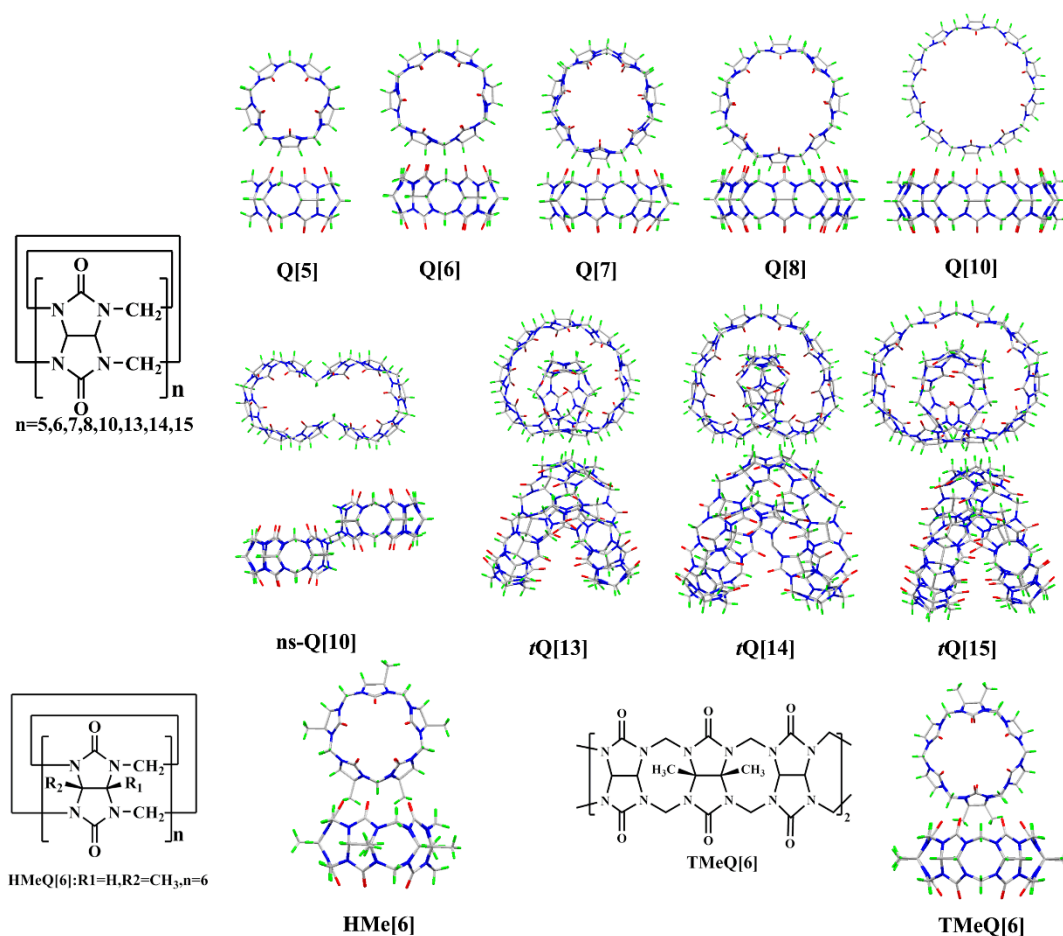
Figure 1. Structures of the cucurbit[*n*]urils.

2.1 Use of cucurbit[6]urils

2.1.1 Use of thiabendazole (TBZ)

The antifungal and antiparasitic agent thiabendazole (TBZ), which is used extensively for the protection of fruits and vegetables, has been complexed with Q[*n*] (n = 6, 7) as well as symmetric tetramethyl-cucurbit[6]uril (TMeQ[6]) in aqueous solution, see figure 2. [19] UV–vis and fluorescent experiments were conducted which revealed the formation of 1:1 host–guest inclusion complexes at pH 6.5. The formation constants, as determined by UV–vis and fluorespectrometry, were found to be $(5.37\pm1.05) \times 10^4$ L mol^{-1} and $(1.47\pm0.41) \times 10^4$ L mol^{-1} for the Q[6]-TBZ system, $(7.76\pm0.51) \times 10^4$ L mol^{-1} and $(9.36\pm0.22) \times 10^4$ L mol^{-1} for the Q[7]-TBZ system, $(1.28\pm0.78) \times 10^4$ L mol^{-1} and $(2.69\pm0.55) \times 10^4$ L mol^{-1} for the TMeQ[6]-TBZ system,

respectively. It was noted that in neutral media, there was an increase in fluorescence intensity associated with TBZ on addition of Q[n], and a linear relationship between fluorescence intensity and TBZ concentration was observed over the range 6.0×10^{-8} mol L^{-1}–8.0×10^{-6} mol L^{-1}. There was little interference from other ions such as Fe^{3+}, Al^{3+}, SO_4^{2-} etc. on the detection of TBZ, and the detection limits were in the range 5.51×10^{-9} mol L^{-1} and 8.85×10^{-9} mol L^{-1}. Use of this method with real samples including tap water and river water, seeded with TBZ, revealed reasonable recovery rates and suggested that the method had potential for use for testing for pesticide residues in different water environments.
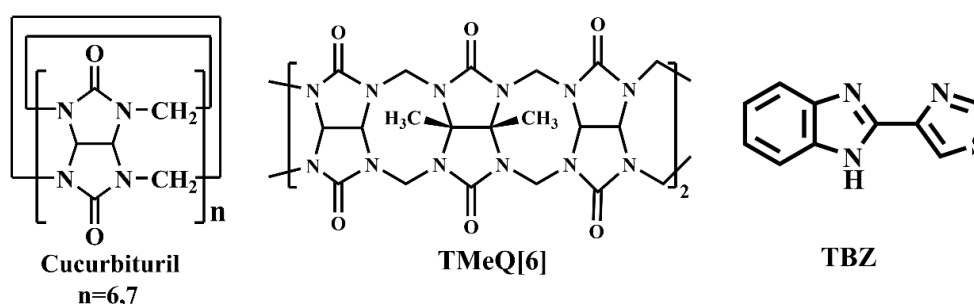
Figure 2. Structures of Q[6 and 7], TMeQ[6] and TBZ.

In later studies, TBZ has been complexed in aqueous solution by symmetrical tetramethylcucurbit[6]uril (TMeQ[6]) and *meta*-hexamethyl-substituted cucurbit[6]uril (HMeQ[6]), as well as by Q[7], in studies conducted in our laboratory. ^{1}H NMR spectroscopy was used to investigate these host-guest systems, and it was found that whilst Q[7] selectively bound the benzimidazole ring moiety of the guest, the thiazole ring was encapsulated by the TMeQ[6] and HMeQ[6] cavities. [14] Phase solubility studies revealed that TBZ solubility increased as a function of Q[7], TMeQ[6] or HMeQ[6] concentration. Importantly, these host-guest complexes enhanced the inhibitory effect of TBZ for *Fusarium graminearum* growth, thereby demonstrating improved antifungal activity for TBZ upon complexation with these Q[n]s.

2.1.2 Use of carbendazim (CBZ)

The interaction of the fungicide carbendazim (2-benzimidazolecarbamate), CBZ, which has seen use in the protection of sports surfaces, with Q[6] has been investigated (figure 3). [24] In particular, the fluorescence of the system at ambient temperature was monitored in aqueous

Na$_2$SO$_4$ solution (pH = 7.61). A fluorescence enhancement (x10) as well as a blue shift (∼11±1 nm) was noted as Q[6] was added and the 1:1 host-guest complex formed. An equilibrium constant (K$_a$) of 271±10 M^{-1} at 25°C was calculated using the Benesi-Hildebrand equation. By measuring the fluorescence at different temperatures, K$_a$ values were used to calculate thermodynamic parameters using the Van't Hoff method, which afforded values for ΔH and ΔS of -15.455 KJmol^{-1} and -5.66 Jmol^{-1}k^{-1} respectively. This suggested enthalpy factors were dominant such as the dipole-dipole interactions between the benzimidazole and Q[6] carbonyl groups. ^{1}H NMR spectroscopic data (upfield methyl shifts) was consistent with encapsulation of the amide-ester fragment of the guest. DSC measurements were also consistent with a 1:1 inclusion complex. It was postulated that for this inclusion complex, the polarity of the benzimidazole was reduced by the surrounding cavity (hydrophobic interactions) and had restricted access to water molecules, all of which led to a reduced excited/ground state energy gap and consequently increased emission. The importance of the presence of the carbonyl groups was highlighted by the less successful use of α and β-cyclodextrins.
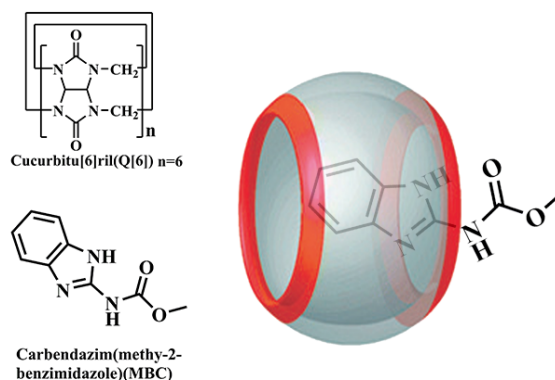
Figure 3. Structures of Q[6] and CBZ. Need to change to CBZ in the figure

2.1.3 Use of fuberidazole (FBZ)

Fuberidazole (FBZ), an ingredient employed in fungicides, has been treated with Q[*n*]s (n = 6, 7, 8), see figure 4, in HCl at pH 2.5, and the system was monitored by ITC, UV-Vis and NMR spectroscopy. [18] The focus of the study was the shift in p*K*$_a$ values together with activity against *Fusarium graminearum* upon interaction with Q[*n*]s (n = 6, 7 or 8). Results revealed increased solubility and p*K*$_a$ shifts upon complexation, and that for Q[6 or 7], activity against *Fusarium graminearum* decreased whereas for Q[8] there was an increase *in vivo*.
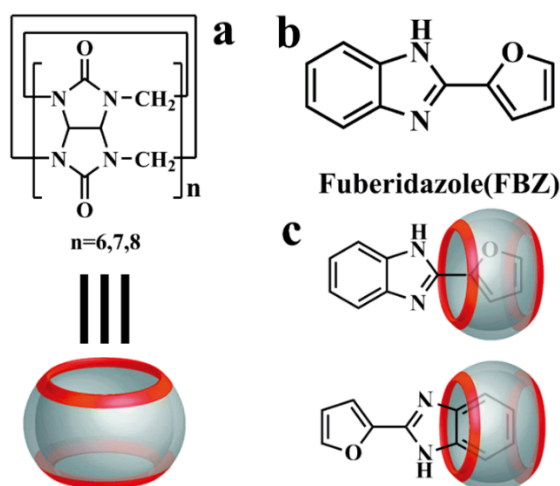
Figure 4. a) Q[*n*]s where n = 6, 7, 8; (b) FBZ; (c) Inclusion of FBZ by Q[*n*]s.

6-Benzyladenine (6-BA), also called 6-benzylaminopurine, is widely used as a plant growth supplement. Its interaction with Q[7], TMeQ[6] and HMeQ[6] (see figure 5) in aqueous solution has been studied using ^{1}H NMR and UV absorption spectroscopies. [20] Results indicated the formation of 1:1 complexes via encapsulation of the phenyl fragments of the guest. Formation constants, via spectrophotometric analysis, were measured at $(5.63 \pm 0.26) \times 10^4$ for Q[7]-6-BA, $(1.94 \pm 0.17) \times 10^3$ for TMeQ[6]-6-BA and $(2.89 \pm 0.23) \times 10^3$ L mol^{-1} for HMeQ[6]-6-BA. From phase solubility diagrams, the complex formation constants were found to be $(1.29 \pm 0.24) \times 10^4$ L mol^{-1} for Q[7]-6-BA, $(3.20 \pm 0.17) \times 10^3$ L mol^{-1} for TMeQ[6]-6-BA and $(3.52 \pm 1.01) \times 10^3$ L mol^{-1} for TMeQ[6]-6-BA. It was clear from these studies that the solubility of the 6-BA increased as a function of the cucurbituril concentration. Furthermore, by evaluating the formation constants over a wide range of temperatures, it was determined that the process was enthalpy controlled, with the dominant driving forces resulting from hydrophobic and van der Waals interactions. This work provided yet another demonstration of solubility enhancement of a substrate (here 6-BA) by host-guest complexation.
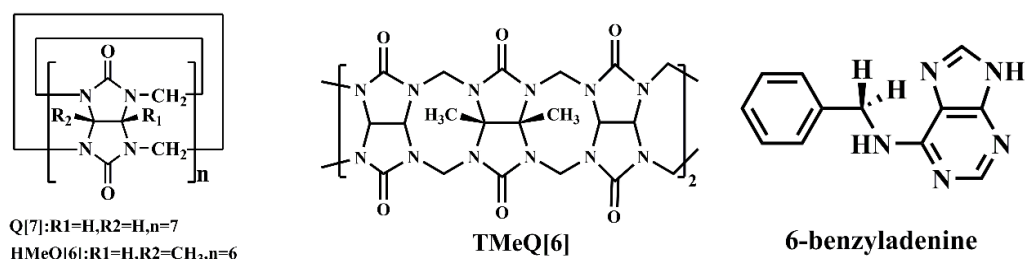
Figure 5. Structures of Q[7], HMeQ[6], TMeQ[6] and 6-benzyladenine.

The well-known and widely used herbicide paraquat (PQ) possesses a toxicity that has serious implications for the ecosystem. If systems can be developed that mask or greatly inhibit this toxicity then this would be widely beneficial. With this in mind, Wang *et al* [12] have employed Q[7] to suppress the toxicity of PQ. In particular, the equimolar reaction of Q[7] with PQ in water affords the species PQ@cucurbit[7]uril (PQ@Q[7]), figure 6, which inhibits the cellular uptake of PQ reducing both the generation of reactive oxygen species together with apoptosis in cellular models. The Wang group conducted a series of experiments to illustrate how this new Q[7]-based PQ species could enhance survival rates for wildlife. For example, reduced hepatotoxicity and better survival rates was witnessed for a zebrafish model when used the Q[7]-based system *versus* free PQ. Extension to mice also revealed the beneficial effects exerted by the Q[7]-based system. Interestingly, the herbicidal activity of the Q[7]-based was not diminished compared to that of free PQ, and so such a system has great potential as a safer herbicide.
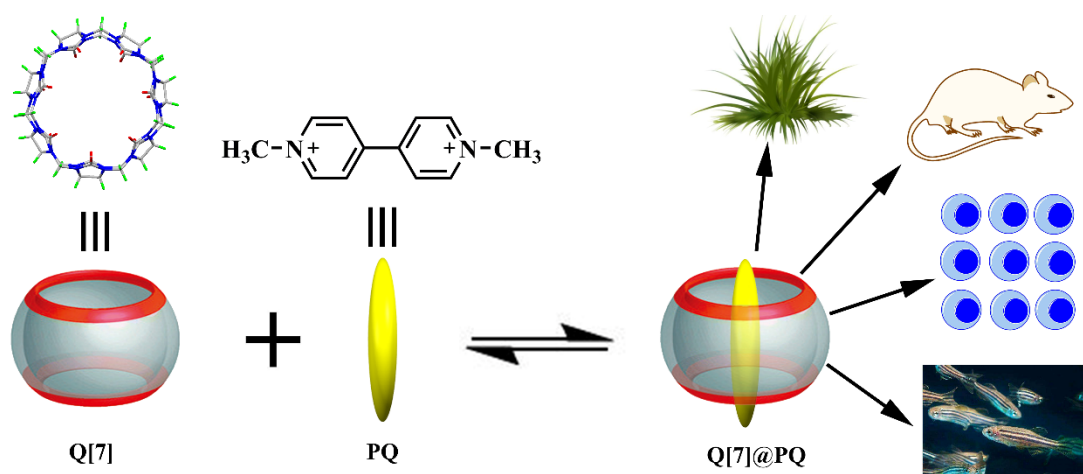
Figure 6. Structures of Q[7], PQ and PQ@Q[7] and illustration of application (cells, zebrafish and mice).

Diquat (DQ^{2+}) and paraquat (PQ^{2+}) are doubly charged quaternary ammonium compounds that are employed as crop desiccants and herbicides. Their interaction with both Q[7] and Q[8], see figure 7, has been studied by Kaifer *et al*. [23] Results indicated that DQ^{2+} was bound better by Q[8] ($K=4.8 \times 10^4$ M^{-1}) than by Q[7] ($K = 350$ M^{-1}). The reversible voltammetric behavior of the dications in the presence of Q[7] or Q[8] revealed that the one electron reduced guest (e.g. $DQ^{\bullet+}$) exhibited an increased binding affinity towards the Q[n] *versus* the dication. From a molecular structure determination, it was evident that the Q[8] formed an inclusion complex with DQ^{2+}, whereas, according the ^1H NMR spectroscopy, with Q[7] there was only partial inclusion of DQ^{2+}. Overall, the results of this study indicated that Q[8] can better tolerate changes to guest features such as charge, charge distribution and shape.
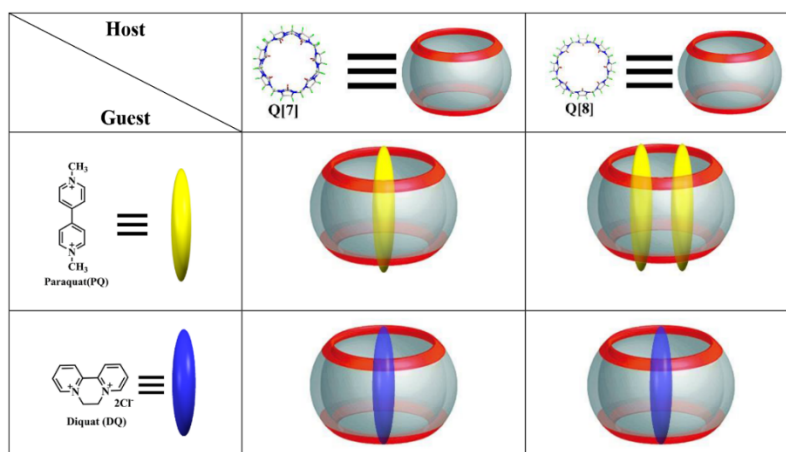
Figure 7. Interaction of Q[7] and Q[8] with paraquat and diquat.

A host-guest complex formed between Q[7] and acridine orange has been employed for the determination of paraquat levels in aqueous solution. [30] The method again is based on changes in fluorescence. In particular, addition of Q[7] results in increased fluorescence of acridine orange, whilst the addition of paraquat to this system results in fluorescent quenching. The system afforded a linear range over the concentrations 3.0–800 nmol L^{-1} with a paraquat detection limit of 1.61 nmol L^{-1}.

Du and coworkers utilized a system comprising Q[7] and the isoquinoline alkaloid coptisine

(COP) in aqueous solution to develop a probe for the detection of paraquat (PQ). [34] The fluorescent intensity of the 1:1 COP/Q[7] host-guest complex was quenched on addition of PQ; the degree of quenching increased with PQ concentration. Both ^{1}H NMR spectroscopy and molecular calculations were employed to shed light on the mechanistic aspects of the host-guest interactions. The method proved to be very sensitive down to ng/mL, and proved to be highly selective. Indeed, deployment of the method for PO detection in the likes of ditch and lake water proved possible, and recoveries were in the range 96.73% to 105.77%.

2.2.2 Use of carbendazim (CBZ)

Fatiha *et al*. [16] have investigated the interaction of the fungicide carbendazim (CBZ), which can be employed as a casting worm control agent, with Q[7] using time-dependent density functional theory. Two models were considered which involved either encapsulation of the benzimidazole or carbamate group of the guest. Results indicated that both forms were stable with limited deformation upon complexation. From calculated UV-vis spectra, it was evident that a charge transfer had occurred between the CBZ and the Q[7].

Our group [17] has been probing the effect of the presence of the hemimethyl-substituted cucurbituril HMeQ[7] on pesticide solubility, and three representative examples, namely 2-(4-thiazolyl)benzimidazole (TBZ), fuberidazole (FBZ), and carbendazim (CBZ) were selected. Such pesticides share a common motif, namely a benzimidazole, and all exhibited limited solubility in water, and this hindered collection of decent ^{1}H NMR spectroscopic data. However, in the presence of HMeQ[7], the situation was improved and informative spectra could be obtained. From ^{1}H NMR spectroscopic titration experiments, it was evident that i) all three systems possess a high binding and unbinding exchange ratio on the NMR time scale, *i.e.* only a single set of resonances is observed for each guest; and ii) proton shifts are consistent with the inclusion of the benzimidazole moiety (a downfield shift is observed as the guest concentration increases), whilst the remainder of the guest resides near the Q[7] portal (upfield shifts).

The high solubility of HMeQ[7] in both water and DMSO suggests further widespread use in host-guest complexation chemistry with practical applications likely.

Hernández and coworkers were able to determine the amounts of carbendazim (CBZ) in oranges by utilizing its complexation with Q[7]. [35] A similar complex was also formed with

Q[6], however the fluorescence intensity exhibited by the Q[7] system was superior. On varying the pH between 1 and 12 at a constant CBZ concentration, it was found that pH4 afforded the optimum results. The concentration of acetate buffer employed was kept low at 10^{-4}M in order to minimize competitive ion dipole interactions. By measuring the fluorescence at different concentrations of Q[7], the stoichiometry of the species formed was determined as both 1:1 and 2:1 (CBZ:Q[7]). Use of the preferred conditions allowed for carbendazim detection down to 5.0 $\times 10^{-9}$M. A matrix solid phase dispersion (MSPD) procedure was used to prepare orange samples, where the MSPD involves making the sample homogeneous, combined with cellular disruption, extraction as well as fractionation and purification. In such prepared orange samples, CBZ levels at concentrations of 0.10 mg/Kg were reproducibly detectable.

Saleh, Nau *et al*. [21] conducted studies on a series of fungicides and anthelmintic compounds, all of which contained a benzimidazole (BZ) motif, focusing on their interaction with Q[7] in water. The chosen compounds were albendazole (ABZ), carbendazim (CBZ), thiabendazole (TBZ), fuberidazole (FBZ), and the parent benzimidazole (BZ), see figure 8, which have found applications ranging from the preservation of fruits, typically citrus fruits, bananas and tomatoes to the treatment of cats and dogs for hookworm. One feature they all share is a limited solubility in water. With this in mind, the interaction with Q[7] was studied by ^{1}H NMR and absorption spectra as well as by fluorescence. Results revealed that pK_a values increased and the guests were protonated leading to strong binding (e.g. K = 2.6 × 10^7 L/mol for ABZ *versus* 6.5 × 10^4 L/mol for the neutral form). The solubility of these host-guest complexes in water was greatly increased *versus* the parent BZ-containing compounds (e.g. from 0.003 to 0.300 mmol/L for ABZ), and was also found to be 5 times higher than if β-cyclodextrin was used instead of Q[7]. It was also found that subjecting these host-guest complexes to UV radiation at pH 2.4, results in far slower decomposition than observed for the parent BZ-containing compounds (e.g. 7 times slower for the FBZ system).
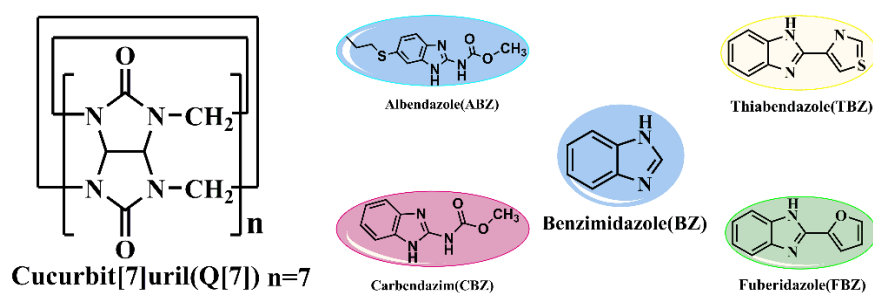
Figure 8. Structures of Q[7], albendazole (ABZ), carbendazim (CBZ), thiabendazole (TBZ), fuberidazole (FBZ), and the parent benzimidazole (BZ).

McCammon *et al.* [15] have determined the pH-dependent changes in binding free energies for complexation between Q[7] and a series of benzimidazole guests, including CBZ, by using calculations to reproduce pK_a shifts. This was accomplished by using a constant pH, and then molecular dynamic simulations were combined with experimental data or thermodynamic integration computations to develop a protocol that allowed for the prediction of pH-dependent free energy profiles (binding free energies). They also noted the importance of correctly assigned guest protonation on such computations.

2.2.3 Use of Cartap (CP)

Cartap (CP), *S,S′*-[2-(dimethylamino)-1,3-propanediyl] dicarbamothioate, has been employed as an insecticide for decades, particularly in Asia. In aqueous solution, CP is not fluorescent, but its presence can be determined via quenching of the fluorescence associated with the host-guest complex formed on interaction of Q[7] with palmatine (PAL) in acidic solution. [32] For CP concentrations between 0.009 and 2.4 µg mL^{-1}, Du and coworkers found that there is a good linear relationship, and from this data, the detection limit was calculated to be 0.0029 µg mL^{-1}. Calculations revealed the partial inclusion of PAL in the Q[7] cavity, with the methoxy isoquinoline fragment encapsulated, whilst the heterocyclic nitrogen is involved in H-bonding with the carbonyls of the portal. The result of this is that there is less exposure to water, and thus there is a fluorescent enhancement. In the presence of other dimethylamino compounds, e.g. thiram, daminozide, the fluorescence remains unaffected. Other experiments evaluated the effect of contaminants, ranging from folic acid to starch, on the detection of CP, and it was found that the system possessed good selectivity. Studies were extended to CP determination in samples of

vegetables (cabbage) and grain (rice). Experiments were each conducted six times, recoveries of 87.4-103% were observed, and the values for the CP concentrations were similar to those obtain by Wu *et al*. [33]

2.2.4 Use of nereistoxin (NTX)

Nereistoxin derivatives are widely used as pesticides, whilst nereistoxin (NTX) itself, *N,N*-dimethyl-1,2-dithiolan-4-amine, is a toxic natural product. Du *et al*. have studied the inclusion complex of Q[7] with the protoberberine alkaloid palmatine (PAL), and have examined the fluorescent behavior in aqueous solution on adding NTX. [29] It was found that the addition of NTX resulted in fluorescent quenching, with the PAL removed from the Q[7] cavity. Data indicated that a 1:1 inclusion complex was formed between NTX and Q[7]. Calculations revealed an association/binding constant of $K_{Q[7]\text{-NTX}} = (1.40 \pm 0.15) \times 10^5$ L mol^{-1} for the Q[7]/NTX complexation process.

2.3 Use of cucurbit[8]urils

2.3.1 Use of paraquat

β-Indoleacetic acid (1*H*-indol-3-yl)acetic acid, IAA) is a common, naturally occurring plant hormone and is known to kill broadleaf plants amongst cereal crops. The interaction of IAA with Q[8] in aqueous solution has been studied using UV-Vis, fluorescence and ^{1}H NMR spectroscopy together with ITC by Huang *et al*. [13] Data indicated the formation of a 1:1 host-guest complex which, in the presence of paraquat (MV^{2+}), exhibits a competitive inclusion process with association constants of $(3.22\pm0.96) \times 10^5$ L·mol^{-1} for Q[8]@ IAA and $(3.90\pm0.91)\times10^6$ L·mol^{-1} for Q[8]@ MV^{2+} (figure 9). The formation of the ternary inclusion complex between Q[8], IAA and MV^{2+} leads to a reduction of the fluorescence and absorption spectra. In this ternary complex, the indole groups of IAA and the bipy group of MV^{2+} end up incorporated into Q[8] cavities as evidenced by ^{1}H NMR spectroscopy.
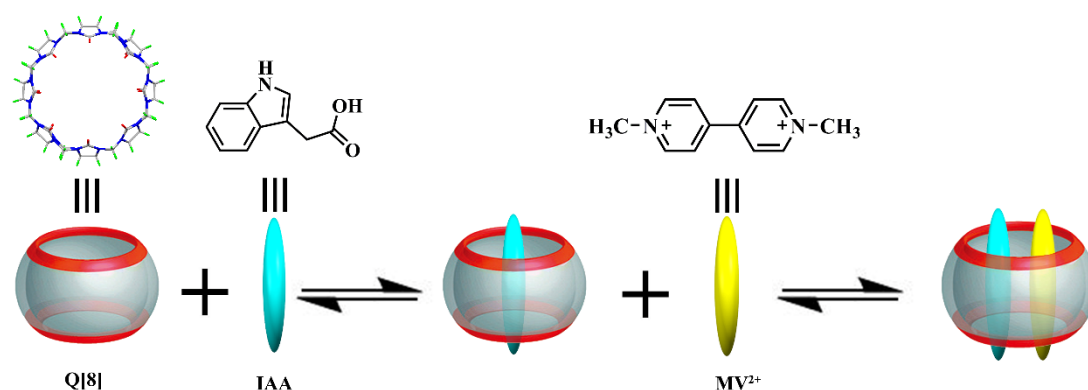
Figure 9. Structures of Q[8], IAA, MV^{2+} and their inclusion complexes with Q[8].

Tan *et al*. found that in the case of Q[8], the cavity is large enough to not only form an inclusion complex with the fluorescent pyrene derivative *N*-allyl-1-pyrenemethylammonium hydrochloride (APA^+), but could also accommodate the paraquat (MV^{2+}) portion of paraquat dichloride. [31] Whilst the fluorescence of the pyrene derivative is diminished upon encapsulation, the further addition of MV^{2+} leads to more quenching and also the emergence of a fresh charge transfer band. These changes can be evaluated by titrations/spectroscopy and used to determine the amounts of both Q[8] and MV^{2+} present with a high degree of sensitivity.

The potential of Q[8] as a host towards amino acids was demonstrated by Rajgariah and Urbach. [36] They employed both Q[8] and the inclusion complex formed from Q[8] and paraquat (MV) in an attempt to encapsulate different amino acids in aqueous solution. All 20 natural amino acids were screened, and it was found, via the use of ^1H NMR spectroscopy and ITC, that there was a preference to only bind with tryptophan (Trp), phenylalanine (Phe), and tyrosine. Such observations reveal the potential of these hosts for selective recognition. It should be noted too that Q[8] favored Phe, whilst Q[8]/MV preferred Trp.

2.3.2 Use of carboxin

The anilide carboxin, which is used as a fungicide for crops such as barley, corn and wheat, has been investigated by Xue *et al*. [22] Its reaction with Q[8] in aqueous solution was monitored by ^1H NMR, electronic absorption and fluorescence spectroscopies. Results revealed the formation of a 1:1 complex in which the phenyl group of the guest was encapsulated in the Q[8] cavity. Further experiments revealed that this host-guest complex improved the antifungal activity of

carboxin, as demonstrated by *in vitro* screening against *Rhizoctonia solani*. It was noted that increasing the amount of Q[8] added led to a better inhibitory effect.

Huang *et al*. reported a system for the detection of benzimidazole fungicides, for example thiabendazole, fuberidazole and carbendazim, which was based on the interaction of Q[8] with pyronine (PyY) in acidic aqueous solution, figure 10. [27] Again, this system employed a turn-on mechanism, and involved the host-guest species 2PyY@Q[8]. The system proved to be highly sensitive, with a reported detection limit of ~10^{-8} mol/L. As well as a series of spectroscopic investigations on the mechanism of the system, DFT calculations were performed.
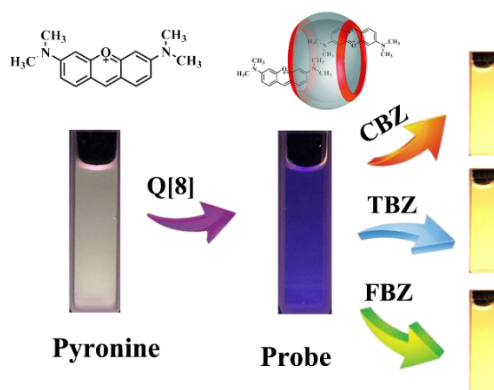
Figure 10. Interaction of PyP with Q[8] and the fungicides thiabendazole, fuberidazole and carbendazim.

Cytotoxicity assays and cell imaging was carried out, and it proved possible to utilize the inclusion complex for the imaging of benzimidazole fungicide in prostate cancer (PC3) cells.

Huang *et al*. also reported the formation of a 1:2 inclusion complex between Q[8] and thionine (TH) in 0.01 mol·L^{-1} HCl solution, figure 11. [28] The fluorescence associated with the Q[8]/TH complex was observed to increase in a linear fashion on addition of increasing amounts of carbendazim (CBZ) over the range 0~3.5 µmol·L^{-1}. A detection limit of 9.39 x 10^{-8} mol·L^{-1} was calculated. The system proved to be tolerant of impurities such as Fe^{3+}, Mg^{2+}, Ca^{2+}, as well as the benzimidazole compounds thiabendazole and fuberidazole.
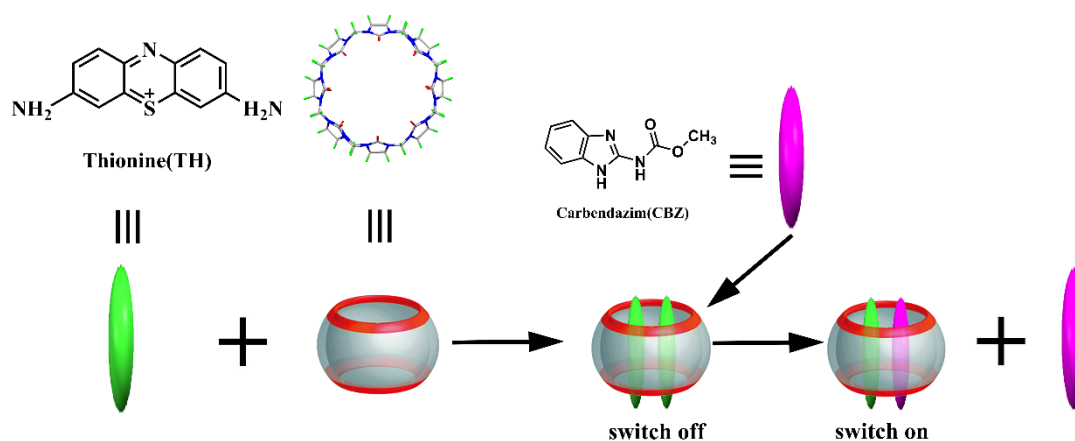
Figure 11. Possible inclusion model of Q[8] and TH with CBZ.

The fungicide and bactericide dodine (DD), 1-dodecylguanidinium acetate, is employed to treat fruits such as apples and pears, and is also effective as an algal growth inhibitor. Our group has reported a Q[10]-based system that can selectively distinguish DD from other pesticides (14 were employed in total). [25] A fluorescence turn-on approach was employed which operates by use of a guest replacement mechanism. The strong fluorescence associated with protonated methyl acridine (MeAD, 10-methylacridin-10-ium iodide) in aqueous solution is key, given the absence of such fluorescence for the homoternary inclusion complex MeAD$_2$@Q[10], figure 12. However, when DD was added to MeAD$_2$@Q[10] in aqueous solution, the MeAD was 'kicked out' which resulted in a return of the strong fluorescence. Use of any of the other 13 pesticides employed in this study did not lead to any return of fluorescence. This suggested that such a system is capable of the selective recognition of DD, and may be applicable for the detection of other relevant analytes.
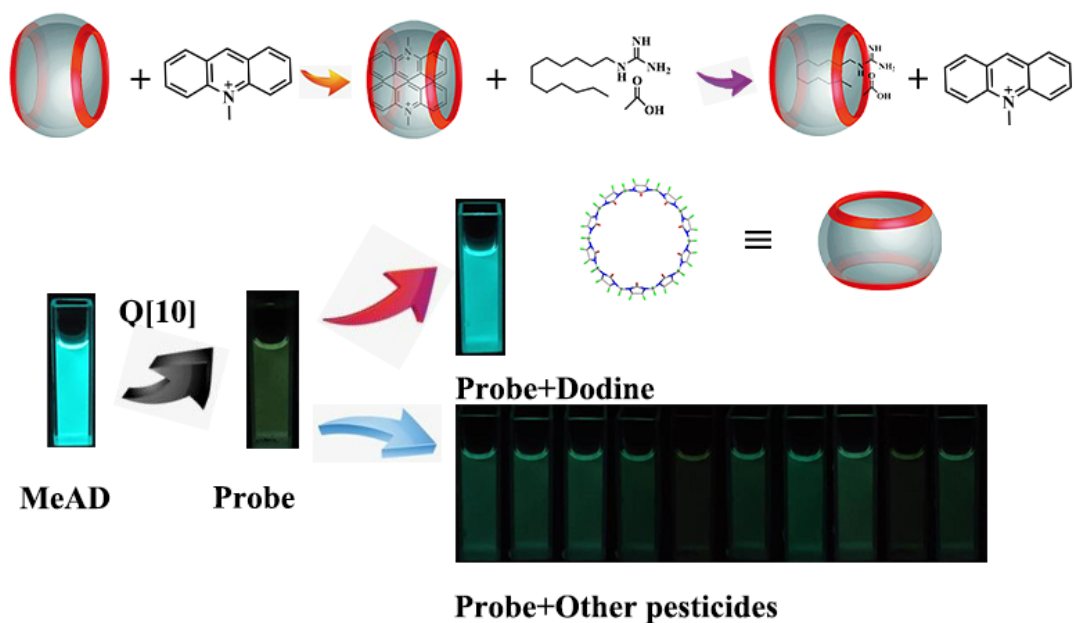
Figure 12. Interaction of Q[10] with dodine and protonated methyl acridine.

The above study was followed up by a second publication on the related $AD_2@Q[10]$ system, where AD = protonated acridine, for DD detection. [26] The system operated using the same guest-replacement fluorescence turn-on mechanism. As well as DD, 19 other pesticides were added, four of which gave some fluorescent enhancements, whilst the remaining 15 did not (figure 13). The concentration range for DD determination was found to be quite wide (0 to 4.0×10^{-5} mol·L−1) with a low limit of detection at 1.827×10^{-6} mol·L^{-1}. Use of the system in real agricultural products was evaluated, for example kidney beans and *G. cusimbua* smeared with DD. Use of UV light allowed for the detection of signals and shows the potential this system has for use in real-world scenarios.
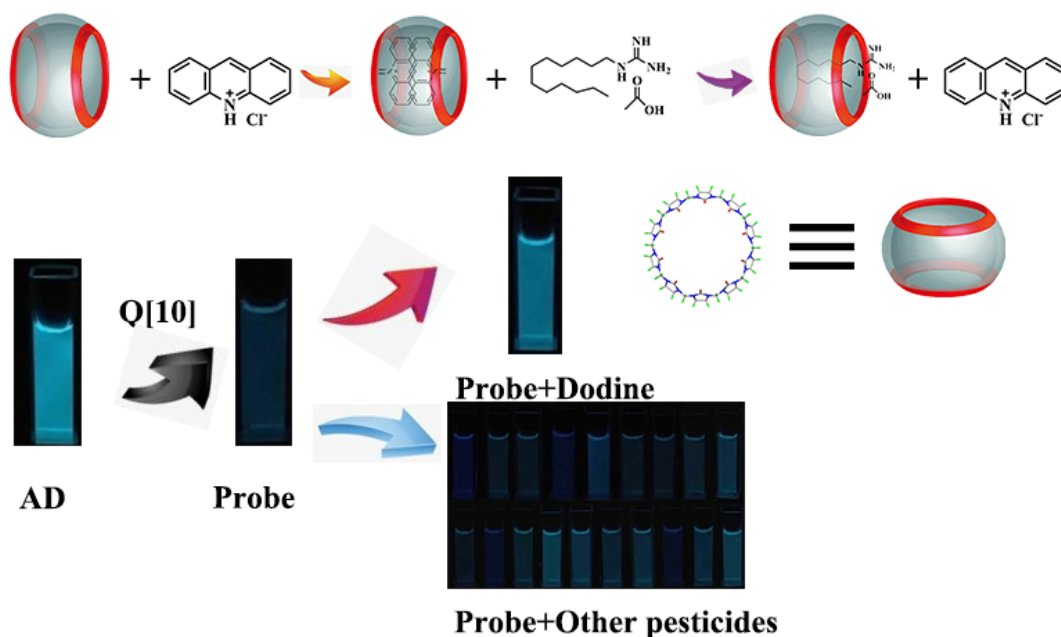
Figure 13. Fluorescent response of AD$_2$@Q[10] in the presence of the 20 pesticides.

3. Supramolecular assembly of pesticides with pillar[n]arenes

3.1. Host-guest complexes of pesticides with pillar[n]arenes

Pillar[n]arenes are a recent addition to the family of macrocycles, with the first observation in the mid-1990s, [37] and the first fully characterized example reported in 2008. [7] They are comprised of hydroquinone groups bridged at the *para* position with methylene linkers, see figure 14. Shape-wise they resemble a cylinder or pumpkin, and like cucurbiturils they possess a cavity capable of binding a variety of species in host-guest fashion. The synthesis and functionalization of pillar[n]arenes has recently been reviewed, [38] whilst Cao and Meier have reviewed the host-guest chemistry of pillararenes with a variety of organic guests, with emphasis on changes of fluorescence (turn-on/turn-off) upon competing complexation. [39] The potential of such systems was recognized, as was the need for much more work in the area.

The section, where possible, discusses pillararenes in order of size, with the majority of reports involving the use of pillar[5]arene. However, given that all but two of the systems involve the use of paraquat, we have not introduced any further sub-sections in this part of the review.
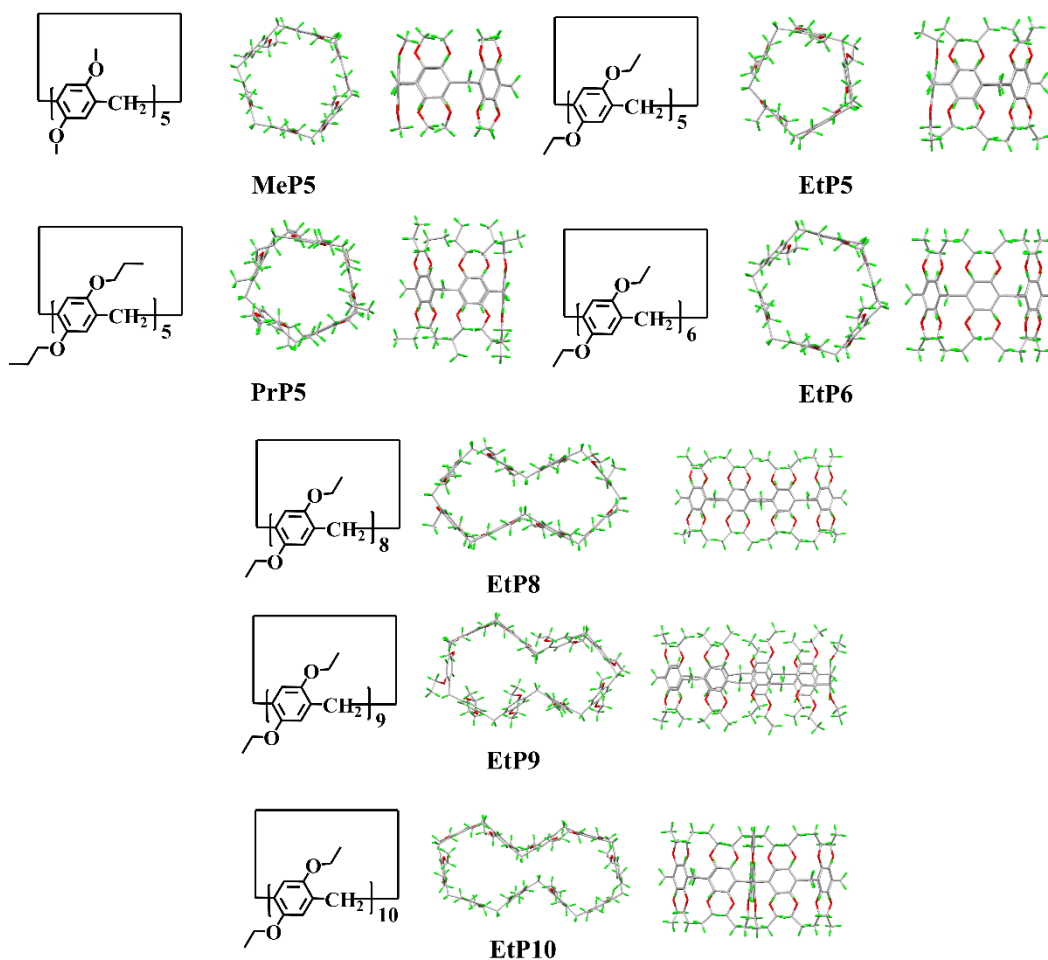
Figure 14. The pillar[*n*]arene family.

Xie, Chen *et al*. have employed density functional theory to probe possible pillar[*n*]arenes (n = 4 to 6) bearing heteroatom bridges of the bora-, aza- or oxa type. [44] In particular, the studies looked at possible geometries, spectroscopy and the influence of different solvents. Studies were extended to include the inclusion complexes of these hosts with paraquat. Results suggested that heteroatom bridged pillar[*n*]arenes with n= 5 or 6 were the ones most likely to be prepared in the laboratory, with n = 5 being the most stable. The aza and oxo-containing structures are quite rigid, whilst the bora systems are looser. The presence of these bridges results in electron rich cavities. From the UV-vis spectral studies, it was found that n → π* and π → π* transitions tend to be present. In terms of solubility, the hosts are soluble in polar solvents. With paraquat, the pillar[5]arenes form 1:1 inclusion complexes, with the aza inclusion system being the most stable (*versus* the bora and oxa systems).

Liu *et al*. [40] have investigated the ability of two water soluble carboxylated pillar[5]arenes bearing arms of different length to encapsulate the 4,4$'$-pyridinium-containing herbicides paraquat (PQ) and diquat (DQ). In particular, they studied the ability of the water-soluble hosts to sequester PQ and DQ from plant foliage, figure 15. In the case of PQ, it was evident from ^{1}H NMR spectroscopic experiments that it was closely associated with the cavities of both the carboxylated pillar[5]arenes. For DQ, the association seems to be somewhat weaker. A Job's plots confirmed 1:1 complexation, and the preference for binding PQ was found to be 30 to 50x that of DQ for both carboxylated pillar[5]arenes. Tests of plants (maize and soybean) revealed the potential of these systems given that spraying with PQ or DQ resulted in rapid deterioration of the leaves (yellow after 6h, withered after 24h), whereas in the presence of the pillararenes, the leaves remained green. Staining experiments revealed that the presence of the pillararene acted to limit the amount of reactive oxygen species present, which in turn restricts the destructive action of the herbicides.
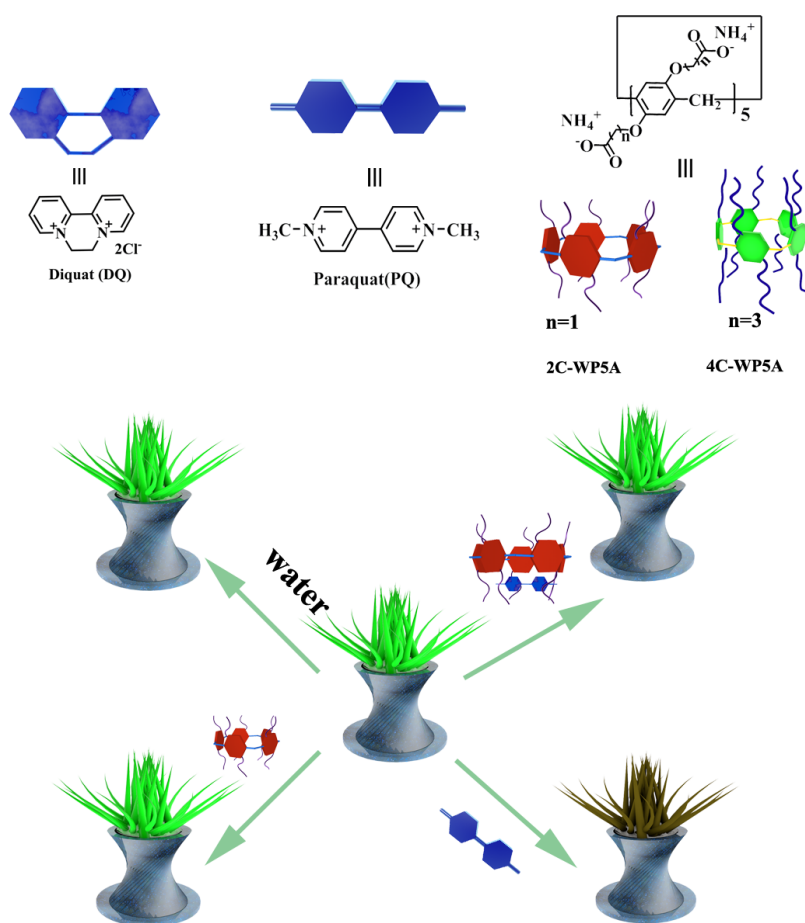
Figure 15. Schematic illustration of inclusion complexes consisting of PQ, DQ, and carboxylated pillararenes for herbicide sequestration from plant foliage.

Ma *et al*. examined the interactions of 22 different guests, including adamantane-containing guests, aromatic guests and ammonium guests, with a number of water-soluble carboxylated pillar[*n*]arene (n = 5-7) in sodium phosphate buffer (pH 7.4). [41] As part of the study, the binding affinity of 51 supramolecular complexes was determined via their Ka values. From the data, it was possible to identify π-π stacking, hydrophobic and electrostatic interactions as the driving force for such encapsulation. The use of di-ammonium guests proved beneficial for high binding affinity, and by incorporating an ethylene linker so that the ammonium motifs were spaced further apart, it proved possible to increase (more than 3-fold) the binding affinity *versus* the guest without the ethylene spacer (namely paraquat).

The herbicide benquitrione (IUPAC name 3-(2,6-dimethylphenyl)-6-[(2-hydroxy-6-oxocyclohex-1-en-1-yl)carbonyl]-1-methylquinazoline-2,4(1*H*,3*H*)-dione), which is used to treat weeds, has been investigated by Yang, Li *et al*. [42] Their study involved the preparation of three water soluble pillar[5]arenes which possessed either different arms of different length terminated by ammonium groups or arms bearing carboxylic acid end groups. Encapsulation of benquitrione was then investigated, and results from UV spectroscopic titration experiments revealed that use of the host **AP5A** (see figure 16) afforded the greatest interaction. Moreover, calculations (Benesi–Hildebrand equation) revealed that this host has the highest binding affinity of the three with benquitrione forming a 1:1 host-guest species. The diffusion of this species over superhydrophobic surfaces was then investigated using a silicon interface. By measuring contact angles, it was observed that the spreading of droplets formed by this species was greater than the spreading observed when benquitrione was used in combination with either of the other two hosts. Calculations revealed that the dynamic spreading area of the droplets formed by **AP5A**/benquitrione significantly increased (by x5) *versus* benquitrione alone. The increased spread was attributed to reduced dynamic surface tension. Similar increased spreading was observed when bamboo and cotton leaves were utilized as the surface. It was also shown, for example by treating grass, that encapsulation of benquitrione by **AP5A** did not impact negatively on the pesticidal properties of benquitrione.
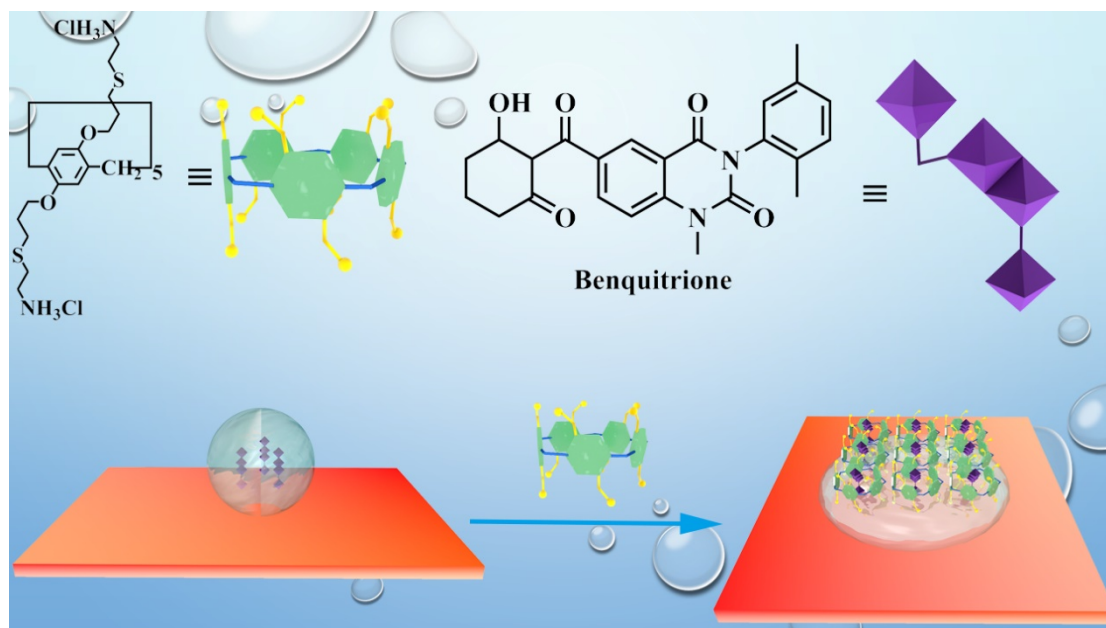
Figure 16. Structures of the host AP5A, benquitrione and an illustration of the droplet spreading ability of the host-guest complex.

Shi, Yao, Huang and coworkers have examined the interaction of three water soluble pillar[5]arenes (figure 17) with paraquat. [43] For two of the pillar[5]arenes (**WP5-2** and **WP5-3**), there was evidence (from ^{1}H NMR spectroscopy) of the formation of strong host-guest complexation, whereas for **WP5-1**, data suggested only a very weak interaction. By using MTT assays and the cell lines HEK 293 and Raw 264.4, all three pillar[5]arenes were found to be of low toxicity. Moreover, cell viability studies revealed that for **WP5-2** and **WP5-3**, the host-guest complexes with paraquat were less toxic than was paraquat alone.
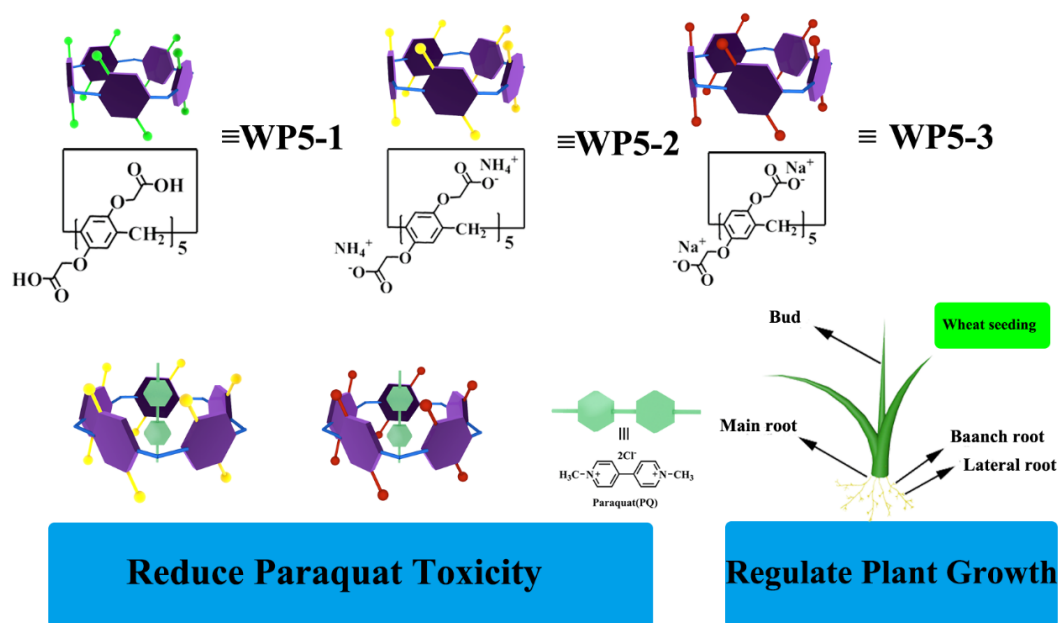
Li *et al*. have studied the interaction of droplets of methyl paraquat at a pillar[5]arene modified surface, the latter acting as a leaf mimic. [45] This was achieved by preparing a pillar[5]arene functionalized with a alkenyl group which allowed, via Click chemistry, the pillararene to be attached to an azide modified silicon surface. Initial solution phase studies were conducted to show that there was a strong interaction between this functionalized pillar[5]arene and methyl paraquat; the association constant of the 1:1 complex was determined to be (1.32 ± 0.08) $10^3 m^{-1}$. Following this, Click chemistry was conducted and the attachment of the pillararene to the surface was confirmed by FTIR, XPS and contact angles. Subjecting this surface to droplets of a number of guests including methyl paraquat revealed different results in terms of contact angle hysteresis following addition of droplets of water. Theoretical slide angles were calculated, with that for methyl paraquat included in the supported pillar[5]arene being 56°; for other guests and water the slides angles were calculated to be between 7 and 13°. Given this, the modified surface was tilted by 45°, and it was observed that all droplets slid off, except for in the methyl paraquat case. The slide angle for methyl paraquat was also found to increase with concentration over the range 10^{-8} to 10^{-3} M; no such trend was observed for droplets of the other guests. Even after seven cycles of adding alternate droplets of water or methyl paraquat, the tilted surface still revealed an

affinity for methyl paraquat. These observations were explained in terms of the enhanced binding between the pillar[5]arene and methyl paraquat.

Huang *et al.* have investigated the use of anionic pillar[5]arenes and their interaction with paraquat. [46] The four constitutional isomers of the precursor ester-bearing pillar[5]arene possess different melting points occurring in the range 102.9 to 116.3 °C, differing ^{1}H NMR spectra and the crystal structure determinations revealed differences in the positions of the pentyl groups. The precursor ester compounds can be readily converted to the corresponding pillararene acids on treatment with sodium hydroxide and ammonium hydroxide. The interaction in water of the four anionic acid isomers with paraquat was investigated by ^{1}H NMR spectroscopy and also by ESI-MS. Data revealed that despite the common cavity, the isomers exhibited different association constants for paraquat, which is related to the orientation of the substituents. It was noted that in three of the isomers, the positions of the substituents led to anionic rims at each end of the cavity, which enhance host-guest interactions.

Yang and coworkers took advantage of a functionalized silica support to encapsulate paraquat. [47] In this case, a silica surface was first treated with $SiCl_4$ and then with either perhydroxyl-pillar[5]arene or perhydroxyl-pillar[6]arene (coverage ≤250 μmol pillar[5, 6]arenes /g). TGAs, FTIR and UV-vis spectra and SEMs were recorded to verify that the pillararenes were indeed attached to the support. Subsequent adsorption experiments using an aqueous solution of paraquat, revealed that the pillar[6]arene-containing system exhibited the greatest absorption (with a saturation value of 0.20 mmol paraquat per gram of supported host) and with first-order kinetics. Overall, the process was endothermic, with desorption of solvents from the cavity contributing greater than the paraquat adsorption. Clearly, the use of such functionalized supports has the potential to be applied to other toxic materials and their removal from contaminated waters.

The [*n*]ethylene glycol-functionalized (n = 1, 3) pillar[5]arenes have been complexed with paraquat. [51] The molecular structure of the 1:1 inclusion complex formed between the n = 1 system and paraquat was reported and revealed that the inclusion complex is stabilized by interactions such as π-interactions (face-to-face stacking and C-H⋯π) together with C-H⋯O bonding interactions. The 1:1 structure in solution for both hosts with paraquat was also verified via the use of ^{1}H NMR spectroscopy, ESI-MS, 2D NOESY and ITC experiments. The results also demonstrated that shorter [*n*]ethylene glycol chain substituents, favor higher association constants.

A reversible reduction process (of the paraquat) was demonstrated on addition of excess (10 equiv.) of zinc powder. The reversible process can be followed by changes in the ^{1}H NMR spectral signals either on addition of the Zn or its removal and subsequent exposure to air.

3.1.3 *Application of pillar[5]arenes and derivatives in pesticides recognition and detection*

Wang, Liang and coworkers devised a method for the detection of paraquat that is based on electrochemistry and nitrogen-doped carbon dots. [53] The nitrogen-doped carbon dots, which are readily prepared in a one-pot procedure, are subject to 1-ethyl-3-(3-dimethylaminopropyl)carbodiimide (EDC)/*N*-hydroxysuccinimide (NHS) coupling with the result that the outer surface is functionalized with carboxylated pillar[5]arenes, figure 18. TEM and FTIR were employed to verify the make-up of the modified pillar[5]arene-coated nitrogen doped carbon dots, and the average size of the latter was found to be 6.3 ± 2.4 nm. TGA results suggested that about 16.7% of the weight loss was associated with the pillararene. The resulting electrochemical sensor works best at pH 7 for pesticide detection. The amount of pillar[5]arene-coated nitrogen doped carbon dots loaded onto the electrode to be employed was found to be 0.50 mg/mL; SEM images also revealed nitrogen doped carbon dots to be present. In the presence of inorganic salts, e.g. 100-fold excess of KCl or NaCl, or organic compounds such as related herbicides e.g. diquat, the electrode system exhibited good tolerance and sensitivity, in other words such species did not interfere with the detection results (of paraquat). A detection limit of 6.4 nmol/L (S/N = 3) was realized, and the system was successfully applied for detection in tap water.
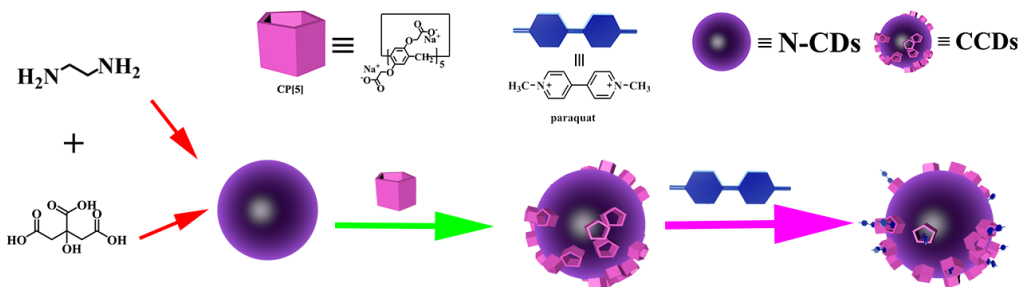
Figure 18. Schematic representation of the synthesis of CCDs via attaching CP[5] at the surface of N-CDs by EDC-NHS coupling reaction, and excellent electrochemical performance in PQ detection exhibited by CCDs/GCE.

Yang, Perrier, Huang and coworkers have employed a polystyrene polymer bearing pendant paraquat and tetraphenylethylene groups to construct, in combination with either water soluble pillar[5]arene (**WP5**) or pillar[6]arene (**WP6**), two amphiphilic polypseudorotaxanes. [54] The properties of these polypseudorotaxanes, such as size and morphology, were measured via the use of DLS, TEM and CLSM; the average diameter of these aggregates was found to be in the region of 80 to 100 nm. In water, these systems undergo self-assembly forming supramolecular polymersomes (**PR5** and **PR6**), figure 19. By adjustment of pH, it proved possible to both breakdown (by adding acid) and reconstruct (by returning to pH 7.4) such polymersomes. Intense fluorescence was also evident in these systems, and this was assigned to tetraphenylethylene-based AIE. As part of the same study, the anti-cancer drug doxorubicin was encapsulated by the vesicles produced above, and this led to quenching of fluorescence. By making the solution more acidic, varying amounts of doxorubicin were released, for example 69% at pH 5.5 over 36h for the pillar[6]arene-based system.
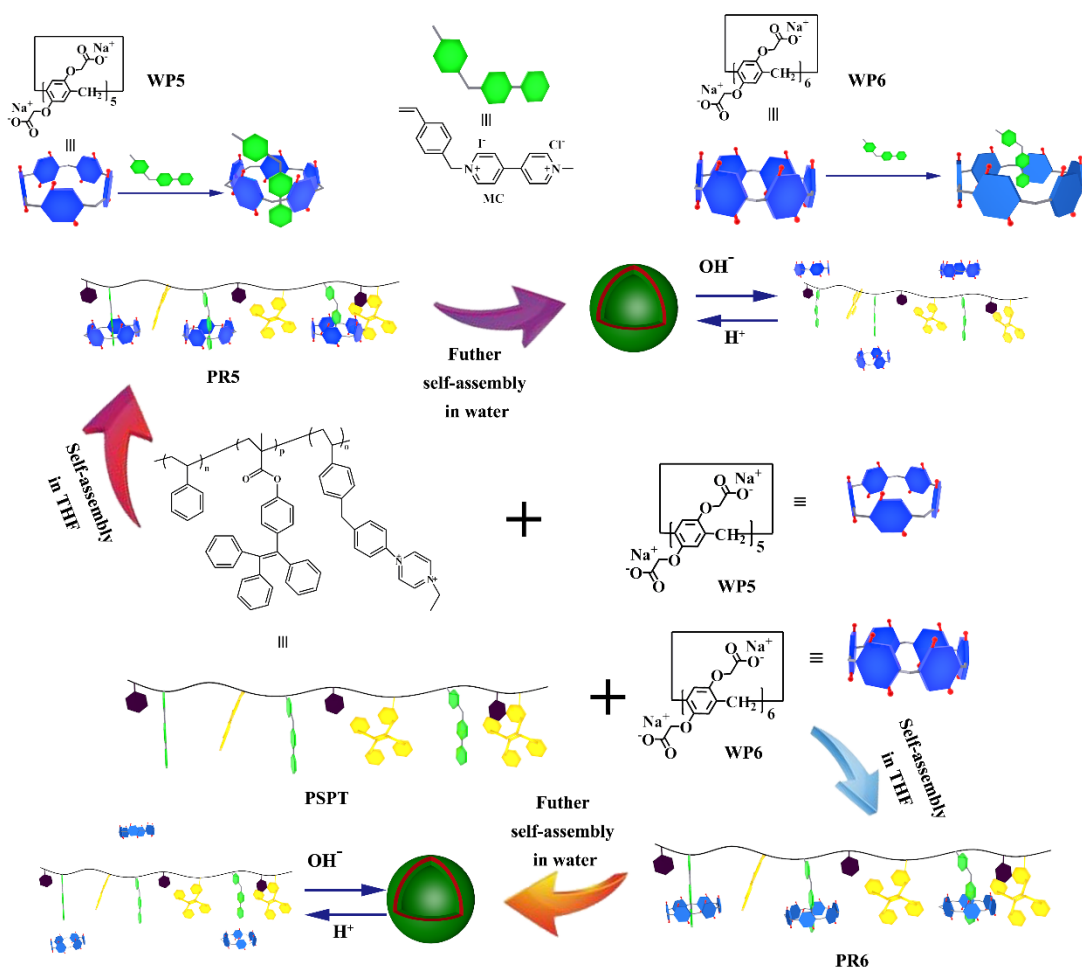
Figure 19. Chemical structures of polymer PSPT, water-soluble pillar[5,6]arenes (**WP5** and **WP6**),

and model guest MC, as well the cartoon representations of host-guest complexations between **WP5** and MC and between **WP6** and MC and pH controlled formation of supramolecular polymersomes from self-assembly of amphiphilic polypseudorotaxanes **PR5** and **PR6** in water.

Yang *et al*. have employed a water soluble ammonium phosphate salt of pillar[5]arene (see figure 20) as a host to construct an inclusion complex with methylene blue. [55] In this system, the fluorescence normally associated with this guest was quenched, however on addition of paraquat, the fluorescence was recovered. This allowed for the detection of paraquat with a minimum detection limit at 3.6×10^{-7} mol•L^{-1}. This system functioned over a relatively wide pH range and was not affected by the presence of other species such as amino acids.
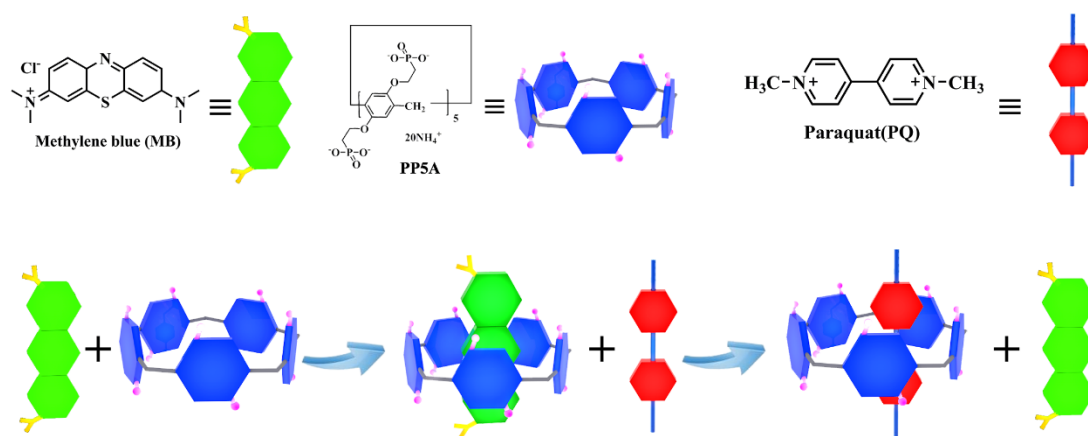
Figure 20. Top: Structures of methylene blue, the ammonium pillar[5]arene and paraquat; bottom: their inclusion complexes.

The insecticide methyl parathion (MP), which is an organothiophosphate, has seen restricted use around the globe. Symptoms resulting from exposure include blurred vision and breathing difficulty and it is classified as an extremely hazardous substance. Thus, methods capable of its rapid detection are highly desirable. With this in mind, Tan and coworkers have reported an electrode system based on a reduced graphene nanocomposite and a cationic pillar[5]arene capable of MP detection via differential pulse voltammetry. [58] Results were compared with a comparable system employing β-cyclodextrin rather than the pillararene, and it was determined (via ^{1}H NMR spectroscopy) that the pillararene system possessed superior recognition toward MP. The selectivity of the method also proved superior and it was possible to detect MP in the presence of

competing species such as KCl, MgCl$_2$ and glucose. The structure of the pillararene/graphene nanocomposite resembled (as observed by TEM) tightly assembled wrinkled sheets. Its MP detection level was found to be 0.0003mM (S/N¼3) with a linear output over the range of 0.001-150mM. It's application with a number of real-world samples, e.g. soil, was tested, and recovery rates were as high as 101.2%.

Xu and Yao have also prepared both micelles and vesicles by making use of a water soluble pillar[5]arene derivative and the recognition ability of paraquat. [62] Paraquat guests with varying lengths of alkyl group (C$_4$H$_9$ to C$_{18}$H$_{37}$) bound to each pyridinium nitrogen were employed, figure 21. Association constants were of the order of 10^{-4} M^{-1} in water. The lengths of these substituents were found to dictate the type of product formed, with shorter chains (<C12) favoring micelles, whilst longer chains (>C12) favoring vesicles. The self-assembly proved to be pH responsive, for example for the system bearing alkyl C$_{12}$H$_{25}$ groups, at pH 4.0, micelles (diameter ~ 7nm) were present, whereas at pH 7.0, vesicles formed. This self-assembly could be reversibly controlled by adjusting the pH. As well as pH, other external stimuli could also be employed such as temperature or addition of other species, e.g. α-cyclodextrins. Hydrophilic guests (e.g. calcein) can be encapsulated by the vesicles, and by adjusting (decreasing) the pH, guest release can be achieved (measured by fluorescence).
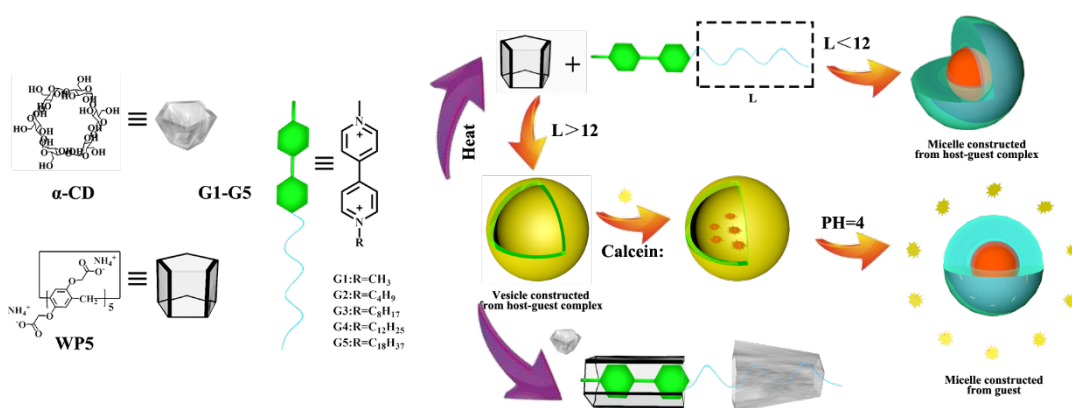
Figure 21. Components used by Xu and Yao to prepare both micelles and vesicles.

Evtugyn *et al*. have utilized a new biosensor for the detection of a number of pesticides including malaoxon, methyl-paraoxon, carbofuran and aldicarb. [64] The system was based on a modified glassy carbon electrode bearing acetylcholinesterase immobilized via carbodiimide on

carbon black and also bearing adsorbed pillar[5]arene. By using a working electrode with stepped potential and measuring the resultant current as a function of time, optimum operating conditions were found to be a potential of 200 mV over 180 seconds. Limits of detection ranged from 5×10^{-9} M (methyl paraoxon) to 4×10^{-12} M (malaoxon). Use of the biosensor on real samples was demonstrated using non-salted raw peanuts and samples of beetroot juice, which were spiked with pesticide. By employing a pillar[5]arene bearing 10 quaternary ammonium arms, reversible inhibition proved possible when it was added, along with acetylthiocholine, to the acetylcholinesterase-based biosensor.

The water-soluble pillar[5]arene **WP5** (figure 22), prepared from the reaction of *per*-hydroxylated pillar[5]arene and tetra(ethylene glycol) monomethyl ether mono-*p*-tosylate, was complexed with a dicationic paraquat derivative which possessed pentyl groups at one end bound to the quaternary nitrogen centres. [65] As anticipated from other results, the dicationic guest was much more tightly held than its neutral counterpart. Following on from this, Huang *et al*. then used the paraquat and a benzyloxy terminated polymer, in conjunction with **WP5**, to form redox-responsive polymeric vesicles via an intermediate pillararene-based amphiphilic macromolecular [2]pseudorotaxane. It proved possible to utilize these vesicles as a drug delivery system, and this was illustrated for the anticancer agent doxorubicin hydrochloride. Drug loadings (~8%) were in the same ballpark as those noted for cucubituril and cyclodextrin-based systems. [66, 67] It was noted that the drug release was more rapid in the presence of a reducing agent such as $Na_2S_2O_4$, and could be controlled by varying the concentration of the reducing agent. Using confocal laser scanning microscopy, it was observed that the vesicles increased in quantity in the cytoplasm of cells, and the drug was released inside the cell. Moreover, the encapsulated drug possessed lower cytotoxicity *versus* the free drug.
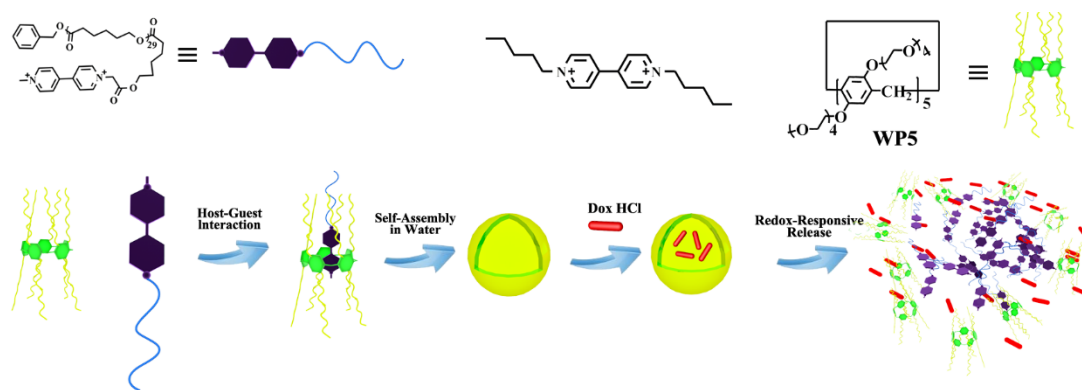
Figure 22. Top: Structure of the benzyloxy terminated polymer, the dicationic paraquat and **WP5**; bottom: use as a drug delivery system.

Li *et al*. have attached a hydrazino pillar[5]arene to a graphene surface, the thickness of which (1.7 ± 0.2 nm) was confirmed by AFM. [68] FTIR and XPS further confirmed the presence of an amide linkage. Addition of the staining agent safranine T led to encapsulation by the pillar[5]arene as evidenced by the upfield shifts in the ^{1}H NMR spectroscopy. Subsequent addition of paraquat led to release of safranine T and the return of fluorescence, the strength of the latter was proportional to the concentration of the paraquat. It was noted that whilst included by the grafted pillar[5]arene, the FRET between the dye and the graphene resulted in 'turn off' of the fluorescence. Cytotoxicity studies using MTT assays and HeLa cell lines indicated that the grafted pillar[5]arene system was not overly cytotoxic; fluorescent quenching of the HeLa cell lines was observed. Given that the fluorescent could be recovered on addition of paraquat to the cells, the system has promise as a probe to image paraquat in living cells. This technique also proved possible *in vivo* with fluorescence turn on and off observable in mice.

Xue *et al*. investigated the 1:1 inclusion complex formed between a carboxylated pillar[5]arene **WP5** (see figure 23) and 10-methylacridinium iodide by ^{1}H NMR spectroscopy, and observed both broadening and upfield shifts for the guest resonances. [69] The initial strong green fluorescence associated with the guest faded upon complexation. Measurements of association constants indicated that the preference for binding paraquat by this system was about 1000 times greater than that for 10-methylacridinium iodide. Given this, it proved possible to utilize the system for the detection of paraquat in water. The host-guest complex could be broken down (by adding acid) and reformed (by adding base) simply by adjusted the pH. The system could also be

employed to detect cyanide ions in aqueous solutions over the pH range 3 to 11. The addition of cyanide involved a change in the color from green to blue.
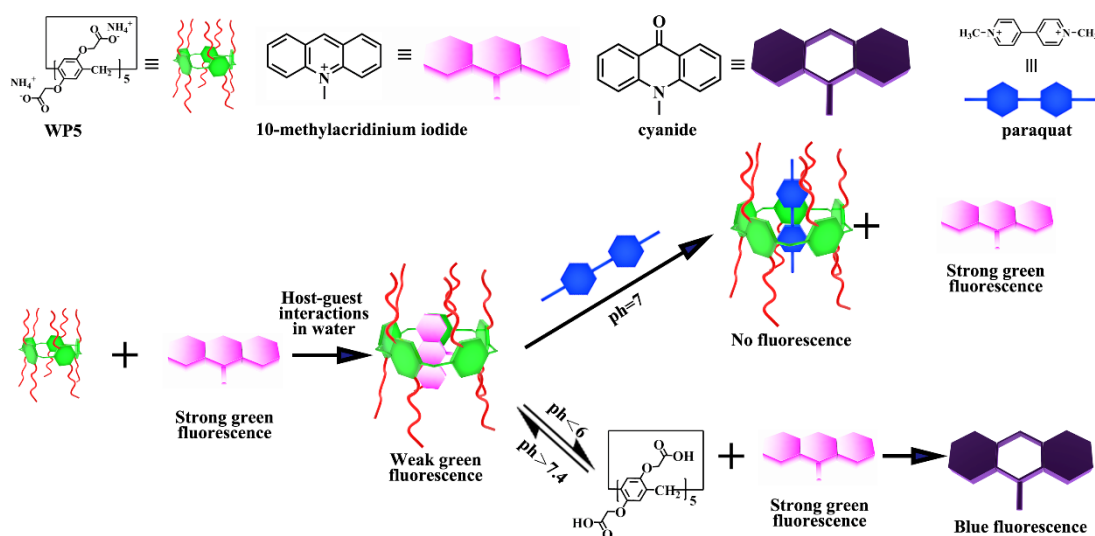
Figure 23. Top: Structures of **WP5**, 10-methylacridinium iodide, cyanide and paraquat; bottom: detection of paraquat and behavior at different pH.

Yang, Jia and coworkers have utilized a system that comprises carboxylatopillar[5]arenes appended on magnetic Fe_3O_4 nanoparticles. [70] The system was characterized by a variety of methods including FTIR, TGA, TEM and XRD. The average diameter of the spheres comprising the pillar[5]arenes and the iron-based nanoparticles was found to be 390 nm. The magnetic properties of the sphere were examined by a vibrating sample magnetometer, revealing super-paramagnetism. Moreover, the extraction capability of the system toward a number of pesticides was evaluated, including metalaxyl, dimethomorph, kresoxim-methyl, flusilazole, cyprodinil, pyrimethanil and triflumizole. In particular, by using magnetic solid phase extraction, in combination with high performance liquid chromatography, the system was evaluated as an adsorbent for trace pesticide determination in spiked and unspiked beverage samples including 5 wines and 5 fruit juices. Following optimization of the conditions, detection limits in the range 5.0 – 11.3 ng mL were determined for the seven pesticides, with recovery ranges of the analytes at 70.6% to 106.8%.

3.1.4 *Use of pillar[6]arene*

Huang *et al*. have investigated the interaction of a water-soluble pillar[6]arene, which possesses carboxylate groups at both rims, with paraquat in water. [52] It was evident from NMR spectroscopic data that a 1:1 [2]pseudorotaxane was formed for which the paraquat was threaded into the cavity. A very high association constant was determined for this system, namely $(1.02\pm0.10) \times 10^8$ M^{-1}, which was attributed to hydrophobic, electrostatic and $\pi-\pi$ stacking interactions. The system proved to be pH sensitive, and the degree of threading of the guest could be manipulated by varying the pH of the solution. Use of an amphiphilic paraquat guest that bears an additional long (C$_{11}$H$_{23}$) alkyl chain in conjunction with the water-soluble pillar[6]arene allowed for controlled aggregation in water. This involved pH control of a reversible process involving micelles and vesicles. Moreover, this allowed for water-soluble dye (calcein was employed) release upon making the solution more acidic as a result of vesicle destruction. As mentioned elsewhere in this review, the toxicity of paraquat is problematic, and involves toxic HO$^{\bullet}$ radicals. By complexing paraquat with the water-soluble pillar[6]arene, the toxicity is reduced partly because the generation of HO$^{\bullet}$ is somewhat reduced, figure 24.
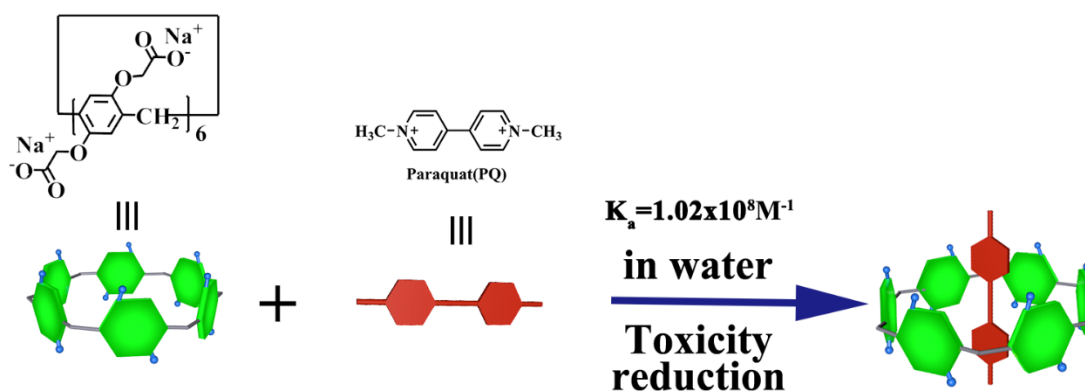
Figure 24. Interaction of water-soluble pillar[6]arene and PQ lead to reduced toxicity.

The first report of the use of pillar[6]arene-modified silver nanoparticles supported on a two dimensional surface (a covalent organic framework, COF) and employed for the detection of paraquat was published by Tan, Zhao *et al*. [56] This heterogeneous system, in which the Ag nanoparticles are the electrocatalysts, the COF is the platform for constructing the sensor, and the pillararene is the host, proved to be highly sensitive in the case of paraquat detection, with a detection limit of 0.014µM. It was operational over 0.01-50µM of paraquat,

and the optimal working potential of the electrode was -0.95 to -0.4 V (*vs* Hg/Hg$_2$Cl$_2$). The system was tolerant of common interferants such as Na$^+$, K$^+$ etc.

Yang *et al*. have employed a water-soluble phosphate pillar[6]arene for the direct exfoliation of a graphene sheet in water. [57] Such a method negates the need for the use of strong oxidizing agents, and is thus a much greener approach compared to previously employed methods. The afforded graphene is highly crystalline, and forms π-π stacking interactions with the pillar[6]arene (figure 25). If this system is used alongside acridine orange, then a FRET interaction with the pillar[6]arene@graphene leads to florescent quenching. However, such quenching is suppressed on addition of paraquat (favored for competitive inclusion *versus* acridine orange), and so paraquat determination is possible; the degree of quenching can be related to the paraquat concentration. The detection limit was found to be 0.06 μM (S/N = 3). The system was screened for its ability to function in the presence of a number of interferents, and was also tested on a number of real water samples.
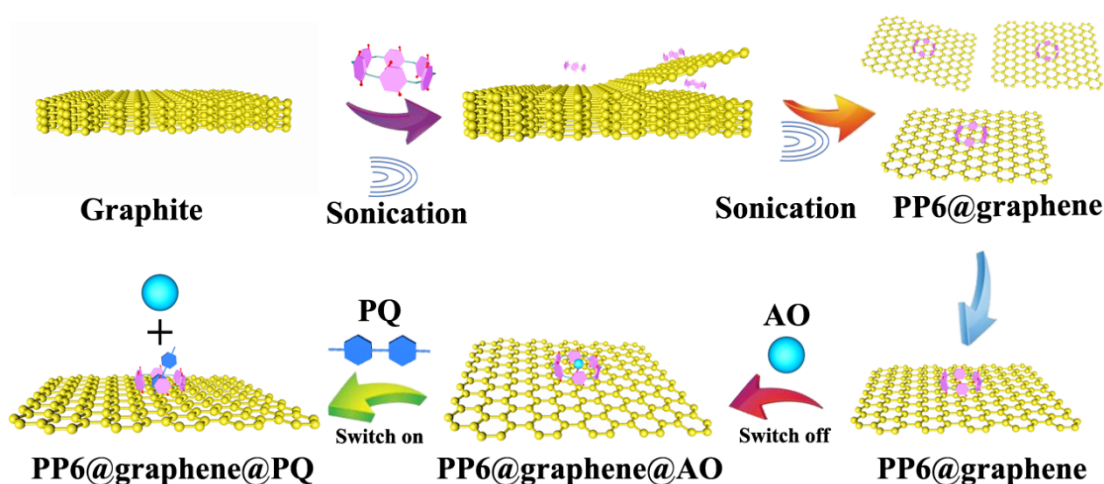
Figure 25. Phosphate pillar[6]arene exfoliation/stabilization of graphene and PQ sensing via host-guest recognition.

Leaning pillar[6]arenes were first reported in 2018, and are so-called because of their unsymmetrical leaning tower-like appearance. [59] Wang *et al*. have utilized such a leaning anionic pillar[6]arene, bearing four carboxylate groups on each rim, in conjunction with *in-situ* generated gold nanoparticles for the detection of the herbicide paraquat, figure 26. [60] A 2:1 host-guest

complex was formed, and the detection limit was 0.02 μM. Such a system also proved to be a useful catalyst for the hydrogenation of *p*-nitrophenol with NaBH₄.
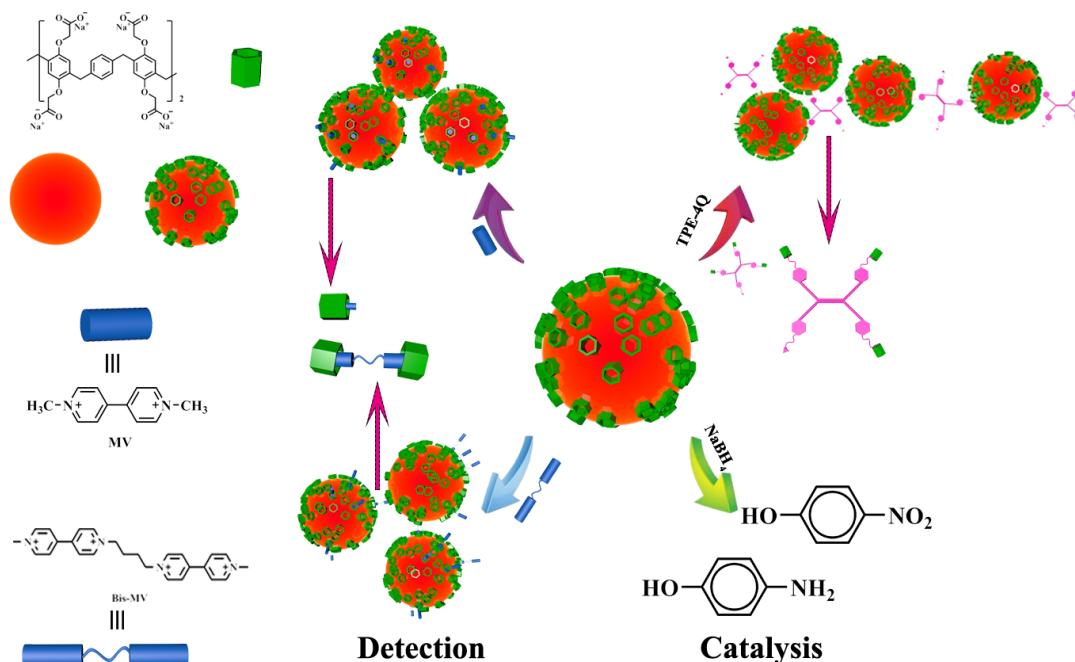
Figure 26. Schematic Illustration of AWLP6-AuNPs and their self-assembly, label-free detection of cationic Methyl Viologen (MV), and efficient catalysis for the hydrogenation of *p*-nitrophenol.

3.1.5 *Use of pillar[7]arene*

Huang *et al*. employed a water soluble pillar[7]arene decorated at both rims with anionic carboxylate groups, and investigated its complexation with paraquat. [48] ^{1}H NMR spectroscopy and 2D NOESY experiments, together with ESI-MS, UV-Vis spectroscopy and fluorescent titrations, were employed to show that the product was a 1:1 [2]pseudorotaxane. The association constant was calculated to be higher than that for either water soluble pillar[5]arene or pillar[6]arene, namely $(2.96 \pm 0.31) \times 10^9$ M^{-1} *versus* $(8.20 \pm 1.70) \times 10^4$ and $(1.02 \pm 0.10) \times 10^8$ M^{-1}, respectively. [49, 50] It was also observed (using ^{1}H NMR spectroscopy) that by adjusting the pH, the degree of threading of the paraquat could be controlled. Studies were then extended to the use of a paraquat derivative with an extra $C_{11}H_{23}$ group at one end to ensure amphiphilic behavior. By utilizing pyrene, it was shown that the water soluble pillar[7]arene and the amphiphilic guest achieved amphiphilic aggregation. The morphology and size of this system was

measured by TEM and DLS experiments. The aggregates were found to have an average diameter of about 164.2 nm (by DLS) and 160 nm (by TEM).

Huang *et al*. reported the formation of a multi-responsive system incorporating two paraquat containing polymers and a water soluble pillar[10]arene, which utilized the willingness of the of the amphiphilic diblock copolymer to form polymeric micelles at ambient temperature in water, figure 27. [61] Such micelles proved to be capable of acting as storage and release vehicles, and this was illustrated using doxorubicin as the cargo. It was also possible to control the rate of cargo release by applying different combinations of external stimuli, for example using both heat and a competitive guest.
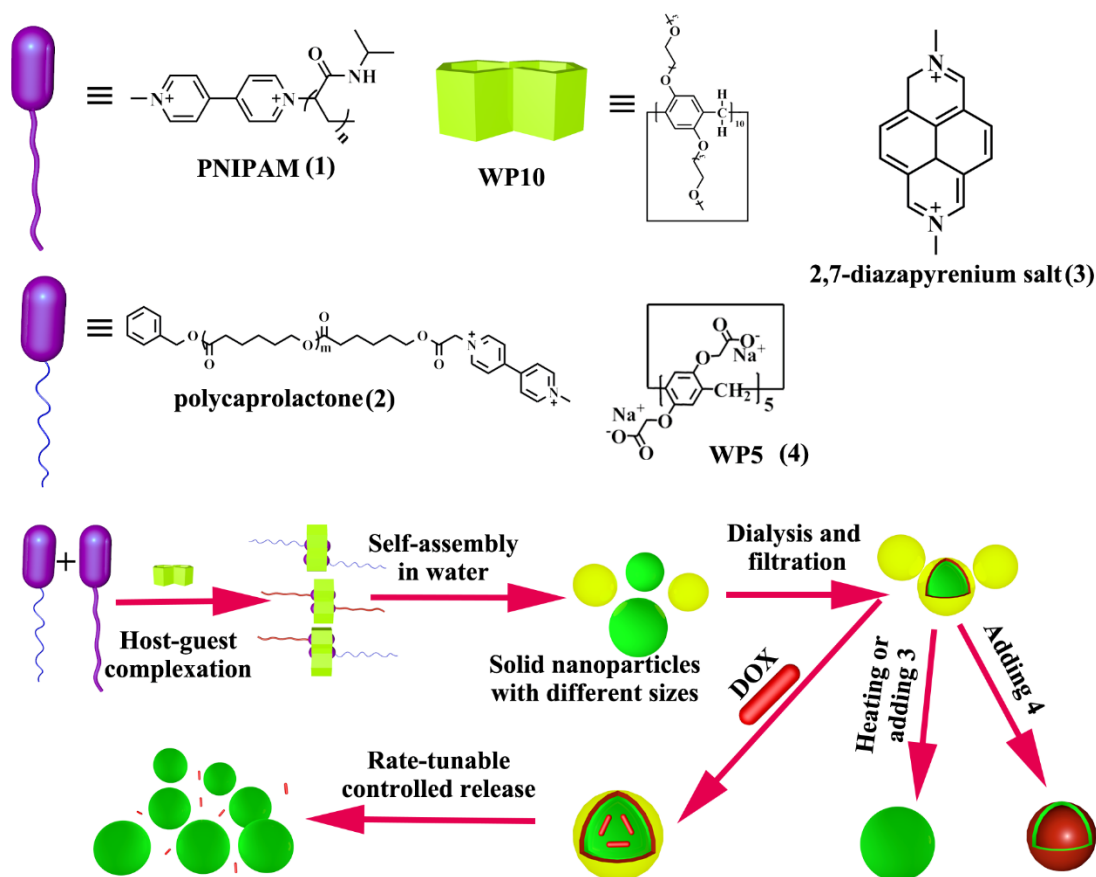
Figure 27. Chemical structures and schematic illustration of preparation of a multi-responsive amphiphilic supramolecular diblock copolymer in water based on pillar[10]arene/paraquat complexation for rate-tunable controlled release.

By utilizing a paraquat derivative with *n*-pentyl groups bound to each pyridinium nitrogen, in combination with a water-soluble pillar[10]arene, a 1:2 [3]pseudorotaxane was formed. [63] Results suggested that there was cooperation between the two pillar[10]arene binding sites upon complexation. In particular, the Scatchard plot (in D_2O at 25 °C) was non-linear and possessed a maximum; the association constants K_1 and K_2 were determined to be $(8.3 \pm 0.1) \times 10^2$ M^{-1} and $(6.2 \pm 0.3) \times 10^3$ M^{-1}, respectively. The studies in this contribution were extended to the synthesis of a gemini-type supra-amphiphiphile by interaction of a homopolymer comprising a paraquat-containing poly(*N*-isopropylacrylamide) and the water-soluble pillar[10]arene. This was reflected in the turbidity experiments, where the plot of light transmittance *versus* temperature changed to a dual-thermo-responsive profile as the concentration of pillar[10]arene was increased. When above the lower critical solution temperature (LCST, 37 °C) of the pillar[10]arene/acrylamide polymer, the system was found to self-assemble into vesicles. Spherical aggregates of diameter ~160 nm were observed by TEM (or 142 nm by DLS), as were the thin walls (18 nm) and cavities. At temperatures below the LCST of the pillar[10]arene/acrylamide polymer, the system adopted random coil conformations, and H-bonding with water led to solubility. A phase change and precipitation were noted as the temperature was increased beyond the cloud point temperature of the pillar[10]arene/acrylamide polymer, which was associated with breakage of the H-bonds and the hydrophobic nature of the components. This thermo-responsive behavior was monitored by the use of DLS over the range 25 to 60 °C. Small molecules could be released from the vesicles on changing (either lowering or increasing) the temperature. For example, in the case of calcein, cooling to 25 °C led to 93%, whilst heating to 60 °C afforded 60% release, over 24h.

4. Supramolecular assembly of pesticides with calix[*n*]arenes and derivatives

Calix[*n*]arenes are comprised of phenolic group linked at the *ortho* position with bridges to form cyclic systems; the bridges are in general of the methylene type. The most common type of calix[*n*]arene has n = 4, and tends to adopt a cone-like conformation; partial cones and 1,2- and 1,3-confirmations also exist. The internal cavity of the cone conformation allows for extensive host-guest chemistry, [4, 5] whilst both the upper and lower rims can be readily modified, and a variety of classes of calixarene are now known, e.g. see examples in figure 28. Calixarenes have

also seen use in many areas, such as catalysis, [71, 72] anti-cancer agents, [73] and even as hair dyes. [74] The recognition of a number of pesticides by calix[*n*]arenes has been reviewed by Español and Maldonado. [75]

<mark>In this section, given the majority of the systems employ calix[4]arene-derived ligand sets, the literature is organized by pesticide type, namely organophosphorus, organochlorine and then other pesticides. Within these sections, further sub-sections relate to the nature of the calixarene system employed, such as whether it is grafted on silica, bound to silver nanoparticles etc.</mark>

p-tertbutylcalix[4]arene   **para-sulfonatocalix[4]arene**

para-sulfonatocalix[6]arene   **para-sulfonatocalix[8]arene**

para-Acyl Calix[4]arenes
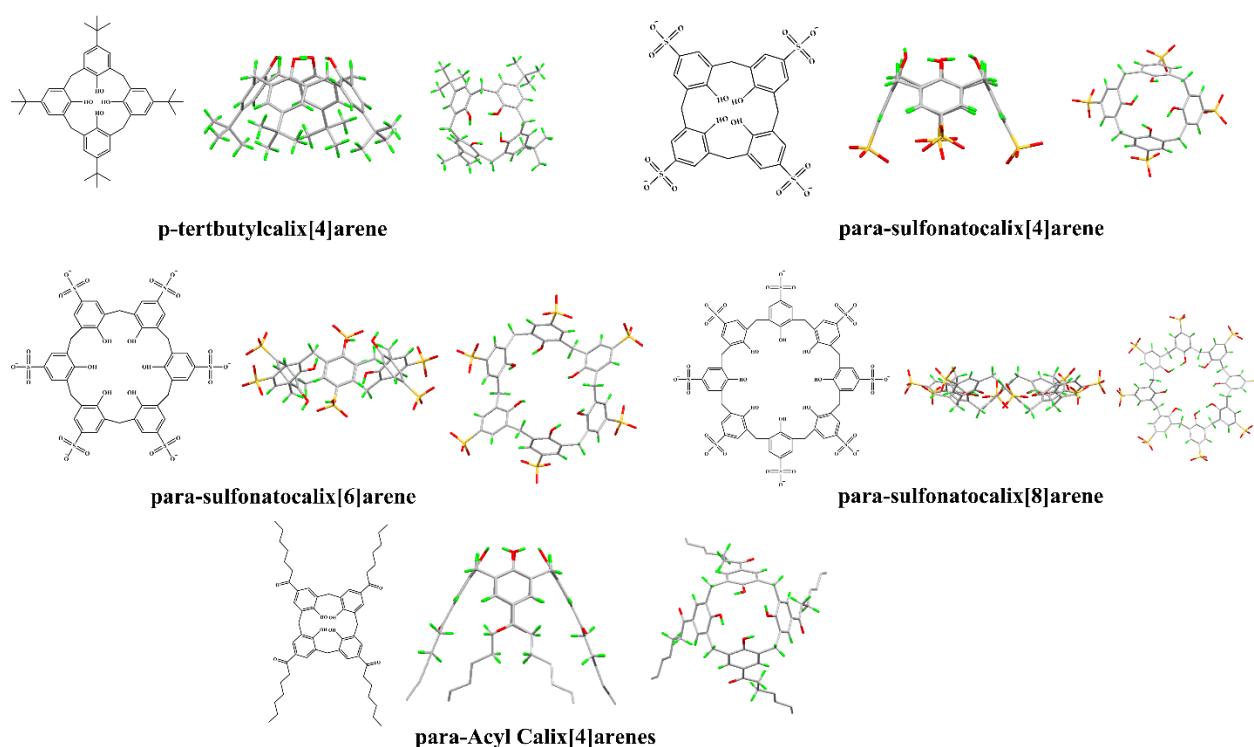
Figure 28. Examples of the types of calixarenes available.

4.1. Detection of organophosphorate compounds with calix[*n*]arenes and derivatives

<mark>4.1.1</mark> *<mark>Silica grafted systems</mark>*

The organophosphorus-based weed killer *N*-(phosphonomethyl)glycine) (glyphosate) has been detected using p-*tert*-butylcalix[4]arene grafted onto the surface of silica nanoparticles. [77] By also appending [Ru(bpy)$_3$]$^{2+}$ groups, a nano-sensor capable of fluorescence resonance energy transfer (FRET) was formed. By addition of glyphosate, FRET with efficiency 87.69% occurred. From the Langmuir isotherm binding plot, a binding constant of 1.16×10^7 M^{-1} was calculated.

The detection limit for glyphosate was found to be 7.91×10^{-7} M, suggesting that such a system could be employed for real world samples. Indeed, the system was shown to function for both ground water and rice grains.

Chlorpyrifos (also known as chlorpyrifos ethyl, *O,O*-diethyl *O*-(3,5,6-trichloropyridin-2-yl) phosphorothioate) is an organophosphorus pesticide used to kill worms and insects associated with both animals and crops, whilst the related pesticide diazinon (*O,O*-diethyl *O*-[4-methyl-6-(propan-2-yl)pyrimidin-2-yl]phosphorothioate) is used to treat cockroaches, fleas etc. Ibrahim and coworkers have utilized an amino functionalized calix[4]arene immobilized on silica functionalized magnetic sporopollenin to remove these two pesticides from water samples. [78] In the pores of the sporopollenin resides the magnetic Fe_3O_4 as evidenced by the SEM images. The removal of the two named pesticides from aqueous solution using this immobilized system was then evaluated at differing pH, concentration, dosage and time. The optimum pH was found to be 7, and over 10 min., 96% and 88% removal was achieved for chlorpyrifos and diazinon, respectively. A chemisorption mechanism was ascribed to the adsorption of both pesticides based on the Langmuir and Dubinin–Radushkevich isotherms, and both followed a pseudo-second-order rate model. The system could also be applied to pesticide contaminated wastewater samples.

4.1.2 Silver nanoparticle bound systems

Acetylcholinesterase (AChE) is a carboxylesterase enzyme, and is a target of organophosphate pesticides. With this in mind, Evtugyn and coworkers [80] have reported an AChE sensor for the detection of both organophosphate and carbamate pesticides. The sensor comprises Ag nanoparticles to which thiacalix[4]arenes are bound, the latter bearing quaternary ammonium groups at the lower rim. At the glassy carbon electrode, a carbon black layer is deposited to which AChE is immobilized. Using this system, it proved possible to detect malaoxon (range 0.4 nM–0.2μM), paraoxon (range 0.2 nM–0.2μM), carbofuran (range 0.2 nM–2.0μM) and aldicarb (range 10 nM–0.20μM), for which the limits of detection were 0.1, 0.05, 0.1 and 10 nM, respectively. The system was applied to spiked food samples, in particular grape fruit juice was spiked with both malaoxon and malathion, whilst peanuts were spiked with carbamate pesticides. Recovery rates were high, for example 95–98% for malaoxon (10 and 100 nM). The weak inhibitory effect exerted on AChE by the quaternary ammonium thiacalixarene was also examined.

Results indicated that use of the thiacalix[4]renes can led to decreased toxicity for anticholinesterase pesticides.

Another widely used organophosphorus insecticide is dimethoate (*O,O*-dimethyl *S*-[2-(methylamino)-2-oxoethyl] phosphorodithioate). Menon *et al*. have reported the use of a system in which sulphonato-calix[4]resorcinarenes (figure 29) are bound to silver nanoparticles. [81] In aqueous media, it proved possible to detect dimethoate with the solution changing color from yellow to red; other pesticides did not afford such a color change. A detection limit as low as 0.8 x 10^{-9} M (80 nM) was possible. When applied to industrial waste samples, 98% dimethoate recovery was observed.
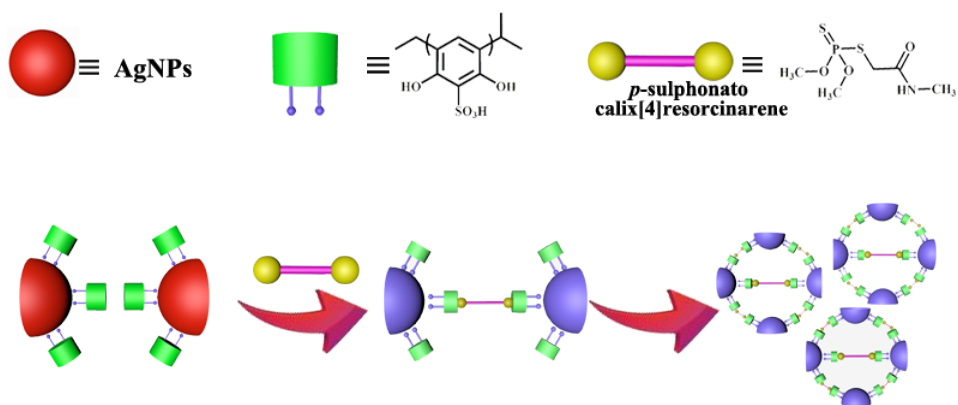
Figure 29. The inclusion complex between dimethoate and sulphonato-calix[4]resorcinarenes bound to silver nanoparticles.

4.1.3 *Systems grafted on titania nanorods*

The organophosphate insecticide profenofos is used to tackle insect problems on cotton, potatoes, soybean and alike and is mostly applied in the USA. Oueslati and coworkers have reported a system that utilizes a calix[4]arene monolayer grafted on 3D nanomaterials based on titania nanorods and nanotubes. [82] The surfaces of these nano systems are responsive to external stimuli such as pressure, heat and light. From Raman spectra, it was evident the neighboring calixarenes were involved in π-π stacking, and are capable of triggering, in the presence of UV light, TiO$_2$ sensitization, and thereby allowing for modulated sensing properties. When applied to the sensing of profenofos, the current density was found to increase 6-fold when the nanorods where submersed in the profenofos solution. This 6-fold increase together with a build-up of solid

are used as signs to detect the profenofos.

4.1.4 *Use of molecular imprinted films/fibers*

Li *et al*. employed the calixarene 5,11,17,23-tetra-*tert*-butyl-25,27-dicyanomethoxyl-26, 28-dihydroxy calix[4]arene to construct, via a sol-gel method, a molecularly imprinted polymer (MIP) fiber. [79] The aim of the study was to employ this MIP fiber for the extraction of organophosphate insecticides, in particular parathion-methyl and related species. It was found that the fiber exhibited good extraction ability and boosted both the excellent thermal and chemical stability as well as solvent resistance. In combination with gas chromatography, and a nitrogen phosphorus detector, the fiber was used to detect the organophosphate insecticides in spiked apple and pineapple samples. The method was compared against other liquid-liquid and solid-phase extraction techniques, and was found to exhibit favorable detection limits and recoveries.

A sensor based on a molecular imprinted film incorporating the calixarene 25-(thioalkyl-alkoxy)-p-*tert*-butylcalix[4]arene has been developed by Cao *et al*. to detect the organophosphorus compounds dimethyl methylphosphonate and diisopropyl methyl-phosphonate. [83] This acoustic wave-based sensor was able to detect low concentration of gases comprising the organophosphorus reagents, and thus has application as a possible early warning system. Competition/interference studies were conducted with 30 other gases, including amines, aromatics, aldehydes etc., and in general there was little interference. Only when certain organic acids and amines were employed at high (100x) comparable concentrations were some issues encountered, and this was thought to be due to such species been adsorbed on the surface of the film.

4.1.5 *Use of 2D nanosheets*

Liu, Ma *et al*. reacted the tetra pyridyl containing calix[4]arene 25,26,27,28-tetra-[(4-pyridylmethyl)oxy]calix[4]arene with 5-nitro-1,3-benzenedicarboxylic acid and $Cd(NO_3)_2 \cdot 4H_2O$ to form 2D layers linked together via weak $\pi - \pi$ interactions to afford a 3D MOF. [76] This 3D MOF, when subjected to liquid ultrasonication (and centrifuging) breaks down into ultrathin colloidal 2D nanosheets, forming either single (2.20 nm) or double-layered (3.73 nm) sheets as evidenced by TEM images. The process was aided by the presence of all the labile methanol solvent molecules that reside in the interspace between the layers in the 3D MOF.

As mentioned in the introductory part to this calixarene section, calix[4]arene can adopt various conformations and tends to adopt a basket-like shape with a cavity. This allows for the encapsulation of guest molecules, and with this in mind, the 2D sheets generated above were used for the sensing of the organophosphorus-based weed killer N-(phosphonomethyl)glycine) (glyphosate), figure 30. Adding glyphosate to the 2D sheets led to increased fluorescence, and a red-shifted absorbance band. A linear range was observed for the concentration of glyphosate (*versus F-F*$_o$, which relates to the change in intensity on addition of glyphosate) over the range 2.5 to 45 µM. The detection limit (2.25 µM) is below that typically seen in drinking water.
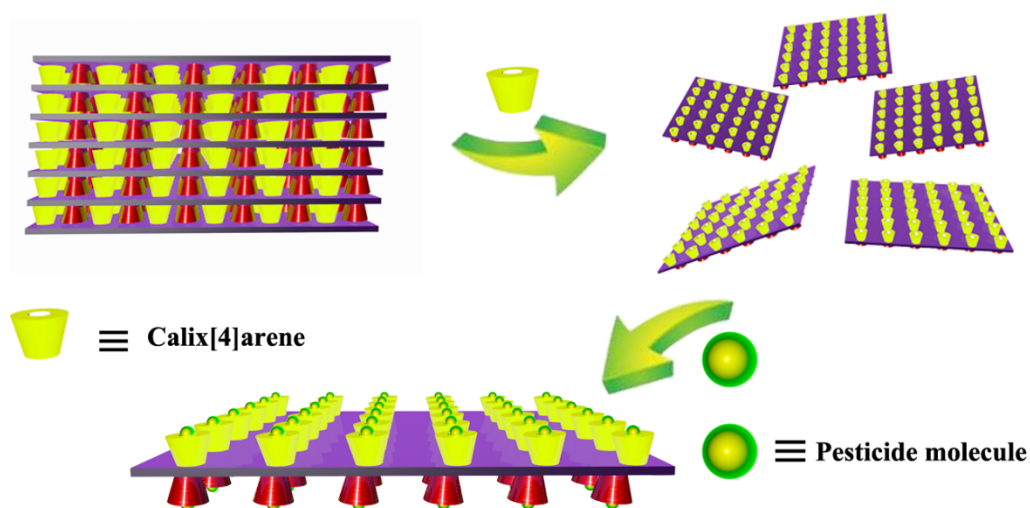
Figure 30. 2D calixarene-containing sheets used for the sensing of the organophosphorus-based weed killer *N*-(phosphonomethyl)glycine) (glyphosate).

4.1.6 *Use of a p-tert-butylcalix[6]-1,4-crown-4 sol-gel film*

In 2005, Hu and coworkers reported the use of a p-*tert*-butylcalix[6]-1,4-crown-4 sol-gel film sensor for the detection of parathion. [84] The sensor was tested by first incubating the sensor in phosphonate buffer (0.1M) over 20 minutes, in the presence of requisite amounts of parathion. The mode of operation was to monitor the electrochemical behavior of parathion, which was achieved via the use of cyclic voltammetry, linear sweep voltammetry, chronoamperometry and alternating current impedance spectroscopy. Results indicated a diffusion-controlled process was in operation, and over the concentration range 5.0×10^{-9} to 1.0×10^{-4}M, a linear response was observed. The detection limit was found to be $1.0 \times$

10^{-9}M (S/N = 3). The system was shown to work when applied to rice samples (sprayed with parathion solution and dried for 2 days), giving results very close to those obtained by HPLC on the same samples.

4.2. Detection of organochlorine compounds with calix[*n*]arenes and derivatives

4.2.1 Calix[4]arene-based systems

4.2.1.1 Fe$_3$O$_4$ nanoparticle containing systems

Hexaconazole (2-(2,4-dichlorophenyl)-1-(1*H*-1,2,4-triazol-1-yl)hexan-2-ol) is employed mainly to treat fungi, and diseases that impact on rice production (e.g. rice sheath blight), primarily in Asia. Another pesticide which sees more widespread use is chlorpyrifos (*O,O*-diethyl *O*-(3,5,6-trichloropyridin-2-yl) phosphorothioate), which is utilized to control pests associated with crops and animals. The removal of both of these pesticides from water samples has been studied by Ibrahim and coworkers. [85] By combining Fe$_3$O$_4$ nanoparticles with graphine oxide and *N*-methyl-*D*-glucamine functionalized calix[4]arene, a new absorbent material was formed, and this was characterized by a range of techniques including SEM and XRD. At pH 6.0, the absorbent was capable of the selective uptake of both hexaconazole and chlorpyrifos achieving adsorption efficiencies in excess of 90%. It was noted that kinetic data could be modelled by a pseudo-second-order model (R2 > 0.99), whilst monolayer adsorption (via physisorption) of pesticide was inferred from the Langmuir isotherm. The system displayed durability in that it could be used at least 20 times (for adsorption/desorption cycles) without any appreciable loss of efficiency. The system could be applied to real world systems including tap water, waste water and river water, with efficiencies of >90%, >81% and >87% (all n=3), respectively.

4.2.1.2 Use of silicone oil coated fibers

Zeng and coworkers have reported a solvent-free method for the extraction of pesticides from water. [88] This involved the use of an extraction/concentration process whereby an analyte from an aqueous solution or just above it is taken in and retained by a silica fiber and then subsequently enters a gas chromatograph where it is detected. The fiber was comprised of a silicone oil, which has been subjected to sol-gel coating using 5,11,17,23-tetra-*tert*-butyl-25,27-

The technique has been applied to radish, and the following analytes were studies: α-,β-,γ- and δ-hexachlorocyclohexane, 1,1,1-trichloro-2-(2-chlorophenyl)-2-(4-chlorophenyl)ethane, 1,1,1-trichloro-2,2-bis(4-chlorophenyl)ethane, 2,4-dichlorobenzophenone, 4,4-dichlorobenzophenone, 1,1-dichloro-2,2-bis(4-chlorophenyl)ethylene, bis(4-chlorophenyl)methane, 1,1-dichloro-2,2-bis(4-chlorophenyl)ethane and endrin. A number of factors were varied during the experiments including temperature, time and the addition of salt in order to optimize sensitivity. When applied to radish samples, which are quite complex, it proved necessary to dilute by a factor of eight to allow for reasonable efficiency *versus* interference from other components. The system exhibited detection limits below 174 ng/kg for the pesticides tested.

A similar type of fiber-based set up was employed by Zeng *et al*. to detect a number of chlorophenols, namely 2-chlorophenol, 2,4-dichlorophenol, 2,4,6-trichlorophenol and pentachlorophenol. [89] In this case, again using a sol-gel approach, silicone oil with end groups derived from 5,11,17,23-tetra-*tert*-butyl-25,27-diethoxy-26,28-dihydroxycalix[4]arene as well as hydroxy groups was prepared and utilized for the analysis. The thermal stability of this coated fiber was as high as 380 °C. Optimization of conditions suggested that the best operating temperature was 40 °C, over 20 minutes at pH 2. The fiber revealed improved carry over (*versus* conventional fibers), particularly for pentachlorophenol, and could be used 180 times without any depreciation of extraction efficiency. Detection limits were found to be between 0.005 to 0.276μg/l for the chlorophenols. Application of the technique to river water and duck lake soil, in conjunction with ultrasonic extraction, led to recoveries >86% for the river water and ≥81% for the soil samples.

Two or four dihydroxyphosphoryl groups have been appended either directly to the upper rim of a calix[4]arene or via an aminomethyl group (figure 31). The interaction of these calixarenes with the herbicides atrazine or 2,4-dichlorophenoxyacetic acid has been studied in water using reverse phase HPLC. [90] Results indicated that the herbicides were captured by the hydrophobic cavity thereby forming 1:1 host-guest complexes with association constants of 2513–6785 M^{-1} and 772–5077 M^{-1} for atrazine and 2,4-dichlorophenoxyacetic acid, respectively. A number of factors were thought to impact on these association constants such as the rigidity of the calixarene conformation. The additional presence of H-bonding can be beneficial, for example in the

aminomethyl-containing derivative, the presence of two strong ArO—H···OPr intramolecular H-bonds stabilizes a flattened-cone conformation, and the latter allows for π-π interactions with the 2,4-dichlorophenoxyacetic acid guest.
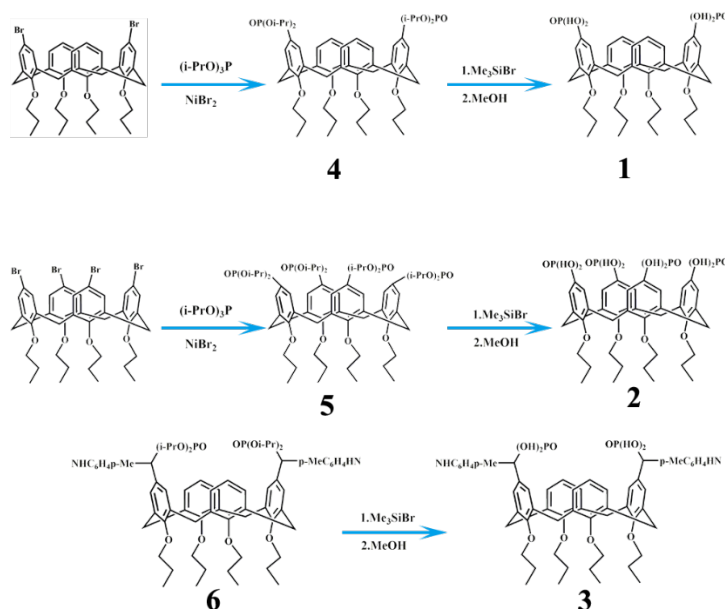
Figure 31. Capacity factors of the guests (k') depended on the calixarene concentration in the mobile phase.

Studies involving larger calix[n]arenes

The gamma isomer of hexachlorocyclohexane (HCH) is an insecticide widely used for the treatment of crops and fruit and is also used in shampoo to counter lice. Some of the other isomers of HCH are problematic to the environment and human health and so there is a drive to develop systems capable of their removal. With this in mind, Memon and coworkers immobilized p-*tert*-butylcalix[8]arene on the surface of silica, as confirmed by FTIR and SEM. [86] To evaluate the effect of pH on the adsorption, they varied the pH between 2 and 10 for the various isomers of HCH. Best results were achieved at pH 8 with an agitation time of 60 minutes. Both the dosage of adsorbent and HCH concentration were also found to impact on the adsorption efficiency. In terms of adsorbent dosage, 5 to 35 mgL^{-1} was tested and 20 mg of modified silica was found to be preferred, whilst for the HCH concentration, the optimum value was 1m g L^{-1}. Analysis of the data indicated that the system was a good fit for the Freundlich adsorption model. Moreover, it followed pseudo-second-order kinetics, and with coefficients for the α, β, γ, δ isomers of 0.054, 0.054, 0.049,

$0.055\ k_{TH}\ cm^3\ mg^{-1}\ min^{-1}$, respectively. Results also suggested that the preferred method for isomer removal was based on column packing rather than a batch method. The modified silica surface could be used for 5 cycles without significant reduction in efficiency. The isomers could be removed from spiked water samples with recoveries between 78 and 87%.

Palleschi *et al*. have investigated the interaction between a number of water soluble 4-sulfocalix[*n*]arenes (with n = 4, 6, 8) and heptachlor (1,4,5,6,7,8,8-heptachloro-3a,4,7,7a-tetrahydro-1*H*-4,7-methanoindene), which is used for fire-ant control, and endosulfan (6,7,8,9,10,10-hexachloro-1,5,5a,6,9,9a-hexahydro-6,9-methano-2,4,3-benzodioxathiepine-3-oxide), which has been used in the past against a range of insects though it is now banned. [87] The main technique employed to investigate the interactions was monitoring the changes in the emission spectra of the calixarene on addition of the pesticide. In the case of heptachlor, studies conducted in ethanol indicated that for n = 4, there was no complexation. By contrast, for the larger calix[6 and 8]arenes, similar decreased emission was observed on addition of heptachlor and thus the associated dissociation constants and stability of the two systems were close. In water, the preferred technique is differential pulse voltammetry, and again this revealed that calix[6 and 8]arene can bind heptachlor, whereas calix[4]arene is too small to act as a host. Stability constants were higher in water (increased hydrophobic interactions) than in ethanol. If endosulfan is the guest, then the behavior of the n = 6 and 8 systems are quite different. For n = 6, the lack of a decreased signal suggested no interaction, whereas for n = 8, a binding constant of $4.7\pm \times 10^5$ was calculated from the observed data. In the case of n = 6 with heptachlor in water, calculations suggested the presence of different interconverting guest configurations and that stability is closely associated with non-specific hydrophobic interactions.

4.3 Detection of others pesticides with calix[*n*]arenes and derivatives

4.3.1 *Calix[4]arene-based systems*

4.3.1.1 *Systems employing a gold surface*

Tian, Li *et al*. have reported a calix[4]arene system that is capable of the selective recognition of the pesticide metolcarb (3-methylphenyl methylcarbamate), which is used to kill ticks and mites. [92] More specifically, the calixarene used has been functionalized in the 1,3-positions at the lower

rim with naphthol groups, and then via Click chemistry, fixed to a gold surface. The unsupported calixarene system was first investigated with a number of pesticides including metolcarb, pirimicarb, carbosulfan, carbofuran, carbaryl, and isoprocarb, and from fluorescence spectroscopic measurements, it was evident that there was enhanced selectivity toward metolcarb (the association constant was calculated to be 1.2 x 10^5 M^{-1}). ^{1}H NMR spectroscopic results were consistent with the guest entering the upper rim of the calixarene.

Following attachment of the calixarene to the gold surface, host-guest interactions were monitored via contact angles. Only in the case of metolcarb did the surface appear hydrophilic, with contact angle measurements implying a hydrophobic surface was formed in the presence of other pesticides employed. The detection limit using this method for metolcarb was found to be 1 x 10^{-7} M.

Click chemistry has been employed to attached a calixarene bearing acetylene groups to a gold surface. [95] The resulting monolayers exhibit hydrophobic properties, but this can be changed by the addition of a guest. In this work, paraquat was utilized as the guest along with three other related analogs, and by measuring the impedance, recognition of paraquat proved most favorable (*vs* the other guests) with a sensitivity limit of 10 pM. The *modus operandi* was thought to be the attraction of the highly polar, positively charged paraquat for the low polarity hydrophobic cavity, and upon entry (inclusion complex formation), there was a switch from a hydrophobic to hydrophilic surface (figure 32).
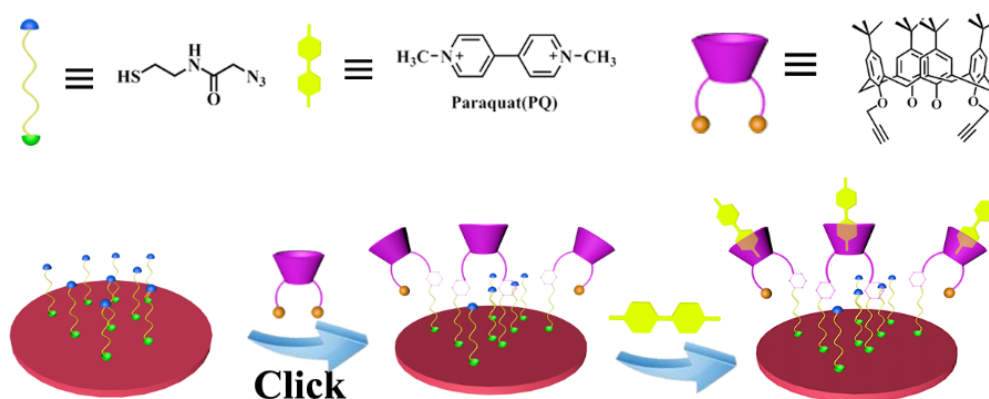
Figure 32. Possible mechanism of C4AE interaction with paraquat on a gold surface causing wettability switch between super-hydrophobicity and excellent hydrophilicity.

Self-assembled monolayers on gold have also been formed by using the calix[4]arene lipoic acid (C4LA) shown below (figure 33), the latter was formed from a Click reaction involving an azide-functionalized calix[4]arene and a thioctic-propyne. [96] The make-up of this modified gold electrode was confirmed by XPS, contact angles measurements and impedance spectroscopy. The pesticides studied in this work were of the carbamate type and included methomyl, san leafhopper, carbosulfan, carbofuran and carbaryl. As was for the case above, changes in wettability on addition of guest were central to the mode of operation. Of the 5 pesticides, only the presence of methomyl had an impact, greatly decreasing the contact angle. At the same time, measurement of the electrochemical impedance also only revealed a change when methomyl was employed as the guest. The selectivity toward methomyl was ascribed to the ability to form a 1:1 complex with the calixarene, whereas UV studies indicated that there were no changes on addition of any of the other 4 guests to the calixarene.
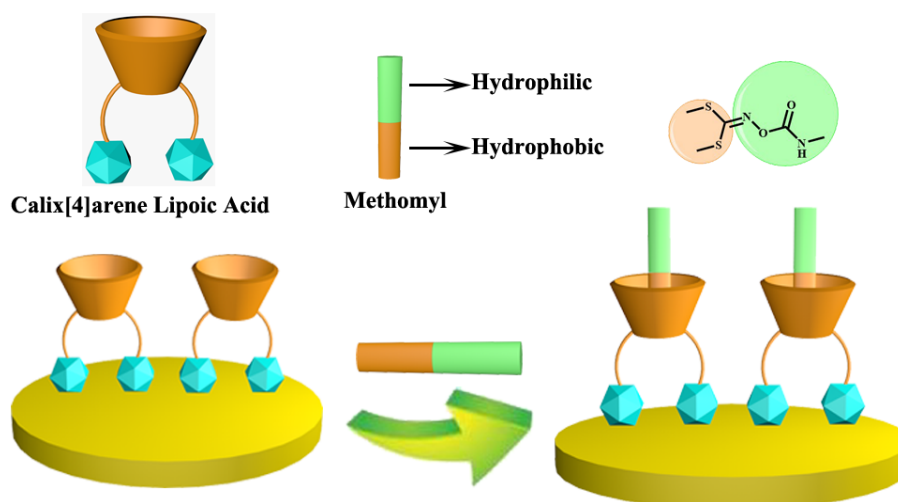
Figure 33. Schematic representation of the possible recognition process for C4LA toward methomyl on the surface of a self-assembled calix[4]arene monolayer via host-guest interaction.

4.3.1.2 *Systems employing a silica surface*

Memon *et al*. have utilized a silica surface modified with *p*-tetranitro-calix[4]arene for the adsorption of carbofuran (2,2-dimethyl-2,3-dihydro-1-benzofuran-7-yl methylcarbamate) from aqueous solutions. [93] The immobilization of the calixarene was confirmed by both FTIR spectroscopy and SEM (images revealed rough white covered areas). Varying the pH over the range 2 to 10 revealed that the amount of carbofuran adsorption decreased as the solution became

more basic, and with this in mind, a pH of 5 was chosen for subsequent experiments. Experiments varying the adsorbent dosage over the range 0.005–0.05 g/10 mL revealed that no increase in adsorption was observed for dosages above 0.03 g/10 mL. Comparative studies *versus* unmodified silica revealed that the percentage of carbofuran more than doubles following modification (98 *vs* 48%). The Morris-Weber model amongst others was applied to the kinetics and data were analyzed with Boyd's model to ascertain the rate determining step. Langmuir, Freundlich and Dubinin–Radushkevich isotherm models were also employed when evaluating the equilibrium. It was concluded that the adsorption follows pseudo second order kinetics with a rate limiting step involving an external mass transfer diffusion process. Data also indicated that the process is exothermic (and spontaneous), with the adsorption of guest decreasing as the temperature increases. The modified silica surface could be readily regenerated by simply shaking with ethyl acetate for 10 minutes and then was good for at least 5 more cycles.

4.3.1.3 *Systems employing quantum dots*

By use of a sol-gel technique, Li and Qu prepared luminescent CdTe quantum dots within composite silica spheres, and the latter were coated with 5,11,17,23-tetra-*tert*-butyl-25,27-diethoxy-26,28-dihydroxycalix[4]arene. [102] IR spectra and TEM images confirmed the presence of the calixarene coating. The fluorescence intensity was increase by 87% by the presence of the calix[4]arene (up to 15 μL), and this was thought to be due to the prevention of any photobleaching; excess calix[4]arene led to precipitation and a rapid decrease in fluorescence intensity. Over time (up to 6 days), the intensity gradually increased and thereafter decreased, and there was no observable shift in the wavelength. The quantum yield in water was 15% (*versus* 12% in the absence of calix[4]arene). Highly acidic or basic media were unfavourable, and a pH of about 8 was deemed best for subsequent experiments. The nano-composite was applied to the determination of various pesticides including methomyl, parathion-methyl, fenamithion, optunal, and acetamiprid. Under the conditions employed (10^{-5} M), only methomyl afforded a significant FL intensity enhancement, which increased linearly over the range 0.1-50μM. The detection limit was determined to be 0.08μM.

4.3.1.4 *Systems employing ionic liquids*

Jia and coworkers have employed a calixarene coated fiber, <mark>prepared via the use of p-*tert*-butylcalix[4]arene in an ionic liquid,</mark> for the detection of the triazines atrazine, simazine, ametryn, and cyanazine, which are used to treat fruit and vegetables. [94] The technique combined the fiber with a chromatography–flame ionisation detector, and under the optimized conditions, detection limits ranged from 3.3 μg kg^{-1} (for atrazine) to 13.0 μg kg^{-1} (for cyanazine). Application of the technique to real samples such as tomato, cucumber and cabbage revealed triazine recoveries in the range 71.5–96.9%.

4.3.1.5 *Other calix[4]arene systems*

Bayrakci and coworkers have investigated the use of fluorescence probes based on calixarene naphthalimides of the type shown in figure 34. [91] The focus of the study was the detection of the pesticides metalaxyl, dimethomorph, flusilazole, cyprodinil, pyrimethanil, triflumizole and in particular kesoxim-methyl, which is the methyl ester of (2E)-(methoxyimino){2-[(2-methylphenoxy)methyl]phenyl}acetic acid. These calixarenes proved to be excellent hosts for kesoxim-methyl, and the process was monitored by use of fluorescence spectroscopy. In the case of the upper rim-modified calixarene naphthalimide, a decrease (94.6%) in the fluorescence of the emission at 442 nm upon addition (20 equiv.) of kesoxim-methyl was observed. Addition of the other pesticides led to less pronounced quenching and so this system was a useful probe for kesoxim-methyl detection. A Job's plot indicated the system was a 1:1 host-guest inclusion complex. At ambient temperature (25 °C), the binding constant was found to be 0.59 x 10^3, decreasing to 0.12 x 10^3 M^{-1} at 45 °C; the trend was aligned with the stability of the complex. The authors also studied the urea-initiated release of kesoxim-methyl, monitoring the process via the use of fluorescence spectroscopy. Controlled release was indeed evident and the color changes (pale to dark turquoise) could be monitored by the naked eye.
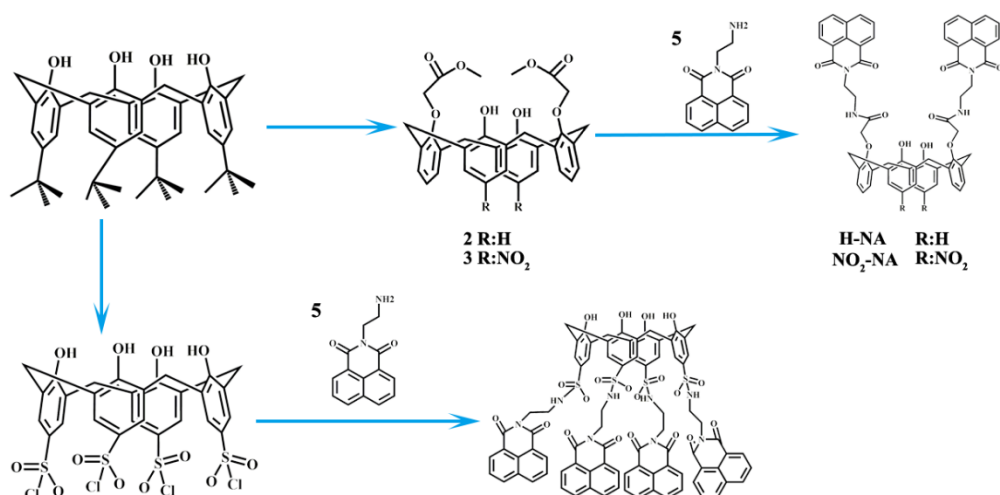
Figure 34. Synthetic route to calixarene-based probes, lower rim-modified NO-NA H-NA and upper rim-modified SO-NA from corresponding starting materials.

The detoxification of paraquat using a *p*-sulfonatocalix[4]arene has been studied by Qi *et al*. [97] The work focused on the physiological disposition of paraquat in rats using HPLC-based *in vivo* pharmacokinetics. Results obtained by analysis of plasma concentration curves indicated that the presence of the calixarene is indeed beneficial in terms of reducing poisoning. Furthermore, *in vitro* studies indicated that 'free' paraquat concentration was reduced in the gastrointestinal tract when the calixarene was present. This suggests that even for oral administration, the formation of a stable inclusion complex between the calixarene and paraquat can lessen the toxicity associated with paraquat.

4.3.2 *Systems including larger calix[n]arene systems*

Ramírez *et al*. have studied the interaction, both in solution and the solid-state, of the larger calix[6 and 8]arenes with paraquat (as the dichloride salt). [98] Data from elemental analysis and neutron activation analysis indicated the formation of 1:1 complexes in the solid-state. In solution, the situation was more complex as the size and shape of the calixarene together with the solvent polarity could impact on product stability. Cation-π interactions were implied from the changes (increases) in luminescence intensity and molar absorption coefficient. From calculations, it was postulated that the pinched conformation adopted by the calix[8]arene in polar solvents was able to trap paraquat in its cavity, whereas the 'in-out' cone conformation of the calix[6]arene can only

partially trap paraquat. Stability studies conducted in tap water with a pH of 7.72 and in distilled water with pH 5.44, indicated that the stability of the calix[6]arene system was pH dependent with dissociation evident at pH<6. The calix[8]arene system was more stable, and would be the receptor of choice here for paraquat stabilization.

Liu and coworkers have studied the interaction between the calixarenes p-sulfonatocalix[4 and 5]arenes and p-sulfonatothiacalix[4]arene with paraquat and diquat. [99] The aim of the study was to reduce the toxicity associated with these pesticides via the formation of host-guest complexes. The binding between the calixarenes and the guest was evaluated at different pH (1.5 and 7.2). Under both neutral and acidic environments, stable host-guest complexes are formed. In the case of diquat, the interaction with the calixarenes was monitored by ^{1}H NMR spectroscopy at pH 2.0 and 7.2. The upfield shifts associated with the guest are consistent with encapsulation within the cavity of the host. From the shift changes, differing degrees of tilt were invoked for the guest within the cavity, with a high tilt seen when p-sulfonatocalix[4]arene is host and a flatter orientation with p-sulfonatocalix[5]arene as host; an intermediate situation was proposed in the presence of p-sulfonatothiacalix[4]arene. Single crystal X-ray diffraction studies also revealed tilted encapsulation, whilst ITC data confirmed the formation of 1:1 species.

It was also noted from electrochemical studies that upon encapsulation, the first reduction potentials of these guests are shifted in the negative direction. In terms of toxicity, this impacted on the production (decreased) of toxic HO▪ given that less guest radical cation would be produced. Other factors that were proposed included hydrogen transfer from the phenolic groups which would again deactivate HO▪, and also the presence of coordinating metal impurities. Mice tests were conducted and the results demonstrated how the presence of the p-sulfonatocalix[n]arenes benefited the health of the mice in terms of lung and liver protection. The poisoning was even somewhat suppressed even if the poison was administered after two hours.

Xiong and Li have screened the ability of silver nanoparticles functionalized with p-sulfonatocalix[4 and 8]arene to act as a sensor for pesticides, figure 35. [101] The range of pesticides investigated included iprodione, acetamiprid, thiabendazole, optunal, pyrimethanil, parathion-methyl and methomyl. Only the combination of p-sulfonatocalix[4]arene and optunal afforded a color change (from yellow to red) along with a large change in the ratio of absorbance for the peaks at 490 and 393 nm. This was thought to be due to the attraction of the calixarene

cavity toward the amino and aromatic moieties of optunal. Optunal concentrations as low as 10^{-7} M can be detected, and results for this method were found to closely match those from HPLC experiments. By contrast, the larger *p*-sulfonatocalix[8]arene because of its increased flexibility, has no such cavity and shows no preference for any of the tested pesticides.
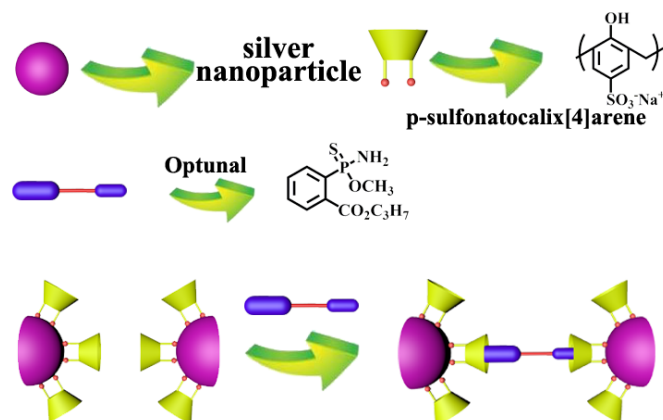
Figure 35. Silver nanoparticles functionalized with *p*-sulfonatocalix[4]arene and inclusion of optunal.

4.3.3 *Resorcinarene systems*

Nikolelis *et al*. have reported a receptor based on a phosphoryl resorcin[4]arene derivative incorporated into a lipid film supported on a methacrylate polymer on a glass fiber. [100] The method employs electrochemical flow injection analysis and was used to detect carbofuran in a large range of foodstuffs including ice creams, canned mushrooms and beans. Central to the detection was the formation of a host-guest complex between the phosphorylated resorcin[4]arene and carbofuran, the strength of which was enhanced by H-bonding. The formation of this inclusion complex leads to a build-up of guest near the lipid membrane surface, and results in electrostatic field variation which can ultimately be correlated with substrate concentration. The detection method proved to be rapid, taking about 1 minute, and could detect down to the nanomolar level, whilst the lipid films can be reused even after prolonged storage (1 month) in air. The possible interference effect of chemicals that are commonly found in foods was screened electrochemically, including caffeine, tartrate and glucose. Results suggested the interference levels were acceptable (errors <5%) and were certainly acceptable at the levels that these chemicals are found in foodstuffs.

5. Supramolecular assemblies involving pesticides with cyclodextrins

Cyclodextrins, which are a family of cyclic oligosaccharides (figure 36), have been known for some time, and have found use in a wide variety of applications. [103] Their use with pesticides has been flagged in a review by Wang *et al.* which discusses inclusion chemistry and applications pre-2013, [104] and in a review by Lay *et al.* which considers the state of the art for applications of cyclodextrins pre-2016. [105] In this section, given the majority of studies involve the use of β-CD, we have structured it in terms of the type of pesticides used, namely organophosphates, organochlorines, neonicotinoids, organic esters and other pesticides, and akin to the calixarene section 4, further sub-sections include the use of supports, nanoparticles, molecular imprinting etc.

α-Cyclodextrin   **β-Cyclodextrin**   **γ-Cyclodextrin**
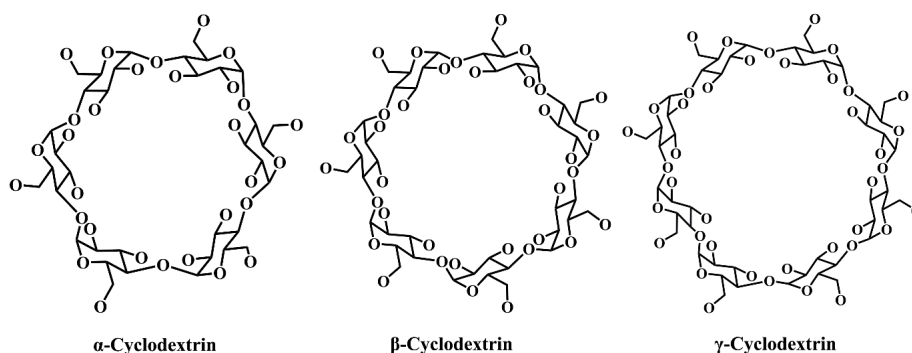
Figure 36. α-, β- and γ-cyclodextrins.

5.1. Detection of organophosphate compounds with cyclodextrins and derivatives thereof.

5.1.1 *Use of nanoparticles*

She, Wang and coworkers reported a pesticide detection method based on the use of β-cyclodextrin-coated silver nanoparticles and 2,3-dihydro-5-oxo-5H-thiazolo[3,2-*a*]pyridine-7-carboxylic acid. [107] The system utilizes FRET, and energy is transferred between the two previously mentioned components when they are combined and this leads to a quenching effect. However, upon addition of the pesticide malathion, the fluorescence is reinstated, and this allows for the detection of the pesticide (limit $0.01\,\mu g/mL$) figure 37; the linear range is 0.1–$25\,\mu g/mL$. When applied to real water samples that were spiked with differing concentrations of malathion,

the %recovery was either 83% (when spiked with 0.4 µg/mL) or about 101% (when spiked with 0.3 or 0.6 µg/mL).
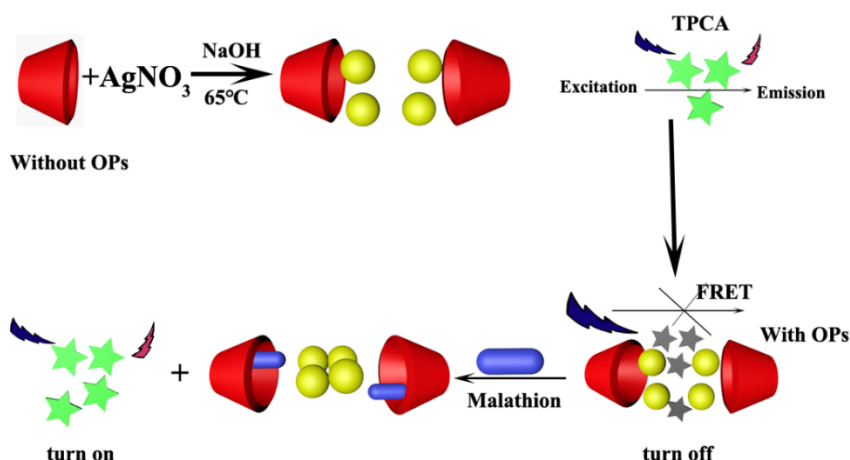
Figure 37. Mechanism of the β-cyclodextrin-coated sensor.

Yang *et al*. have employed the electrodeposition of Pt-Au nanoparticles on a multi-walled carbon nanotube modified glass carbon electrode to construct a new biosensor. [110] The sensor was applied for the detection of a number of pesticides (e.g. malathion, chlorpyrifos, dufulin and methyl parathion) in food (cabbage) and drink (water and milk). To complete the biosensor, bio-composites of acetylcholinesterase and choline oxidase were co-immobilized at the electrode surface in the presence of *L*-cysteine. The generated hydrogen peroxide greatly increased the electrochemical luminescent signal associated with the luminol, the latter was selected given its cost, low oxidation potential and high emission yield. It was expected that the addition of pesticide would result in reduced levels of H_2O_2 and so diminish the luminescent signal. Results indicated that there was indeed a signal decrease and that this decrease was more pronounced on increasing the pesticide concentration. This led to detection rates of 0.16 nmol L^{-1}(malathion), 0.09 nmol L^{-1} (methyl parathion), 0.08 nmol L^{-1} (chlorpyrifos) and 29.7 nmol L^{-1} (dufulin), for the latter, the linear range was 50 to 500 nmol L^{-1}. When applied to cabbage samples, pesticide recoveries were as high as 108.43%.

Ji, Ren and coworkers have reported an acetylcholinesterase biosensor for the detection of the pesticides malathion and carbaryl. [111] The acetylcholinesterase was immobilized on a nanocomposite film comprised of electrochemically reduced graphite oxide, gold nanoparticles,

β-cyclodextrin and Prussian blue/chitosan on a glass carbon electrode. The graphite oxide/gold nanoparticle combination was able to enhance electron transfer between Prussian blue and the electrode surface, enhancing the thiocholine electrochemical oxidation. Moreover, the presence of the Prussian blue/chitosan shifted the oxidation potential of thiocholine to 0.2 V (from 0.68 V), thereby significantly improving the sensitivity of the system. The selectivity of the sensor was enhanced by the presence of the β-cyclodextrin.

For pesticide detection, concentration studies were conducted using malathion, and it was found that, at pH 6.5, the oxidation peak current decreased as the malathion concentration increased until the saturation point was reached. By measuring the shift in the oxidation peak current, the concentration of pesticide could be determined. Low detection limits of 4.14 pg mL^{-1} for malathion and 1.15 pg mL^{-1} for carbaryl were established, with wide linear ranges (e.g. 4.3 to 1.00×10^3 pg mL^{-1} for carbaryl). When applied to the detection of pesticides in vegetables, recoveries as high as 106.7% (malathion) and 101.5% (carbaryl) were achieved.

5.1.2 *Use of a silica surface*

Mauri-Aucejo *et al*., have screened a number of mesoporous silica materials as sorbents during the detection (extraction) of organophosphorus pesticides in water. [109] The sorbents were comprised of the M-UVM-7 structure to which Ti or Fe dopants had been added; cyclodextrin silica-based supports were also screened. Pores sizes and volumes as well as BET surface area were measured. Detection was via a gc coupled to a nitrogen-phosphorus selective detector. The pesticides employed were ethoprophos, diazinon, methyl chlorpyrifos, methyl tolclofos, fenitrothion, malathion, chlorpyrifos and parathion. From the results, the sorbent that exhibited the highest extraction was the Ti-doped material Ti25-UVM-7. Various parameters such as pH and volume (eluent and breakthrough) were tuned in order to verify the optimum conditions. This led to recoveries as high as 104.5%, with relative standard deviation of less than 7.8% over one day (*i.e.* 3 replicants in one day) and 12% for different days (*i.e.* 3 series of 3 different experiments on 3 different days). The limits of detection using GC-MS were found to be 0.2-1.4 µg L^{-1}. The system was also applied to some spiked water samples, and results were found to be similar to those obtained with commercial C18 cartridges. It was noted that the reusability of the reported system exceeded that of commercial C18 cartridges.

5.1.3 *Use of molecular imprinting*

Wei and coworkers have employed a solid-phase microextraction probe, which was produced via sol–gel molecular imprinting (template quinalphos), for the determination of pesticides in food (e.g. tomato and cabbage) and water. [106] Five pesticides were screened, namely quinalphos, triazophos, parathion, fenthion and chlorpyrifos-methyl. The extraction ability of the probe was found to depend on factors such as pH, and the extraction performance was found to increase on changing the pH from 5.6 to 6.2, but thereafter decreased on further increasing the pH. Such a trend was explained in terms of the ability to form H-bonds with the pesticide. Temperature was also found to be an influencing factor, and 35 °C was deemed optimal. Other factors that were found to be influential included stirring rate and extraction time. The simultaneous detection of the five pesticides proved possible with a linear range of 0.02 to 2.0 μg mL^{-1}, and detection limit between 3.0 – 10.0 μg mL^{-1}. When used with the likes of tomato, cabbage and water, recovery rates in the range 82-98% were recorded.

By use of molecular imprinting, Pan *et al*. have prepared mono[6-deoxy-6-[(mercaptodecamethylene)thio]]-β-CD and employed it in a surface acoustic wave sensor to detect the nerve agent sarin (propan-2-yl methylphosphonofluoridate). [112] The β-CD containing film was characterized by AFM and electrochemical impedance spectroscopy, which indicated the formation of rough regions at the gold coated areas. Detection experiments were conducted with films of different composition to verify the beneficial effect of the mono[6-deoxy-6-[(mercaptodecamethylene)thio]]-β-CD film. In the absence of the film, no frequency changes were observed. The film in the absence of templates (*i.e.* not molecularly imprinted) was tested, and there was only minimal interaction with sarin. However, use of the mono[6-deoxy-6-[(mercaptodecamethylene)thio]]-β-CD film led to a very different response which was quick and of high frequency. For sarin detection at ambient temperature, the frequency shift was 300 Hz, and the low detection limit was 0.10 mg/m^3 (linear range 0.7 mg/m^3~3.0 mg/m^3). On increasing the temperature to 50 °C, the frequency shift diminishes as do both the response and recovery time. In terms of storage, the system could be used at ambient temperature over a 60-day period without appreciable loss of response frequency.

Lee and Lee *et al*., have utilized a biocatalytic compound that is capable of the rapid decomposition of methyl paraoxon. [108] By embedding the compound (organophosphorus hydrolase) in a matrix of poly-β-cyclodextrin, it proved possible to capture methyl paraoxon via a host-guest interaction in preference to its less hydrophobic decomposition product *para*-nitrophenol. An adsorption ratio of 1.7:1 for methyl paraoxon *versus para*-nitrophenol was recorded. By operating in this way, the system can neutralize the toxic effects associated with the organophosphate pesticide. The preferred operating pH was 8.6, as at higher pH, the *para*-nitrophenol isomerized to the phenolate for which the adsorption decreased. It was noted that for the immobilized organophosphorus hydrolase, the reaction rate was less (by 23%) than that of the free enzyme. The immobilized system exhibited good shelf-life in that it could be used for extended periods (*e.g.* 4 days) prior to degradation (*i.e.* hydrolysis of methyl paraoxon).

5.1.5 *Other β-cyclodextrin systems*

The three pesticides fenitrothion [*O,O*-dimethyl *O*-(3-methyl-4-nitrophenyl) phosphorothioate], fenthion [*O,O*-dimethyl *O*-[3-methyl-4-(methylthio)phenyl] phosphorothioate] and acetochlor [2-chloro-*N*-(ethoxymethyl)-*N*-(2-ethyl-6-methylphenyl)acetamide] have been treated with permethylated β-cyclodextrin and the molecular structures of the resulting isostructural (space group $P2_12_12_1$) inclusion complexes have been determined by X-ray crystallography. [113] In the two organophosphate structures, the guest has the dimethyl phosphorothioate units close to the rims of the host, and these rims are blocked by a number of methoxy groups. In the case of the chloroacetanilide system, the guest is orientated somewhat differently. In particular, the aryl group is completely encapsulated, and the ethyl and chloro-ethoxymethyl acetamide groups protrude out of the secondary rim of the host cavity. Methoxy groups block off the primary rim and orientate in such a way that the host resembles a cup shape. The thermal profiles for these complexes displayed two distinct mass losses, attributed to guest release and decomposition. The dissociation of the guests was investigated by isothermal and non-isothermal thermogravimetry, and two mechanisms were invoked, a first-order reaction model and a three-dimensional diffusion model. The activation energies calculated (using non-isothermal thermogravimetric methods) for the loss of guest for these species were, on average, of the order

of 149 to 158 KJmol^{-1}.

5.2. Detection of organochlorine compounds with cyclodextrin derivatives

Use of magnetic nanoparticles

Ding, Ren and coworkers have designed a method for the detection of organochlorine pesticides in soil, which uses magnetic solid phase extraction in combination with GC-QTOF-MS. [114] Central to the method was the synthesis of a lipid bilayer nanocomposite containing Fe$_3$O$_4$@β-cyclodextrin. The nine pesticides employed were α-chlordane, chlordecone, hexachlorobenzene, lindane, α-hexachlorcyclohexane, *o,p'*-dichlorodiphenyltrichloroethane, mirex, *p,p'*-DDT and pentachlorobenzene. Following magnetic solid phase extraction, the combination of inclusion complex formation and the hydrophobicity allowed for selective pesticide adsorption, with detection limits as low as 4.5 to 34 pg g^{-1}. Recoveries from soil (seven soils of differing pH and %C content were used) varied from 78% to 107% with good precision (≤6.9%).

4-Chlorophenoxyacetic acid and 2,3,4,6-tetrachlorophenol exhibit only moderate levels of toxicity and so have seen increased use, and this in turn has led to their unwanted presence in the environment. A method for their detection has been devised by Jara *et al*. [118], which involves the use of β-cyclodextrin (the polymers of which were described in the paper as a nano-sponge) decorated with magnetic nanoparticles (Fe$_3$O$_4$). The performance of this β-cyclodextrin-based system was compared against granulated activated carbon. The inclusion complexes formed on addition of either pesticide to the 'nano-sponge' were characterized by a multitude of techniques including ^{1}H NMR (high field chemical shifts) and UV-vis spectroscopies, TGA (improved thermal stability), SEM, EDS and PXRD. The UV-vis studies revealed the ability of the 'nano-sponge' to remove these chlorinated pesticides from aqueous solution. Steric effects were most favorable for the formation of 4-chlorophenoxyacetic acid inclusion complexes on the 'nano-sponge'. The system proved to be reusable, and interestingly by incorporation of Fe$_3$O$_4$ (magnetite), the 'nano-sponges' could even be recovered using a magnet (neodymium-based) from aqueous solution, and this without any loss of absorption efficiency.

Mahpishanian and Sereshti reported a system for the extraction of organochlorine

pesticides (16 were screened) from honey. [121] The system involved a composite involving β-cyclodextrin/iron oxide <mark>(magnetic Fe_3O_4)</mark> reduced graphene oxide, which could be prepared in one-step from non-toxic materials. The synthesis of the composite was validated by a variety of techniques including SEM, XRD, FT-IR, Raman spectroscopy, and VSM. In combination with vortex-assisted magnetic solid phase extraction and gas chromatography-electron capture detection, it was applied to the detection of the 16 pesticides. Following optimization, the method proved to be rapid with very low detection rates (LOD: 0.52–3.21 ng kg^{-1}), and recoveries were in the range 78.8% to 116.2%. The speed of the technique was due to the ability of the vortex to enlarge the area of contact between the pesticides and the absorbent.

<mark>5.2.2 *Use of carbon nanotubes/activated carbon*</mark>

Dichlorophen (4-chloro-2-[(5-chloro-2-hydroxyphenyl)methyl]phenol) is most commonly employed to tackle tapeworm. Skrzypek and coworkers have devised a method for its detection based on the use of square-wave adsorptive stripping voltammetry. [117] The method employed β–cyclodextrins and multi–walled carbon nanotubes at a glassy carbon electrode. The makeup of the electrode was verified by AFM, EIS and cyclic voltammetry.

At pH 6.5 (phosphate buffer), the voltammetry afforded a linear curve over the concentration range 5.0×10^{-8} mol L^{-1} to 2.9×10^{-6} mol L^{-1}. A low detection limit (10^{-8} molL^{-1}) with good repeatability was possible, and the system could be applied to river water without the need for any pretreatment. It was suggested that for the immobilized (on the glassy carbon electrode) 1:1 host-guest complex, part of the guest was buried in the cavity and protected, whilst part of the guest remained outside and could be readily oxidized.

Chlordecone (decachloropentacyclo[5.3.0.0$^{2.6}$.0$^{3.9}$.0$^{4.8}$]decan-5-one) is a pesticide which is now banned in many countries, but residual contamination, particularly in rivers and soils, still exists leading to serious diseases. Its detection and removal is therefore seen as a priority, and with this in mind, Levalois-Grützmacher and coworkers have investigated the use of both cyclodextrin@chlordecone host-guest complexes as well as a hybrid material comprising activated carbon modified with cyclodextrins. [122] It was found that both β- and γ-cyclodextrins form 1:1 inclusion complexes, and that, given their lack of solubility in most solvents, can be separated out by filtration (over activated carbon) to, for example, purify water. Best results were achieved for

the system employing the activated carbon decorated with cyclodextrins, and the improvement could be equated to the amount of cyclodextrin present. Both the methods reported proved to be better than the use of only activated carbon.

5.2.3 *Use of molecular imprinting*

Forchlorfenuron (*N*-(2-chloropyridin-4-yl)-*N'*-phenylurea) is generally used to treat grapes and kiwifruit. Nie *et al*. have made use of molecular imprinting to form a polymer based on β-cyclodextrin (as the monomer) and 1,6-hexamethylene diisocyanate (as the cross-linking agent). [120] In DMSO, an inclusion complex, promoted by hydrophobic interactions, can form between the imprinted polymer and forchlorfenuron; the binding recognition is specific and reversible, figure 38. Adsorption equilibrium experiments were conducted in ethanol which showed that the amount of forchlorfenuron adsorbed increased with time until the saturation point was attained (26.79 mg/g); the process was completed over 30 min.
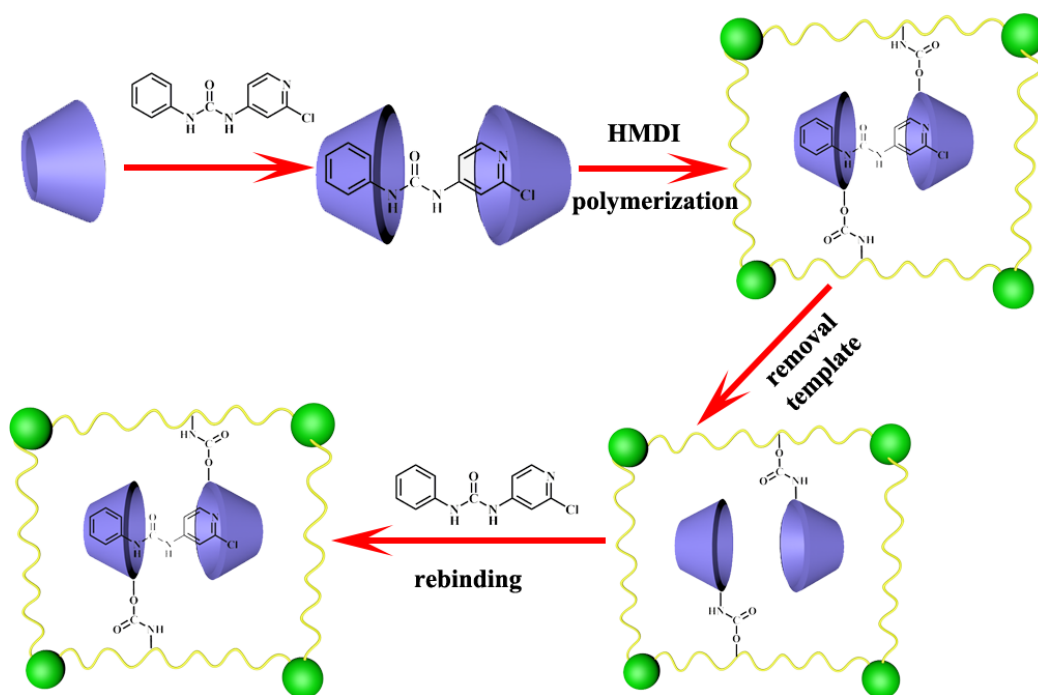
Figure 38. Schematic demonstration of molecular imprinting and rebinding of chlorfenuron.

For spiked (0.05 – 0.5 mg/kg) fruit samples (strawberry), the amount of forchlorfenuron was determined, and the amount found (recovery) was between 84.5 and 90.8% with a limit of detection of 0.023 µg/kg. A comparison with other methods of detection was made, and it was

flagged that this system has both economic advantages and good repeatability (it can be used at least 5 times).

5.2.4 *Use of CD-assisted fluorescence*

Levine *et al*. have utilized cyclodextrin-assisted fluorescence modulation to detect the organochlorine pesticides *cis*-chlordane, heptachlor, lindane and mirex in samples of water collected from different regions of Rhode Island. [119] The fluorophore employed was 4,4-difluoro-1,3,5,7,8-pentamethyl-4-bora-3a,4a-diaza-*s*-indacene, commonly known as bodipy, and was chosen given its high quantum yield. When in close proximity to a pesticide, the emission changes and this can be measured and linked to a specific analyte. Detection limits are at the micromolar level, and closely related pesticides (e.g. *cis*-chlordane and *trans*-chlordane) can be fully distinguished from one another. The system proved to be quite versatile and could operate with water samples of differing pH value, salinity and temperature.

DiScenza and Levine reported the previously mentioned cyclodextrin-promoted fluorescence modulation for the detection of the four pesticides mirex, *cis*-chlordane, heptachlor and lindane. [123] A number of cyclodextrins were screened including α and β-cyclodextrins, methyl-β-cyclodextrin and 2-hydroxypropyl-β-cyclodextrin. The high quantum yield fluorophores employed were bodipy, rhodamine 6G and coumarin 6. Upon addition of the pesticide, the changes that occur in the fluorescence depended upon the interaction with the fluorophore and on the cyclodextrin, and these changes allowed for 100% selectivity to be achieved. The detection limits were as low as 5.2 mM. Control experiments including in the absence of any cyclodextrin revealed that best separation was achieved when using the larger cyclodextrins.

5.2.5 *Use of other β-CD systems*

Chlorothalonil (2,4,5,6-tetrachlorobenzene-1,3-dicarbonitrile) is used mostly with peanuts, potatoes and tomatoes, but its limited water solubility has somewhat restricted its uses. With this in mind, Ye *et al*. have investigated the use of β-cyclodextrin and hydroxypropyl-β-cyclodextrin in the hope that the resulting inclusion complexes would possess enhanced water solubility (and activity). [116] Molecular simulations and spectroscopic data (FTIR and ^{1}H NMR) together with XRD, SEM and TGA, revealed that during complexation, chlorothalonil was encapsulated by both

of the hosts. TGA revealed that the thermal stability improved upon complexation. Moreover, from fungicidal activity experiments it was deduced that both the water solubility and antifungal activity improved following complexation.

Jáuregui-Haza *et al*. have synthesized the iodine labeled compounds 1-iodochlordecone and β-1-iodo-pentachlorocyclohexane and subsequently formed inclusion complexes with cyclodextrins. [115] The driving force for this work was the problematic detection of the pesticides chlordecone and β-hexachlorocyclohexane, which are typically found in low concentration and are therefore hard to detect. The stability of the inclusion complexes was measured using a variety of calculation techniques, and it was determined that γ-CD formed the most stable complexes of the form I-CLD@CD and I-β-HCH@CD. This stability *versus* the other CD isomers was ascribed to the increased cavity size for γ-CD (*versus* α and β-CD) which allowed for total inclusion. The calculations revealed close similarities between the inclusion processes for both labeled and non-labeled pesticides. The work suggests that there is promise in using such labeled systems as radiotracers for tracking the removal of these and other pollutants.

5.3. Detection of neonicotinoid pesticides compounds with cyclodextrins and derivatives

5.3.1 *Use of activated carbon surfaces*

Imidacloprid (*N*-{1-[(6-chloro-3-pyridyl)methyl]-4,5-dihydroimidazol-2-yl}nitramide) is widely used for pest control. Zhang, Cai, Wu *et al*. have reported a method for its controlled release based on infrared light. [124] The method employs hollow carbon microspheres with a PEG and α-cyclodextrin modified surface, and this gel-like network can sequester the pesticide. The *modus operandi* then involves local heat generated by the carbon nanospheres upon irradiation, resulting in breakdown of the network and release of pesticide. This method shows significant improvement compared to exposure to only sunlight, *viz* 77% *versus* 29% pesticide release. The elevated temperature was found to be crucial for enhanced release, and experiments revealed that once the sol-gel transition temperature was achieved (63 °C here), the network collapse led to a large

increase in the release. Such a system has great potential for pest control, and this was illustrated on corn borers.

Valente and coworkers have employed an absorbent and controlled release technique, based on activated carbon-poly(β-cyclodextrin) composites, for the pesticides cymoxanil and imidacloprid. [125] The cross-linker used to polymerize the β-cyclodextrin was hexamethylene diisocyanate, and composites with 5 and 10 wt% activated carbon were prepared. The swelling degree of the gel seemed to be influenced by the presence of the activated carbon, with the latter possibly acting also as a cross-linker. Good stability was exhibited, with an observed sorption capacity of about 50 mg g^{-1}. A Sips model was invoked for the sorption, which would imply both chemical and physical interactions occurring (as evidenced by the surface morphology). The presence of either NaCl (to influence ionic strength) or the soil additive urea had little effect on the results. In terms of release, about 30% of the initial amount sorbed could readily be released, and the system experienced no loss of efficiency over three sorption/desorption cycles.

Determination of the neonicotinoid insecticides imidacloprid, clothianidin, thiamethoxam in honey (pollen and beeswax samples were also examined) has been reported by Pereira *et al*. using an electrochemical sensor. [127] The sensor comprised a glassy carbon electrode modified with reduced graphene oxide and β-cyclodextrin. In the honey samples, high recovery rates (up to 116%) were achieved, whereas for pollen (<68%) and beeswax (<55%), recovery values were lower. The sensitivity toward imidacloprid was superior to that for either clothianidin or thiamethoxam, which was thought to be due to the ease with which imidacloprid can form an inclusion complex with the β-cyclodextrin. Indeed, results compared to use of a glassy carbon electrode only, revealed significant increases in response rates, namely 1300% for imidacloprid, 670% for clothianidin by 670 % and 630% for thiametoxam. Experiments were also conducted in the presence of a number of interferents including Ca^{2+}, Mg^{2+}, Fe^{2+}, K^+, Na^+, NH_4^+ and the insecticides acetamiprid and dinotefuran, and the experiments showed they did not impact on the results.

A similar method was also employed by the same group for the determination of imidacloprid. [128] In this case, compared to the use of a glassy carbon electrode alone, the β-cyclodextrin containing sensor exhibited a 947% increase in peak current variation. Optimization of conditions by varying factors such as pH, potential, dissolved oxygen content, stirring, β-cyclodextrin concentration and scan rate led to an increase in the peak current variation of 57%.

Paichongding, launched in 2008, is a Chinese pesticide used to control insects on the likes of rice. Its electrochemical determination has been investigated by Yang, Wang *et al*. [132] The method utilized a β-cyclodextrin-graphene modified glassy carbon electrode, which exhibited increased peak current for paichongding *versus* that observed when using either just the glassy carbon electrode or the graphene glassy carbon electrode. The best operational temperature proved to be 0 °C with an accumulation time of 7 minutes at a pH of 7.2. The system could be stored at ambient temperature for a week without appreciable loss of current response. Ions such as Mg^{2+}, Ca^{2+}, Fe^{2+}, K^+, Na^+, and NH_4^+ did not interfere with the measurements, and for 10 different batches of the sensor, reproducible results were produced.

A linear range was observed from 1 to 10 µM, 10 to 55 µM, with a detection limit of 0.11 µM. When applied to 10 g samples of spiked (1.6, 6.4, 8.0, 10.0 µM) grains, the detection of paichongding via electrochemistry gave similar results to HPLC.

5.3.2 *Use of magnetic nanoparticles*

The neonicotinoid insecticides thiamethoxam, imidacloprid, acetamiprid, nitenpyram, dinotefuran, clothianidin and thiacloprid have been adsorbed by a magnetic (Fe_4O_3), copper-based MOF in aqueous solution. [130] The MOF was constructed from benzene-1,3,5-tricarboxylate and copper acetate, with a magnetic core comprising Fe_4O_3/graphene oxide/ β-cyclodextrin as support (figure 39). The supramolecular recognition properties of the system, including the presence of hydrophobic cavities, led to increased adsorption (both capacity and rate) of the pesticides. The surface area (Brunauer–Emmett–Teller) of the MOF was 250.33 m^2g^{-1}, and was thought to possess a thin single surface layer coating of Fe_4O_3/graphene oxide/β-cyclodextrin. The system exhibited super-paramagnetism (saturation magnetization of 10.47 emu g^{-1}). Modelling revealed differing adsorption behavior for the pesticides with Langmuir monolayer adsorption adopted by thiacloprid, whilst Freundlich bimolecular layer adsorption was the best fit for the other pesticides. For spiked tap water samples (0.1, 0.2, and 0.5 mg/L), treatment with the magnetic MOF (20 mg) resulted in near complete removal of pesticide.
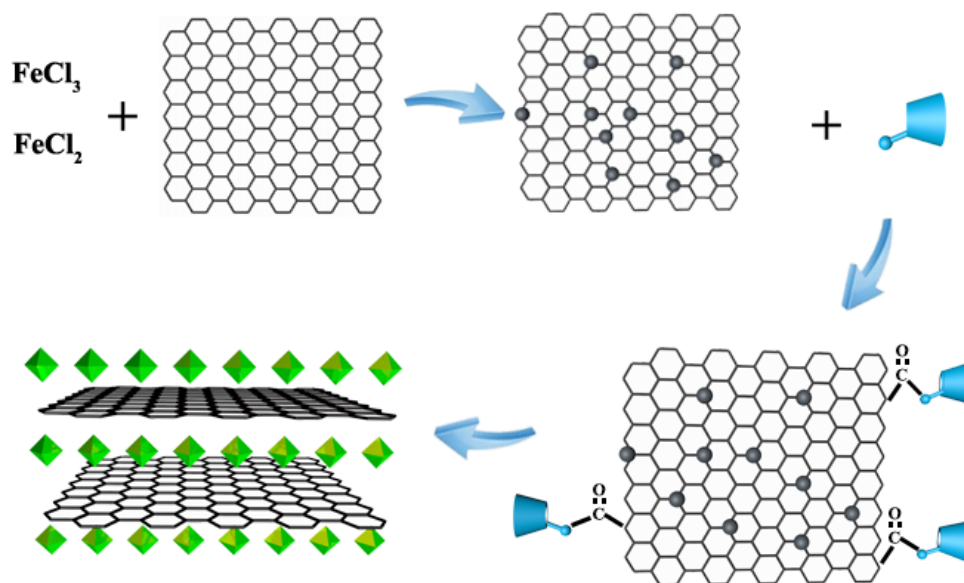
Figure 39. MOF constructed from benzene-1,3,5-tricarboxylate and copper acetate, with a magnetic core comprising Fe_4O_3/graphene oxide/ β-cyclodextrin as support.

5.3.3 *Use of liquid-liquid microextraction*

Vichapong *et al*. reported a microextraction method for the detection of the neonicotinoid pesticides thiamethoxam, clothianidin, imidacloprid, acetamiprid and thiacloprid. [126] The system was based on β-cyclodextrin assisted liquid–liquid microextraction, which involved a solidification process (of floating droplets) in combination with HPLC. The presence of the β-cyclodextrin (disperser solvent) aided, along with centrifugation, the process by increasing the organic and aqueous phase contact area, whilst at the same time reducing the interfacial tension. The extraction solvent employed was 1-octanol; toluene, *n*-hexane, and 1-dodecanol proved to be unsuitable. After optimizing the conditions by varying the likes of the 1-octanol, β-cyclodextrin and salt addition, a linear range was obtained over 0.0003 to 1 µg mL^{-1}. For the named pesticides, the limits of detection were 0.0001 to 0.0005 µg mL^{-1}, with good recoveries (83 – 132%).

5.3.4 *Use of polypropylene*

The inclusion complex between the pesticide imidacloprid (*N*-{1-[(6-chloro-3-pyridyl)methyl]-4,5-dihydroimidazol-2-yl}nitramide) and β-cyclodextrin was prepared by Özen *et al*. and then incorporated into polypropylene. [129] The embedded system demonstrated high

thermal stability, and by use of HPLC was shown to exhibit a prolonged (*versus* the inclusion complex alone) release profile whereby 84wt% of imidacloprid was released over several weeks.

5.3.5 *Use of other β-CD systems*

Alonso and coworkers have characterized, both in solution and the solid-state, the inclusion complex resulting from the interaction of β-cyclodextrin with acetamiprid ((*E*)-N1-[(6-chloro-3-pyridyl)methyl]-N2-cyano-N1-methyl-acetamidine). [131] Spectroscopic data were consistent with the adoption of a 1:1 inclusion complex in solution, whilst in the molecular structure, determined by X-ray diffraction, 2:2 dimers were observed arranged in channel-type fashion. All the data presented indicated that in both solution and in the solid-state, the nitrile of the pesticide pointed toward the primary rim of β-cyclodextrin, whilst the chloropyridine fragments pointed toward the secondary rim.

The inclusion complex of pyrimethanil (4,6-dimethyl-*N*-phenylpyrimidin-2-amine), which is usually applied to fungus, with hydroxypropyl-β-cyclodextrin has been studied by Garrido *et al*. [133] Upon complexation, ^{1}H NMR spectroscopy reveals downfield shifts for the pyrimethanil protons, with integration consistent with a 1:1 host:guest ratio. The solubility in aqueous solution was about 5x that of the free fungicide. Moreover, encapsulation also resulted in about a 4x increase (in half-life) for the photostability (simulated solar irradiation) *versus* the free fungicide, in various types of aqueous solution.

5.4. Detection of organic ester compounds with β-cyclodextrins and derivatives

5.4.1 *Use of magnetic Fe_3O_4*

Using solvent-free conditions, Zhou *et al*. have prepared the sorbent 1-octyl-3-methylimidazolium hexafluorophosphate functionalized magnetic (Fe_3O_4) poly β-cyclodextrin. [134] Given the toxic nature of the pyrethroids cyhalothrin, fenvalerate, etofenprox, bifenthrin, the sorbent was utilized for their determination in a variety of teas via magnetic solid-phase extraction. Using the optimized extraction conditions, a linear range of 2.5–500 µg L^{-1} was established, with low limits of detection of 0.32–0.54 µg L^{-1}. For the named pyrethroids, the precision of the extraction experiments was good with intra-day at 2.6– 7.0%, and inter-day at 3.5–7.6%). Using Huoshan Huangya, Jinjunmei

and Tieguanyin teas, which were separately spiked with 10, 50, and 250 µg L^{-1} of each of the four pyrethroids, the recovery rates ranged from 70% to 101% (SD < 9.1%).

Li *et al*. have employed magnetic (Fe$_3$O$_4$) molecularly imprinted polymer gold nanoparticles based on mono-6-thiol-β-cyclodextrin for the extraction of carbendazim, figure 40. [139] The adsorption capacity of the system was measured at 190 mg·g^{-1}. When applied to spiked cabbage, lettuce, tomato, cauliflower and cowpea, the recoveries were between 90.5 % to 109 %; the detection limit was 3.0 pg·M L^{-1}.
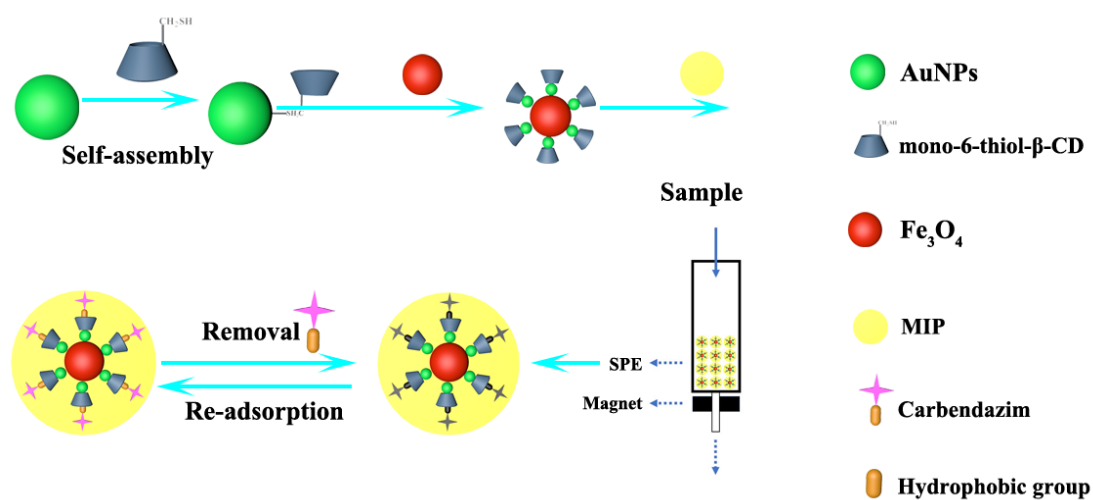
Figure 40. The procedure used to construct the SPE column and adsorb carbendazim.

5.4.2 *Use of carbon surfaces*

Qu, Lu *et al*. employed a composite prepared from Mxene, comprised of 2D layers (a few atoms thick) of transition metal carbides, carbon nano-horns which are horn-shaped graphene sheets, and β-cyclodextrin MOFs (prepared from β-CD and KOH), as an electrochemical sensor for carbendazim. [135] The MOFs utilized in this study not only possessed the porous structure typical of MOFs, but also exhibited the recognition properties of the cyclodextrin. Given also the beneficial large surface area, plentiful active sites and conductivity available to the Mxene/carbon nano-horns, the system as a whole had a much-improved mass transfer/catalysis capacity. This led to an electrode performance with a broad linear range (3.0 nM to 10.0 µM), as well as a low limit of detection (1.0 nM). The reproducibility of the system was tested with 5 different batches of the composite, and the RSD was around 4.6%. Moreover, for one specific composite, the current was measured 15 times with RSD 3.5%. A variety of interferents were screened including Cl$^-$, SO$_4^{2-}$,

Na$^+$, Cu^{2+}, Al^{3+} and 250.0 μM uric acid, ascorbic acid, glucose, malathion, thiabendazole, chlorophene, fenitrothion, none of which interfered with the results. When applied to spiked tomato juice, recoveries of between 97.77 to 102.01% were achieved.

Song and coworkers have modified carbon nanotubes with β-cyclodextrin and then immobilized, via sol-gel, this composite onto the walls and lumen of a hollow fiber. [138] The system was then utilized for the determination of carbaryl and 1-naphthol in four different batches of tomatoes using solid phase microextraction/HPLC. Carbaryl was detected in the concentration range 0.71 to 17.82 ng/g, whilst 1-naphthol was detected at 0.11 and 9.32 ng/g. Using this set up, the low limits of detection were 0.05 and 0.15 ng/g for 1-naphthol and carbaryl, respectively. Spiked recoveries were in the range 84.2% to 108.9%. The small hollow fiber helped to clean up the samples.

5.4.3 *Use of molecular imprinted polymers*

Nie *et al*. have reported a molecularly imprinted polymer containing β-cyclodextrin for the determination of carbendazim, figure 41. [136] Using dispersive solid-phase extraction combined with analysis by HPLC fitted with a UV detector, the capacity for the adsorption of carbendazim was investigated. A maximum adsorption capacity of 3.65 mg/g over 30 min was observed, and the system could be used at least 7 times with only 10% loss of efficiency. Linearity was displayed over the range 0.05–2.0 mg/L. Albendazole and benomyl, which have structures related to carbendazim, showed far less affinity toward the polymer. In fact, for albendazole, the adsorption capacity was reduced 3-fold, whilst that for benomyl was 4-fold less than for carbendazim. When applied to spiked apple, banana, orange, and peach samples, recoveries were in the range 81.33–97.23% (RSD 1.49–4.66%); the limit of detection was 0.03 mg/L.
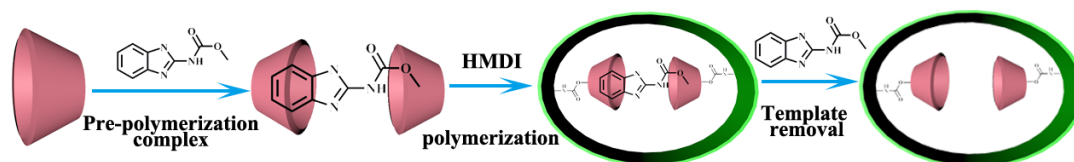
Figure 41. Schematic illustration of β-cyclodextrin based MIPs synthesis for CBZ determination.

The extraction of the pyrethroid pesticides fenpropathrin, cyhalothrin, and ethofenprox from aqueous solution has been investigated by Lu and coworkers. [137] They reported a method which exploited dispersive solid-phase extraction, a hyperbranched polymer functionalized with β-cyclodextrin, and HPLC. Optimization of the conditions revealed best conditions were experiments conducted with 30 s extraction time, with addition of 2% NaCl (ionic strength) at pH 9 using acetonitrile as the desorption solvent. For fenpropathrin, the linear range was 10–500 ng/mL, whilst for cyhalothrin and ethofenprox, it was 5–500 ng/mL. Detection limits spanned 1.0 ng/mL to 2.1 ng/mL, and recoveries ranged from 83.1% to 91.6%. For reproducibility, the RSD was < 6% for intra-day and inter-day. Samples from the Yongding River were spiked at two concentrations, namely 50 ng/mL and 100 ng/mL, and for the three named pesticides, recoveries were between 82.9 to 97.23% (RSD <9.44%).

5.5. Recognition and detection of other pesticides with cyclodextrins and derivatives

5.5.1 *Use of Ag/Au nanoparticles/colloids*

Jadeja, Thakore and coworkers have investigated the use of a gold (and silver) nanoparticle-based sensor, which was prepared from a cyclodextrin crosslinked polymer with phthalic anhydride, *i.e.* a cyclodextrin phthalate ester polymer, for the detection of sulfur-containing compounds. [140] SEM and TEM images indicated that the sensor was spherical in appearance and its size was < 15nm. This sensor has been applied to the detection of both amino acids (cysteine) and compounds of agricultural interest (diethyldithiocarbamate). Upon interaction of either guest, a clustering of gold particles was induced and this led to a rapid (<5s) red shift (524 to 670 nm), which can be monitored. A linear range of 0.01–0.25 μM was found, with limits of detection at 0.05 (sodium diethyldithiocarbamate) and 0.07 μM (cysteine). Best experimental conditions included pH 6 (cysteine) and 10 (sodium diethyldithiocarbamate), in the presence of 0.02 M NaCl. The related silver-based system was less effective. When tested on onion and garlic extracts, the sensor changed color from red to blue, thereby recognizing allicin. These experiments were extended to water samples spiked with the sulfur containing pesticides Phorente and Tafgor, and similar observations (red to blue) were evident.

Methyl parathion has been electrochemically (square wave anodic stripping voltammetry) determined in aqueous solution at pH 7.0. For this, Fu *et al.* employed a glassy carbon electrode comprised of a self-assembled monolayer of 6-thio-β-cyclodextrin with gold nanoparticles and single-walled carbon nanotubes. [162] The presence of the cyclodextrin monolayer greatly improved both selectivity and sensitivity. Indeed, when methyl parathion was bound by all the named ingredients above, the electrochemical response was some 3.9x and 5.1x that when bound to the glassy electrode bearing only the cyclodextrin/gold nanoparticles or gold nanoparticles/carbon nanotubes, respectively. A linear range of 2.0–80.0 nM was determined together with an LOD of 0.1 nM (S/N = 3). Other aromatic insecticides (chlorpyrifos, 2,4-dichlorophenoxy acetic acid, methamidophos, triazophos, parathion) hardly affected the detection of methyl parathion. By dipping in nitric acid (1.0 mM) for about 10 mins, the sensor could be regenerated and used again with little degradation. The RSD was 2.3% after 5 repeat measurements. The system was applied to spiked (25-70 nM) river water, and recoveries in the range 92.3 to 109.6% were achieved.

Bleta and coworkers have investigated the use of nanocomposites for the visible light drive photodegradation of the herbicide phenoxyacetic acid in water. [157] The composite preparation employed a methylated β-cyclodextrin as a structure directing agent, which was capable of the self-assembly of both gold and titania colloids. The resulting composite possessed a uniform dispersion of metals and controllable porosity. Use of other types of cyclodextrin led to composite materials with different size metal particles present and differing porosity. For example, the use of α-CD, β-CD and γ-CD afforded small gold particles and a less porous material. As mentioned above, in this work, a methylated β-cyclodextrin was selected for the self-assembly process, given it afforded the best combination of properties, including high crystallinity and surface area, required to optimize the photocatalytic activity (*i.e.* enhancing the likes of the electron transport and photo-adsorption over a wider wavelength range). In terms of reuse for photodegradation of phenoxyacetic acid, there was a drop-off in activity from 85% to 54% over the second run, and thereafter for the third run, it remained at 52%. This reduction was in part thought to be due to the lack of adsorption sites available for water following repeated runs.

5.5.2 *Use of chitosan-derived nanoparticles*

Carvacrol (2-methyl-5-(propan-2-yl)phenol) and linalool (3,7-dimethylocta-1,6-dien-3-ol) are monoterpenoid phenols, and show activity against fungi. The high volatility of both of these compounds is problematic and restricts their use. Given this, Fraceto *et al* have investigated their 1:1 inclusion complexes with β-cyclodextrin with a view to reducing the volatility. [152] Complexation efficiencies at 20 °C were 86.2% (carvacrol) and 74.2% (linalool), which were lower than previous reports, which was thought to be due to the method of preparation (involving maceration and drying steps). Using an ionic gelation method, nanoparticles were prepared from a hybrid polymer comprising the polyaminosaccharide chitosan and β-cyclodextrin. These nanoparticles were then used for the encapsulation (efficiencies <90%) of carvacrol and linalool, and the mean diameters of the products were 175.2 and 245.8 nm, respectively. The biological activity against mites (*Tetranychus urticae*), and repellency, acaricidal activity, and effect on oviposition were monitored over a 72h period. Despite a slow start *versus* the unencapsulated compounds, repellency activities were of the order of 80%. However, in terms of acaricidal activity and hindered oviposition, the encapsulated species proved to be more effective.

5.5.3 *Use of microporous silica*

Feng, Du *et al*. have utilized cyclodextrin/benzimidazole-based nano-valves for the targeted delivery of pesticides. [141] The valves acted as the shell structure embedded on a MoS$_2$ mesoporous silica core, and this was capable of pesticide transportation. By adjusting the conditions (low pH, α-amylase hydrolysis, competitive wax (fatty acids or triterpenoids) for binding, or near-IR irradiation), the controlled release of pesticide could be triggered, figure 42. Furthermore, the wetting agent (Aersosol OT) was also applied to prevent loss via splashing or bouncing, *i.e.* enhanced efficiency and less environmental pollution. When tested against pathogenic fungi Rhizoctonia solani (rice sheath blight) and Fusarium graminearum (wheat head blight) using the fungicide tebuconazole, the fungicidal efficacies observed were better than benchmark tests with commercial alternatives.
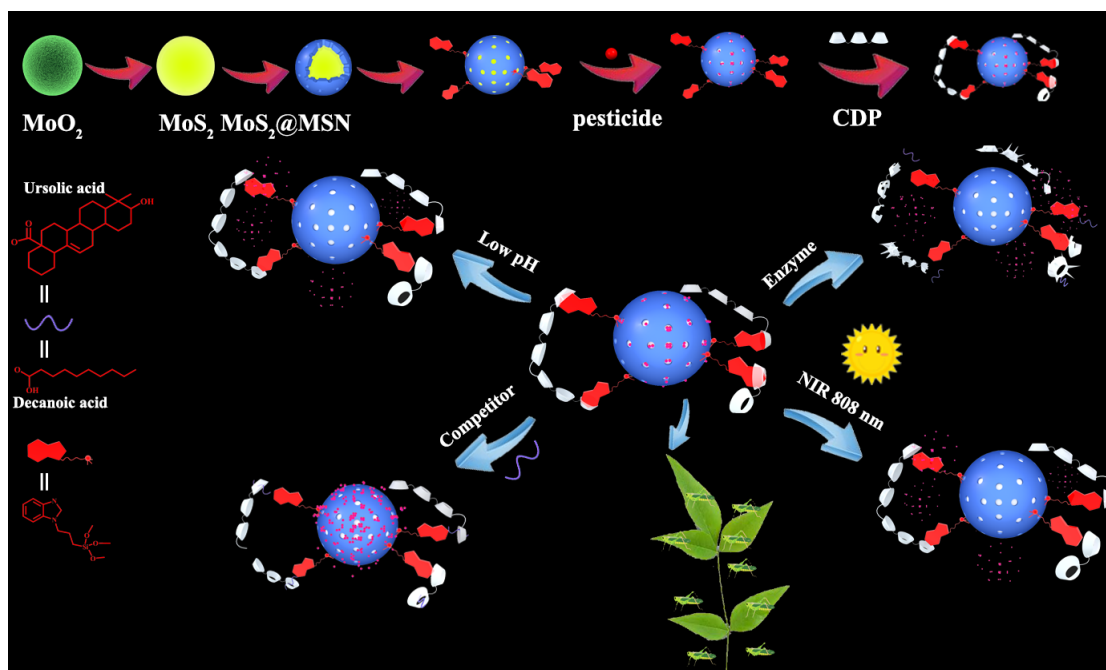
Figure 42. Controlled release of encapsulated pesticide from cyclodextrin/benzimidazole-based nano-valves.

A controlled release system was reported by Xu, Zhang and coworkers who employed hollow amino functionalized mesoporous silica capped with carboxylated β-cyclodextrin. [143] The pesticide chosen for release was indoxacarb (methyl 7-chloro-2,5-dihydro-2-[[(methoxycarbonyl)[4-(trifluoromethoxy)phenyl]amino]carbonyl]indeno[1,2-e][1,3,4]oxadiazine-4a(3*H*)-carboxylate), which is used against the larvae of moths and butterflies and related insects, and the loading efficient was 26.42% w/w. The release could be triggered by pH, with best results at pH 5 and 10, or by enzymatic action (α-amylase hydrolysis). The system also offered protection from UV radiation, thereby protecting the pesticide from degradation. When applied to the treatment of *Spodoptera frugiperda*, the system exhibited greater insecticidal activity *versus* indoxacarb emulsifiable concentrate under the same conditions. Moreover, when applied to zebrafish, the toxicity of the loaded indoxacarb was over 5 times less, which suggests that the use of this new delivery system can reduce collateral damage to the surrounding environment.

Li *et al*. reacted 4,4'-stilbene di-carboxylic acid with 6-deoxy-6-amino-β-cyclodextrin to afford a stilbene diamido-bridged bis(β-cyclodextrin), which was then bonded to the surface of an ordered mesoporous silica gel (SBA-15). [150] The resulting bridged bis(β-cyclodextrin)-bonded chiral

stationary phase was applied to the separation of 23 racemic drugs and pesticides using chromatography in the reversed-phase or polar organic mode. The analytes screened included β-blockers and triazoles, flavanones, praziquantel and trimeprazine. Chromatographic results were compared against those of a 'normal' β-cyclodextrin stationary phase, and it was found that the bridged chiral stationary phase performed better in terms of enantioselectivity and diasterioselectivity. High resolution (1.51~5.15) and fast times (25 min.), and is some cases increased enantioseparation resolutions were achieved. It was postulated that the having the two cyclodextrins in close proximity resulted in the formation of a pseudo cavity capable of synergistic encapsulation that enables it to trap large analytes (and enhancing chiral discrimination). The new stationary phase was also able to operate at temperatures between 30 and 60 °C, whilst maintaining good enantioselectivity and diastereoselectivity.

He *et al*. reported a system triggered by an enzyme (α-amylase) that comprised α-cyclodextrin capped hollow mesoporous silica spheres. [153] α-Cyclodextrin provides a convenient entry point to this system given its ability to form a more stable complex with *N*-alkylaniline than does β-cyclodextrin. Both the α-cyclodextrin and the *N*-alkylaniline form caps/stoppers on the hollow silicon sphere. The loading of avermectin by the controlled release formulation was around 38% w/w. The release profile of avermectin was evaluated under a variety of conditions including variation of pH and temperature, as well as with and without α-amylase present. The release of avermectin could be greatly increased by the addition of α-amylase, and the system exhibited improvements in both UV and thermal stability. The toxicological activity of avermectin controlled release system against *Plutella xylostella* larvae was evaluated, and results revealed that the enzymes could remove the α-CD caps *in vivo* thereby providing a route for larva death. When compared to commercial avermectin containing products, the mortality (of the insect) at 14 days (83.33%) was greater by 40%.

5.5.4 *Use of polysilicon systems*

Amino, carboxyl, phenyl, alkyl and β-cyclodextrin ends groups were introduced to hyperbranched polysilicons by Gao, Xu *et al*. [149] These systems were then screened for their ability to adsorb benzoylurea insecticides, which are insect growth regulators and are often applied to combat flees on cats and dogs. Calculations were used to probe the binding model of

diflubenzuron with each of the polysilicons modified with different end groups. Adsorption experiments were then used to verify the calculations and it was found that the hydrogen bonding associated with the presence of an amino end group provided the most favorable system. Given this, further experiments were conducted with other pesticides including hexaflumuron, flufenoxuron, teflubenzuron, lufenuron, and chlorfluazuron to give insight into the influence of adsorption time and concentration on uptake. For dipyridamole, the adsorption peaked at 3h for an initial concentration of 120 mg L^{-1} (of the amino end group absorbent). In the case of a β-cyclodextrin end group, the insecticide can form a host-guest coating by entering the cavity.

5.5.5 Column-based/solid phase extraction systems

Castells *et al*. have investigated the enantio-separation of racemic mixtures of the polar pesticides mecoprop, dichlorprop, fenoprop and hydroprop esters, fenoxaprop ethyl, metalaxyl, and haloxyfop esters, using achiral polymers and permethyl-β-cyclodextrin. [155] The capillary columns (of Fused-silica of 250 μm i.d.) were coated with permethyl-β-cyclodextrin which had been dissolved in one of (14%-cyanopropylphenyl)(1%-vinyl)-86%-methylpolysiloxane, (5%-phenyl)(1%-vinyl)-95%-methylpolysiloxane or polyethyleneglycol. Results were compared against a commercial column, Hydrodexβ-PM. For the majority of the chiral pesticides, the use of the 30% permethyl-β-cyclodextrin in the less polar (5%-phenyl)(1%-vinyl)-95%-methylpolysiloxane afforded best enantioseparations. Such a column could also separate enantiomers that the more polar phases could not, showing that this system had the potential to be applied to a wider range of polar pesticides.

Li *et al*. prepared a β-cyclodextrin-bonded chiral stationary phase incorporating a thiocarbamated benzamide linker, and investigated, using chiral HPLC, its ability to separate out a number of pesticide and drug samples. [146] In total, 24 analytes were selected, and these included 11 triazole pesticides, 8 flavanone drugs and 5 β-blocker drugs. Results revealed 18 of the analytes to be fully separated, with the enantio-resolution range for the triazoles at 1.45-3.33, that for the flavanones was 0.35-2.45 and that for the β-blockers was 1.26-1.58. Tebuconazole exhibited the best resolution at 3.33 over 13 min, whilst four peaks were noted for bitertanol, which contains two chiral centres, and for the *cis*/*trans* isomers of triticonazole. The usually difficult to separate myclobutanil was also completely resolved. The enhanced separation ability of the system

was ascribed to the ability of the thiocarbamated benzamide spacer to contribute to coordination and hydrogen bonding.

The determination of the four benzoylurea insecticides diflubenzuron, triflumuron chlorfluazuron and hexaflumuron in honeys has been investigated by Lu *et al*. [158] They employed acidified Attapulgite, which is a hydrated magnesium silicate clay with a presumed formula of $(Al_2Mg_2)Si_8O_{20}(OH)_2(OH_2)_4 \cdot 4H_2O$, and β-cyclodextrin linked together in a composite via KH-560 (an epoxy functional resin). The composite was then utilized as the sorbent in a dispersed micro-solid phase extraction, which in combination with HPLC, allowed for insecticide determination. The conditions (e.g. extraction time, amount of sorbent, ionic strength) of use for this absorbent were then varied to optimize efficiency. This led to detection limits of 0.2–1.0µg/L, and when applied to spiked vitex honey and acacia honey, recoveries ranged from 14.2 to 82.0%. These results revealed a strong preference for the adsorption of hydrophobic compounds, e.g. chlorfluazuron and hexaflumuron, and could indeed be related to logP_{ow} (which is a measure the hydrophobicity). A selling point of this system is that the sorbent is relatively cheap in comparison to alternatives.

Gao, Li and workers have employed an ionic liquid-modified β-cyclodextrin/attapulgite adsorbent for the recognition of the benzoylurea insecticides hexaflumuron, flufenoxuron, lufenuron and chlorfluazuron in honey and tea. [160] The solid-phase microextraction method was coupled with HPLC, and following optimization, the linear range was 5–500 ng mL^{-1} with limits of detection between 0.12 to 0.21 µg L^{-1}. The accuracies for the four insecticides were hexaflumuron (93.3%), flufenoxuron (84.5%), lufenuron (104.7%) and chlorfluazuron (103.6%) with intraday precision < 3.71% and interday (over two days) <3.85%. For the spiked (50 µg L^{-1} and 200 µg L^{-1}) honey and tea samples, recoveries ranged between 76.8–94.5%, with the lowest results associated with flufenoxuron.

5.5.6 ==*Use of magnetic materials*==

Madj and Nojavan have used a maltodextrin/β-cyclodextrin-functionalized magnetic graphene oxide containing composite to co-extract triazines (atrazine, tribenuron methyl, and metribuzin) and triazoles (cyproconazole, tebuconazole, penconazole, and diniconazole) from potato, tomato, and corn. [145] Epichlorohydrin was used as the linker to bind β-cyclodextrin and

maltodextrin to the magnetic graphene oxide surface. The co-extraction was accomplished due to the presence of both hydrophobic cavities (β-cyclodextrin) and numerous hydroxyl groups (maltodextrin). Linearity over the range 1.0–1000 µg L^{-1} was observed under optimum conditions, which included a pH of 7.0 and extraction time of 20 min. For the 7 pesticides examined, the extraction efficiencies ranged between 66.4–95.3%; limits of detection were 0.01–0.08 µg L^{-1}. In samples of tomato (36.0 µg kg^{-1}) and corn (166.0 µg kg^{-1}), diniconazole was detected, whilst in tomato, atrazine (680.0 µg kg^{-1}) was also detected and in corn, tebuconazole (176.0 µg kg^{-1}) was detected. When the samples were spiked, recoveries were in the range 88.4–112.0% with decent intra- and inter-day precision (RSDs < 9.0%, n = 3).

Yang, Li and coworkers have modified the magnetic MOF Fe$_3$O$_4$@MIL-100(Fe) by using the cross-linker tetrafluoroterephthalonitrile to append β-cyclodextrin to the MOF shell. [148] The new cyclodextrin-containing MOF was then applied to the removal of the triazole fungicides epoxiconazole, flusilazole, tebuconazole, and triadimefon from water samples. Under the optimized conditions, which included 1.0 g L^{-1} of absorbent, pH 7.0, adsorption equilibrium time of 50 min, high adsorption capacity was observed. After 5 cycles of adsorption and desorption, there was only a small change in extraction efficiency, and no significant change in the adsorption was noted in the presence of different concentrations of humic acid. When applied to wastewater and lake water, the adsorption efficiencies for the four named fungicides were in the range 64.52 to 102.10 mg g^{-1}.

5.5.7 *Use of nanofibers formed via electrospinning*

A delivery system has also been reported by Ye, Fu and coworkers. [142] They employed electrospinning to complex thiram as the guest molecule and thereby create self-supporting inclusion complex nanofibers based on high concentrations (180% w/v) of hydroxypropyl-β-cyclodextrin. In this way, the solubility of thiram, together with its thermal stability, was greatly improved; the increased solubility was proportional to the hydroxypropyl-β-cyclodextrin content. Moreover, the system was found to increase the antifungal activity of thiram, as demonstrated against *Gibberella sp*.

5.5.8 *Use of nanorods*

Porous and rigid composites based on cross-linked cyclodextrin polymers, and which contain ordered MnO_2 nanorods, have been prepared by oxidation using $KMnO_4$. [144] This method allowed for the oxidation of short chains within the polymer network and thereby imparted mechanical stability. The influence of the amount of $KMnO_4$ used on the structure and properties of the composites was examined. Whilst cross-linked cyclodextrin polymeric materials showed linear changes with oxidant dosage, the changes for the γ-cross-linked cyclodextrin polymeric materials were less noticeable. Various factors such as degree of cross-linking, cyclodexrin content and pore volume were varied and their effect on the resulting composite properties was investigated, for example increased cross-linking was found to improve stability in water. More importantly, such factors were found to impact upon the sorption capacity. For the γ-cross-linked cyclodextrin polymeric materials, the adsorption capacity exhibited toward the pesticides flufiprole, firponil and benalaxyl were high at 24.1%–43.7% *versus* those of the beta system; the trend was reversed for other pesticides. The sorption capacity relies on both the number and access to the adsorption sites, and in such materials the mechanisms which dictate the sorption contribute in the order association complexation ≥network meshing ≫ inclusion complexation. In water samples spiked (80–400 µg/L) with the hydrophobic pesticides benalaxyl, butachlor, flufiprole, and fipronil, removal efficiency was in the range 60 to 80%; the removal of other pesticides was far lower (10 to 60%). Reusable experiments for both the β– and γ–systems increased after use, and this was thought to be due to repeated swelling and washing improving access to the sorption sites.

5.5.9 *Use of hydrogels*

Liu *et al*. have produced an amphiphilic copolymer by conjugating camptothecin with low molecular weight polyethylene glycol. [147] This copolymer either self-assembled into micelles, or in the presence of α-cyclodextrin (for cross-linking) produced a hydrogel. Both micelles and the hydrogel were used to transport camptothecin with acetamiprid or nitenpyram. The results revealed that both micelles and hydrogels were capable of the transportation and release of combinations of pesticides. In particular, the micelles released the pesticides (camptothecin, pegalated camptothecin, and acetamiprid or nitenpyram) quickly at the same time. In the case of the hydrogels, the release of acetamiprid or nitenpyram (phase one) was sustained over 168h,

accompanied by (phase two) an amount of camptothecin (and no free camptothecin). The first phase was associated with diffusion and destruction of cross-links, whilst phase two involved hydrolysis. The micelles and hydrogels, loaded with acetamiprid or nitenpyram, were tested against the insects *Brevicoryne brassicae, Tetranychus cinnabarinus,* and *Bursaphelenchus xylophilus.* Impressive insecticidal activities were observed, which together with LC_{50} results, indicated that these systems were more potent that free camptothecin. Even with doses as low as 5µg/mL, high insecticidal activities were possible.

5.5.10 *Use of liposomes*

Greige-Gerges and coworkers have explored the possibility of encapsulating eucalyptol, with a view to improving its volatility and hence usability. [154] To do this, they studied three systems, employing an ethanol injection method to prepare liposomes and drug-in-cyclodextrin-in-liposomes; the hydroxypropylcyclodextrin/eucalyptol inclusion complex was also studied. During the freeze dry process, hydroxypropylcyclodextrin, which does not affect the fluidity of the liposomes, was used as the cryoprotectant. Particle size distribution and zeta potentials were measured (pre- and post-freezing) to ensure reproducibility of the batches. The eucalyptol loading rate was determined post analysis by HPLC. Its release from all three systems was evaluated at 4 °C over 6 months using multiple headspace extraction. It was found that the eucalyptol loading for the drug-in-cyclodextrin-in-liposomes was some 38 times greater than that found for conventional liposomes. Moreover, both the hydroxypropylcyclodextrin/eucalyptol inclusion complex and the drug-in-cyclodextrin-in-liposomes exhibited superior eucalyptol retention (and decreased eucalyptol evaporation) *versus* conventional liposomes studied.

5.5.11 *Molecular imprinted polymers*

Bulk polymerization techniques have been employed by Shen and coworkers to access pirimicarb-imprinted polymers. [156] The molecular imprinted polymers were used to enrich the pirimicarb content via solid-phase extraction, which is subsequently followed by liquid chromatographic analysis. SEM images revealed these imprinted polymers to be quite rough and porous, which contrasts with the smooth and compact non-imprinted polymers. The adsorption solvent (methanol) contains a significant amount of water and this leads to a local hydrophobic

environment involving the template and monomer. In fact, the best ratio was found to be 95:5 v/v water:methanol, as this promoted host-guest complexation between pirimicarb and allyl-β-cyclodextrin. For the columns tested, the average of selective retention recovery of pirimicarb ranged between 76.96 to 96.38%, with best results for that containing a combination of allyl-β-cyclodextrin and methacrylic acid; non-imprinted columns gave the lowest results. The results also showed that the use of methacrylic acid was preferable to acrylonitrile in terms of the formation of molecular imprinted polymers. By shaking 20 mg of mass polymers in pirimicarb solution at 30 °C, it was found that much more polymer formed in the presence of the template. Indeed, the capacity factor for binding affinity was found to greatly increase for both allyl-β-cyclodextrin/methacrylic acid (13.05 to 16.55 mg g^{-1}) and for allyl-β-cyclodextrin/acrylonitrile (10.33 to 14.73 mg g^{-1}). Experiments were conducted on spiked (1, 3.33 and 10 μg. g^{-1}) vegetables (cabbage, broccoli, lettuce, *Brassica chinensis var parachinenis* and cauliflower), and recovery rates ranged from 88.23 to 97.54% with RSD ≤ 5.07%.

5.5.12 *Fluorescent systems*

Ling and coworkers prepared, via Click chemistry, a pyrene appended β-cyclodextrin probe, which, in water, self-assembled into fluorescent aggregates. [151] By virtue of intra- and intermolecular interactions, including hydrophobic π–π interactions between pyrenes, there was strong excimer and weak monomer emission. The fluorescent aggregates were employed for the selective detection of pirimicarb (2-(dimethylamino)-5,6-dimethylpyrimidin-4-yl dimethylcarbamate), and the monomer to excimer ratio exhibited an impressive enhancement (*i.e.* a x85 increase in the intensity ratio). It was thought the presence of pirimicarb led to an increased separation between pyrenes and hence a weakening of the π-π interactions. A detection limit of 60nM was recorded, and the system seemed relatively unaffected by pH changes over the range 4.12 to 10.02. The other carbamate pesticides screened failed to produce any significant changes.

The pyrene appended β-cyclodextrin probe was also applied (at pH 7.2) to the discrimination/detection of the trinitro-aromatic compounds 2,4,6-trinitrotoluene, 1,3,5-trinitrobenzene and picric acid, which are of interest due to their explosive nature. A range of other nitro and dinitro-aromatics were also screened, but none afforded significant selectivity. Observations on the emission for 2,4,6-trinitrotoluene and 1,3,5-trinitrobenzene suggested that the

modus operandi was different to that in operation with pirimicarb, and the formation of thermodynamically driven, short lived dimers between the nitroaromatics and the probe was proposed. In the case of picric acid, quenching of the emission was observed, due to an energy transfer between the pyrene (excited states) and the picric acid (ground state). DLS and TEM images of the aggregates following addition (50 or 100 equivalents) of pirimicarb, 2,4,6-trinitrotoluene, 1,3,5-trinitrobenzene or picric acid revealed that the average size (~164 nm) of the aggregates reduced considerably suggesting a partial disruption of aggregation.

Levine *et al*. have employed the energy transfer from polychlorinated biphenyls, tamoxifen, and diethylstilbestrol, facilitated by γ-cyclodextrin, to the fluorophores BODIPY, Coumarin 6 or Rhodamine 6G, as a means of detecting these pesticides at micromolar level. [161] The analytes were detected in both buffer solution (pH 7.4) and in unpurified apple juice. In the buffered solution, results using different fluorophores revealed different trends. For example, in the case of BODIPY, most energy transfer efficiencies increased in the presence of 10 mM of γ-cyclodextrin, whilst for Coumarin the opposite was true and for Rhodamine 6G, the presence of the γ-cyclodextrin made little difference. Results with apple juice tended to result in quite noisy spectra, though for two pesticides (the organochlorines), energy transfer (24-25%) was evident, particularly in the presence of BODIPY, with LODs in the range 2.1-14.2 μM.

5.5.13 *Use of functionalized nanoporous carbon*

The extraction of *p*-nitrophenol and pesticides (β and γ-hexachlorocyclohexane, aldrin, dieldrin and three different *p,p'*-chlorodiphenyl compounds) from aqueous solutions has been investigated by Zolfaghari by using cyclodextrin functionalized nanoporous carbons. [159] The cyclodextrin (13.8×7.9 Å) was grafted onto (and inside the pores which had diameter 4.1 nm) the nanoporous carbon surface, which had been oxidized using HNO_3, using a 1,4-phenylene diisocyanate linkage. A number of absorbents were prepared including the parent nanoporous carbons, their oxidized form and a number of cyclodextrin functionalized nanoporous carbons, the latter containing different ratios of cyclodextrin to 1,4-phenylene diisocyanate linkage. The largest adsorption capacity (100 mg/g) for *p*-nitrophenol was found for the system employing the cyclodextrin nanoporous carbon. It proved possible to remove 90% of the *p*-nitrophenol for the

systems with higher cyclodextrin content. For the pesticides, those bearing the *p,p'*-chlorodiphenyl motif appeared to have a good geometric match with the cyclodextrin cavity which led to good adsorption. The results for the other pesticides were not so good. Successive adsorption–desorption cycles were possible by using ethanol to release the *p*-nitrophenol, and it was found that the cycles could be repeated without significant reduction in the adsorption capacity.

5.5.14 *Other inclusion complexes*

Tonelli *et al.* have reported inclusion complexes resulting from the interaction of pyriproxyfen, which is used against mosquito larvae, with β- and γ-cyclodextrins; the guest was too large (length *ca*. 18.4 Å, diameter 5.3Å) to form an inclusion complex with α-cyclodextrin. [163] From ^{1}H NMR spectroscopic measurements, the ratio of guest to cyclodextrin was proposed as 1:1.3. In the case of γ-cyclodextrin, XRD data suggested a change in structure from cage to columnar upon complexation with pyriproxyfen. The formation of the inclusion complexes also reduced the potential for evaporation of pyriproxyfen.

Capsaicin ((6*E*)-*N*-[(4-hydroxy-3-methoxyphenyl)methyl]-8-methylnon-6-enamide) can be used in sprays to deter pests, but its uses are restricted by solubility and instability. With this in mind, Shan, Yang *et al.* have investigated its guest–host complexation with β-cyclodextrin and hydroxypropyl-β-cyclodextrin using a co-evaporation method. [164] Data suggested the formation of 1:1 complexation in both cases. Complexation greatly improved the solubility of capsaicin, with a 50-fold increase in the presence of hydroxypropyl-β-cyclodextrin (60 mM) and a smaller increase (5-fold) for β-cyclodextrin (6 mM). Preparing the inclusion complexes by co-evaporation led to improvements in guest dissolution and degradation *versus* systems prepared by a grinding method. In the samples prepared via co-evaporation (1:0.5–1:5 molar ratios of CP/CDs), the ratio of guest to β-cyclodextrin was 1:5 and for hydroxypropyl-β-cyclodextrin 1:3. In soil, adsorption–desorption experiments revealed that use of HP*β*CD could significantly lower the amount of adsorbed CP in soil.

5.5.15 *Computational studies*

Ferencz and Balog have looked at soil contamination from the pesticide types organochlorine, triazine, carbamate, phenoxy acid and organophosphorus. [165] These studies took place in

Romania, and a number of pesticides were found that are banned under EU rules. With a view to making such pesticides less harmful, computational studies involving steric energy were conducted on possible host-guest complexation with cyclodextrins. The calculations revealed the presence of water required increased energy and also in some cases, the presence of partial inclusion was observed. Steric energy evaluations revealed that a number of the pesticides could readily be abstracted from the soil, e.g. diazinon, carbaryl and fenthion, given they formed very stable inclusion complexes. Deltamethrine and brodifacoum were studied in detail with results indicating that although stable complexes are formed, they involved interactions with external hydrophilic areas. Studies on potato beetles using deltamethrine or its inclusion complex with β-cyclodextrin revealed that on exposure to the inclusion complex, half the beetles died after 45 mins, whereas it took 65 mins using the pesticide alone. This was thought to be due to a change in properties such as taste, odor etc. which suggests if administered as an inclusion complex then the pesticide can be applied in lower dosage.

6. Conclusion

Whilst the use of pesticides has proved crucial over the years in controlling pests for agricultural and related purposes, their impact on the environment has been extremely detrimental. Methods which can reduce toxicity, lower necessary dosage and make pesticide delivery more targeted will clearly be highly beneficial. With this in mind, many research groups have chosen to focus on the use of macrocycles as a way of making pesticides greener. The types of macrocycles which are central to these studies tend to have available cavities and the capacity to form stable host-guest inclusion complexes. In this review, we have discussed the literature relating to the use of cucurbiturils, pillararenes, calixarenes and cyclodextrins. In many cases, the resulting host-guest complexes not only exhibit less toxicity than the parent pesticides, but retain the potent herbicidal activity. When used for the detection of pesticides, these host-guest systems can be very selective for specific pesticides and can tolerant a large range of impurities without interference. Many operate over large linear ranges and have very low detection limits (down to ng/mL), and can be used multiple times with little or no impact on efficiency. The host-guest complexation also helps to improve solubility and can slow down pesticide decomposition. To-date, most work has been

done with cyclodextrins, but the results herein indicate that the newer members of the macrocyclic family also hold much potential in this area. As for most products, the key to the widespread use of these systems will be cost and the ability to up-scale the macrocyclic syntheses.

Acknowledgements

Author Contributions

All authors had full access to all the data in the study and take responsibility for the integrity of the data and the accuracy of the data analysis. Pei hui Shan and Jian hang Hu can contribute equally as first authors.

Conflicts of interest

There are no conflicts to declare.

References

1. Aktar, M. W.; Sengupta, D.; Chowdhury, A. *Interdiscip. Toxicol*. **2009**, 2, 1-12.
2. Alewu B, Nosiri C. Pesticides and human health. In: Stoytcheva M, editor. *Pesticides in the Modern World – Effects of Pesticides Exposure*. InTech, **2011**, 231–250.
3. Nicolopoulou-Stamati, P.; Maipass, S.; Kotampasi, C.; Stamatis, P.; Hens, L. *Front. Public Health*, **2016**, 4, 148.
4. Ariga, K.; Kunitake, T. Supramolecular chemistry: Fundamentals and applications, Springer, Heidelberg, **2006**.
5. Wagner, B. D. Host-Guest chemistry: Supramolecular inclusion in solution. Walter de Gruyter GmbH & Co KG, **2020**.
6. Freeman, W. A.; Mock, W. L.; Shih, N. –Y. *J. Am. Chem. Soc*. **1981**, 103, 7367-7368.
7. Note the original reaction was conducted much earlier: Behrend R.; Meyer, E.; Rusche, F. *Justus Liebigs Ann. Chem*. **1905**, 339, 1-37.
8. Ogoshi, T.; Kanai, S.; Fujinami, S.; Yamagishi, T.-a.; Nakamoto, Y. *J. Am. Chem. Soc*. **2008**, 130, 5022-5023.
9. Gutsche, C. D. Calixarenes; The Royal Society of Chemistry: Cambridge, **1989**.

10. Villiers, A. *Compt. Rend. Acad. Sci.* **1891**, 536–538.

11. Nau, W. M.; Florea, M.; Assaf, K. I. *Isr. J. Chem.* **2011**, 51, 559-577.

12. Zhang, X. J.; Huang, Q. X.; Zhao, Z. Z.; Xu, X. Q.; Li, S. K.; Yin, H.; Li, L. L.; Zhang, J. X.; Wang, R. B. *J. Agr. Food Chem.* **2019**, 67, 7783-7792.

13. Song, G. X.; Tang, Q.; Huang, Y.; Zhang, J. X.; Tao, Z.; Zhu, Q. J.; Wei, G. *Spectrosc. Spect. Anal.* **2015**, 35, 3134-3139.

14. Liu, Q.; Tang, Q.; Xi, Y. Y.; Huang, Y.; Xiao, X.; Tao, Z.; Xue, S. F.; Zhu, Q. J.; Zhang, J. X.; Wei, G. *Supramol. Chem.* **2015**, 27, 386-392.

15. Kim, M. O.; Blachly, P. G.; Kaus, J. W.; McCammon, J. A. *J. Phys. Chem. B* **2015**, 119, 861-872.

16. Fatiha, M.; Faiza, B.; Ichraf, K.; Leila, N.; Eddine, K. D. *J. Taiwan Inst. Chem. E* **2015**, 50, 37-42.

17. Zhao, W. X.; Wang, C. Z.; Chen, L. X.; Cong, H.; Xiao, X.; Zhang, Y. Q.; Xue, S. F.; Huang, Y.; Tao, Z.; Zhu, Q. J. *Org. Lett.* **2015**, 17, 5072-5075.

18. Guo, G.; Tang, Q.; Huang, Y.; Tao, Z.; Xue, S.; Zhu, Q. *Chinese J. Org. Chem.* **2014**, 34, 2317-2323.

19. Huang, Y.; Wang, J.; Xue, S. F.; Tao, Z.; Zhu, Q. J.; Tang, Q. *J. Incl. Phenom. Macro.* **2012**, 72, 397-404.

20. Zhang, H.; Huang, Y.; Xue, S. F.; Tao, Z.; Zhu, Q. J. *Supramol. Chem.* **2011**, 23, 527-532.

21. Koner, A. L.; Ghosh, I.; Saleh, N. i.; Nau, W. M. *Can. J. Chem.* **2011**, 89, 139-147.

22. Liu, H.; Wu, X.; Huang, Y.; He, J.; Xue, S. F.; Tao, Z.; Zhu, Q. J.; Wei, G. *J. Incl. Phenom. Macro.* **2011**, 71, 583-587.

23. Ling, Y.; Mague, J. T.; Kaifer, A. E. *Chemistry* **2007**, 13, 7908-7914.

24. Saleh, N.; Al-Rawashdeh, N. A. *J. Fluoresc.* **2006**, 16, 487-493.

25. Lian, C. J.; Xu, W. T.; Luo, Y.; Zhu, X. Y.; Fan, Y.; Redshaw, C.; Tao, Z.; Xiao, X. *Microchem. J.* **2021**, 167, 106309.

26. Xu, W. T.; Luo, Y.; Zhao, W. W.; Liu, M.; Luo, G. Y.; Fan, Y.; Lin, R. L.; Tao, Z.; Xiao, X.; Liu, J. X. *J. Agr. Food Chem.* **2021**, 69, 584-591.

27. Tang, Q.; Zhang, J.; Sun, T.; Wang, C. H.; Huang, Y.; Zhou, Q. D.; Wei, G. *Spectrochim. Acta A* **2018,** 191, 372-376.

28. Xi, Y. Y.; Tang, Q.; Huang, Y.; Tao, Z.; Zhu, Q. J. *Spectro. Spec. Anal.* **2016**, 36, 1809-1812.

29. Zhang, C. X.; Jing, X.; Du, L. M.; Liu, H. L.; Li, J.; Zhao, S. G.; Fu, Y. L. *Prog. React. Kinet. Mec.* **2015**, 40, 154-162.

30. Xing, X. Q.; Zhou, Y. Y.; Sun, J. Y.; Tang, D. B.; Li, T.; Wu, K. *Anal. Lett.* **2013**, 46, 694-705.

31. Chen, H.; Yang, H.; Xu, W. C.; Tan, Y. B. *Chinese Chem. Lett.* **2013**, 24, 857-860.

32. Jing, X.; Du, L. M.; Wu, H.; Wu, W. Y.; Chang, Y. X. *J. Integr. Agr.* **2012,** 11, 1861-1870.

33. Wu, G.; Yu, H. F.; Bao, X. X.; Chen, H.; Ye, Q. F. *Chin. J. Chromatography*, **2007**, 25, 214-216.

34. Yao, F. H.; Liu, H. L.; Wang, G. Q.; Du, L. M.; Yin, X. F.; Fu, Y. L. *J. Environ. Sci.* **2013**, 25, 1245-1251.

35. del Pozo, M.; Hernandez, L.; Quintana, C. *Talanta* **2010**, 81, 1542-1546.

36. Rajgariah, P.; Urbach, A. R. *J. Incl. Phenom. Macro.* **2008**, 62, 251-254.

37. Rathore, R.; Kochi, J. K. *J. Org. Chem.* **1995**, 60, 7479-7490.

38. Li, M. –H.; Lou, X. –Y.; Yang, Y. –W. *Chem. Commun.* **2021**, 57, 13429-13447.

39. Cao, D. R.; Meier, H. *Chinese Chem. Lett.* **2019**, 30, 1758-1766.

40. Tang, M.; Bian, Q.; Zhang, Y. M.; Arif, M.; Luo, Q.; Men, S. Z.; Liu, Y. *RSC Adv.* **2020**, 10, 35136-35140.

41. Liu, Y. M.; Zhou, F.; Yang, F.; Ma, D. *Org. Biomol. Chem.* **2019**, 17, 5106-5111.

42. Song, Q. Q.; Mei, L. C.; Zhang, X. J.; Xu, P. P.; Dhinakaran, M. K.; Li, H. B.; Yang, G. F. *Chem. Commun.* **2020**, 56, 7593-7596.

43. Shangguan, L.; Shi, B. B.; Chen, Q.; Li, Y.; Zhu, H. T. Z.; Liu, Y. Z.; Yao, H.; Huang, F. H. *Tetrahedron Lett.* **2019**, 60, 150949.

44. Xie, J.; Shen, C.; Shi, H. Z.; Luo, S. S.; He, M. X.; Chen, M. *Struct. Chem.* **2020**, 31, 329-337.

45. Luo, L.; Nie, G. R.; Tian, D. M.; Deng, H. T.; Jiang, L.; Li, H. B. *Angew. Chem. Int. Ed.* **2016**, 55, 12713-12716.

46. Zhou, Y. J.; Yao, Y.; Huang, F. H. *Chinese J. Chem.* **2015**, 33, 356-360.

47. Zhou, T.; Song, N.; Yu, H.; Yang, Y. W. *Langmuir* **2015**, 31, 1454-61.

48. Li, Z. T.; Yang, J.; Yu, G. C.; He, J. M.; Abliz, Z.; Huang, F. H. *Org. Lett.* **2014**, 16, 2066-2069.

49. Ogoshi, T.; Hashizume, M.; Yamagishi, T.; Nakamoto, Y. *Chem. Commun.* **2010**, *46*, 3708-3710.

50. Yu, G.; Zhou, X.; Zhang, Z.; Han, C.; Mao, Z.; Gao, C.; Huang, F. *J. Am. Chem. Soc.* **2012**, *134*, 19489−19497.

51. Chi, X. D.; Xue, M.; Yao, Y.; Huang, F. H. *Org. Lett.* **2013**, 15, 4722-4725.

52. Yu, G. C.; Zhou, X. R.; Zhang, Z. B.; Han, C. Y.; Mao, Z. W.; Gao, C. Y.; Huang, F. H. *J. Am. Chem. Soc.* **2012**, 134, 19489-19497.

53. Zhang, H.; Huang, K.-T.; Ding, L.; Yang, J.; Yang, Y.-W.; Liang, F. *Chinese Chem. Lett.* **2022**, 33, 1537-1540.

54. Zhao, R.; Zhou, Y. J.; Jia, K. C.; Yang, J.; Perrier, S.; Huang, F. H. *Chinese J. Polym. Sci.* **2020**, 38, 1-8.

55. Yang, Y. H.; Bao, Q. L.; Luo, J. P.; Yang, J. L.; Li, C. H.; Wei, K. K.; Chuan, Y. M.; Yang, L. J. *Chinese J. Org. Chem.* **2020**, 40, 1680-1688.

56. Tan, X. P.; Zhang, Z.; Cao, T. W.; Zeng, W. J.; Huang, T.; Zhao, G. F. *ACS Sustain. Chem. Eng.* **2019**, 7, 20051-20059.

57. Qian, X. C.; Zhou, X. J.; Gao, W.; Li, J.; Ran, X.; Du, G. B.; Yang, L. *Microchem. J.* **2019**, 150, 104203.

58. Tan, X.; Liu, Y.; Zhang, T.; Luo, S.; Liu, X.; Tian, H.; Yang, Y.; Chen, C. *RSC Adv.* **2019**, 9, 345-353.

59. Wu, J.-R.; Mu, A. U.; Li, B.; Wang, C.-Y.; Fang, L.; Yang, Y.- W. *Angew. Chem., Int. Ed.* **2018**, 57, 9853−9858.

60. Wang, X.; Wu, J. R.; Liang, F.; Yang, Y. W. *Org. Lett.* **2019**, 21, 5215-5218.

61. Chi, X. D.; Ji, X. F.; Shao, L.; Huang, F. H. *Macromol. Rapid Comm.* **2017**, 38, 1600626.

62. Xu, H. X.; Yao, Y. *Supramol. Chem.* **2017**, 29, 161-166.

63. Chi, X.; Yu, G.; Shao, L.; Chen, J.; Huang, F. *J. Am. Chem. Soc.* **2016**, 138, 3168-74.

64. Shamagsumova, R. V.; Shurpik, D. N.; Padnya, P. L.; Stoikov, I. I.; Evtugyn, G. A. *Talanta* **2015**, 144, 559-568.

65. Zhao, J.; Chen, C.; Li, D.; Liu, X.; Wang, H.; Jin, Q.; Ji, *J. Polym. Chem.* **2014**, 5, 1843−1847.

66. Shen, J.; Wang, Q.; Hu, Q.; Li, Y.; Tang, G.; Chu, P. K. *Biomaterials* **2014**, 35, 8621−8634.

67. Chi, X.; Yu, G.; Ji, X.; Li, Y.; Tang, G.; Huang, F. *ACS Macro. Lett.* **2015**, 4, 996-999.

68. Mao, X. W.; Liu, T.; Bi, J. H.; Luo, L.; Tian, D. M.; Li, H. B. *Chem. Commun.* **2016**, 52, 4385-4388.

69. Wang, P.; Yao, Y.; Xue, M. *Chem. Commun.* **2014**, 50, 5064-5067.

70. Tian, M. M.; Chen, D. X.; Sun, Y. L.; Yang, Y. W.; Jia, Q. *RSC Adv.* **2013**, 3, 22111-22119.

71. Homden, D. H.; Redshaw, C. *Chem. Rev.* **2008**, 108, 5086-5130.

72. Santoro, O.; Redshaw, C. *Coord. Chem. Rev.* **2021**, 448, 214173.

73. Basilotta, R.; Mannino, D.; Filippone, A.; Casili, G.; Prestifilippo, A.; Colarossi, L.; Raciti, G.; Esposito, E.; Campolo, M. *Molecules*, **2021**, 26, 3963.

74. Non-toxic hair dyeing compsn. - contg. calixarene coupler and *N,N*-disubstd. diamine developer, giving blue tone. Noack, H. D. D.; Weinelt, H. L. D.; Noll. B. W. N. Patent number DE4135760A1, Germany, **1993**.

75. Español, S. E.; Maldonado, M. *Crit. Rev. Anal. Chem.* **2019**, 49, 383-394.

76. Yu, C. X.; Hu, F. L.; Song, J. G.; Zhang, J. L.; Liu, S. S.; Wang, B. X.; Meng, H.; Liu, L. L.; Ma, L. F. *Sensor Actuat. B-Chem.* **2020**, 310, 127819.

77. Ashwin, B.; Saravanan, C.; Stalin, T.; Muthu Mareeswaran, P.; Rajagopal, S. *Chemphyschem.* **2018**, 19, 2768-2775.

78. Kamboh, M. A.; Ibrahim, W. A. W.; Nodeh, H. R.; Sanagi, M. M.; Sherazi, S. T. H. *New J. Chem.* **2016**, 40, 3130-3138.

79. Li, J. W.; Wang, Y. L.; Yan, S.; Li, X. J.; Pan, S. Y. *Food Chem.* **2016**, 192, 260-267.

80. Evtugyn, G. A.; Shamagsumova, R. V.; Padnya, P. V.; Stoikov, II; Antipin, I. S. *Talanta* **2014**, 127, 9-17.

81. Menon, S. K.; Modi, N. R.; Pandya, A.; Lodha, A. *RSC Adv.* **2013**, 3, 10623-10627.

82. Oueslati, I.; Ghrairi, A.; Ribeiro, E. S.; de Carvalho, L. A. E. B.; Gil, J. M.; Paixao, J. A. *J. Mater. Chem. A* **2018**, 6, 10649-10654.

83. Cao, B.-Q.; Huang, Q.-B.; Pan, Y. *Amer. J. Analyt. Chem.* **2012**, 3, 664-668.

84. Li, C.; Wang, C.; Guan, B.; Zhang, Y.; Hu, S. *Sens. Actuators B: Chem.* **2005**, 107, 411-417.

85. Nodeh, H. R.; Kamboh, M. A.; Ibrahim, W. A. W.; Jume, B. H.; Sereshti, H.; Sanagi, M. M. *Environ. Sci-Proc. Imp.* **2019**, 21, 714-726.

86. Memon, S.; Memon, S.; Memon, N. *Desalin. Water Treat.* **2013**, 52, 2572-2582.

87. Bocchinfuso, G.; Mazzuca, C.; Saracini, C.; Venanzi, M.; Micheli, L.; Palleschi, G.; Palleschi, A. *Microchim. Acta* **2008**, 163, 195-202.

88. Dong, C.; Zeng, Z.; Li, X. *Talanta* **2005**, 66, 721-727.

89. Li, X.; Zeng, Z.; Zhou, J. *Anal. Chim. Acta* **2004**, 509, 27-37.

90. Kalchenko, O.I.; Solovyov, A. V.; Cherenok, S.A.; N.F. Starodub, N.F.; Kalchenko, V.I. *J. Incl. Phenom. Macrocycl. Chem.* **2003**, 46, 19–25.

91. Yilmaz, B.; Aydin, N.; Bayrakci, M. *J. Environ. Sci. Heal. B* **2018**, 53, 669-676.

92. Zeng, X. F.; Ma, J. K.; Luo, L.; Yang, L. L.; Cao, X. L.; Tian, D. M.; Li, H. B. *Org. Lett.* **2015**, 17, 2976-2979.

93. Memon, S.; Memon, S.; Memon, N. *J. Iran. Chem. Soc.* **2014**, 11, 1599-1608.

94. Tian, M. M.; Cheng, R. M.; Ye, J. J.; Liu, X. T.; Jia, Q. *Food Chem.* **2014**, 145, 28-33.

95. Zhang, G. F.; Zhu, X. L.; Miao, F. J.; Tian, D. M.; Li, H. B. *Org. Biomol. Chem.* **2012**, 10, 3185-3188.

96. Zhang, G. F.; Zhan, J. Y.; Li, H. B. *Org. Lett.* **2011**, 13, 3392-3395.

97. Wang, G. F.; Ren, X. L.; Zhao, M.; Qiu, X. L.; Qi, A. D. *J. Agr. Food Chem.* **2011**, 59, 4294-4299.

98. Garcia-Sosa, I.; Ramirez, F. D. *J. Mex. Chem. Soc.* **2010**, 54, 143-152.

99. Wang, K.; Guo, D. S.; Zhang, H. Q.; Li, D.; Zheng, X. L.; Liu, Y. *J. Med. Chem.* **2009**, 52, 6402-6412.

100. Nikolelis, D. P.; Raftopoulou, G.; Psaroudakis, N.; Nikoleli, G. P. *Electroanal.* **2008**, 20, 1574-1580.

101. Xiong, D; Li, H. *Nanotechnology* **2008**, 19, 465502.

102. Li, H. B.; Qu, F. G. *Chem. Mater.* **2007**, 19, 4148-4154.

103. Shieh, W. J.; Hedges, A. R. *J. Macromol. Sci. A*, **1996**, 33, 673-683.

104. Wang, J.; Feng. J. G.; Ma. C.; Fan. T. F.; Wu. X. M. *Chinese J. Pestic. Sci.* **2013**, 15, 23-31.

105. Lay, S.; Ni, X.; Yu, H.; Shen, S. *J, Sep, Sci.* **2016**, 39, 2321–2331.

106. Huang, X. C.; Ma, J. K.; Feng, R. X.; Wei, S. L. *J. Sci. Food Agr.* **2019**, 99, 6998-7007.

107. Wang, M.; Su, K.; Cao, J.; She, Y.; Abd El-Aty, A. M.; Hacimuftuoglu, A.; Wang, J.; Yan, M.; Hong, S.; Lao, S.; Wang, Y. *Talanta* **2019**, 192, 295-300.

108. Moon, Y.; Jafry, A. T.; Bang Kang, S.; Young Seo, J.; Baek, K. Y.; Kim, E. J.; Pan, J. G.; Choi, J. Y.; Kim, H. J.; Han Lee, K.; Jeong, K.; Bae, S. W.; Shin, S.; Lee, J.; Lee, Y. *J. Hazard Mater.* **2019**, 365, 261-269.

109. Pellicer-Castell, E.; Belenguer-Sapina, C.; Amoros, P.; El Haskouri, J.; Herrero-Martinez, J. M.; Mauri-Aucejo, A. *Talanta* **2018**, 189, 560-567.

110. Miao, S. S.; Wu, M. S.; Ma, L. Y.; He, X. J.; Yang, H. *Talanta* **2016**, 158, 142-151.

111. Zhao, H.; Ji, X.; Wang, B.; Wang, N.; Li, X.; Ni, R.; Ren, J. *Biosens. Bioelectron.* **2015**, 65, 23-30.

112. Pan, Y.; Mu, N.; Shao, S.; Yang, L.; Wang, W.; Xie, X.; He, S. *Sensors* **2015**, 15, 17916-25.

113. Cruickshank, D. L.; Rougier, N. M.; Maurel, V. J.; Rossi, R. H.; Buján, E. I.; Bourne, S. A.; Caira, M. R. *J. Incl. Phenom. Macrocycl. Chem.* **2012**, 75, 47-56.

114. Wang, H.; Yan, S.; Qu, B.; Liu, H.; Ding, J.; Ren, N. *New J. Chem.* **2020**, 44, 7727-7739.

115. Jauregui-Haza, U.; Ferino-Perez, A.; Gamboa-Carballo, J. J.; Gaspard, S. *Environ. Sci. Pollut. Res. Int.* **2020**, 27, 41105-41116.

116. Gao, S.; Liu, Y. Y.; Jiang, J. Y.; Ji, Q. Y.; Fu, Y.; Zhao, L. X.; Li, C. Y.; Ye, F. *J. Mol. Liq.* **2019**, 293, 111513.

117. Sipa, K.; Brycht, M.; Leniart, A.; Urbaniak, P.; Nosal-Wiercinska, A.; Palecz, B.; Skrzypek, S. *Talanta* **2018**, 176, 625-634.

118. Salazar, S.; Guerra, D.; Yutronic, N.; Jara, P. *Polymers* **2018**, 10, (9), 1038.

119. DiScenza, D. J.; Lynch, J.; Miller, J.; Verderame, M.; Levine, M. *ACS Omega* **2017**, 2, 8591-8599.

120. Cheng, Y.; Nie, J. Y.; Li, Z. X.; Yan, Z.; Xu, G. F.; Li, H. F.; Guan, D. K. *Anal. Bioanal. Chem.* **2017**, 409, 5065-5072.

121. Mahpishanian, S.; Sereshti, H. *J. Chromatogr. A* **2017**, 1485, 32-43.

122. Rana, V. K.; Kissner, R.; Gaspard, S.; Levalois-Grutzmacher, J. *Chem. Eng. J.* **2016**, 293, 82-89.

123. DiScenza, D. J.; Levine, M. *New J. Chem.* **2016**, 40, 789-793.

124. Liu, B.; Zhang, J.; Chen, C.; Wang, D.; Tian, G.; Zhang, G.; Cai, D.; Wu, Z. *J. Agric. Food Chem.* **2021**, 69, 6981-6988.

125. Utzeri, G.; Verissimo, L.; Murtinho, D.; Pais, A.; Perrin, F. X.; Ziarelli, F.; Iordache, T. V.; Sarbu, A.; Valente, A. J. M. *Molecules* **2021**, 26, 1426.

126. Vichapong, J.; Moyakao, K.; Kachangoon, R.; Burakham, R.; Santaladchaiyakit, Y.; Srijaranai, S. *Molecules* **2019**, 24, 3954.

127. Oliveira, A. E. F.; Bettio, G. B.; Pereira, A. C. *Electroanal.* **2018**, 30, 1918-1928.

128. Oliveira, A. E. F.; Bettio, G. B.; Pereira, A. C. *Electroanal.* **2018**, 30, 1929-1937.

129. Turan, A. C.; Özen, İ.; Gürakın, H. K.; Fatarella, E. *J. Eng. Fibers Fabr.* **2017**, 12, 75-83.

130. Liu, G.; Li, L.; Xu, D.; Huang, X.; Xu, X.; Zheng, S.; Zhang, Y.; Lin, H. *Carbohydr. Polym.* **2017**, 175, 584-591.

131. Alonso, M. L.; Sebastian, E.; San Felices, L.; Vitoria, P.; Alonso, R. M. *J. Incl. Phenom. Macro.* **2016**, 86, 103-110.

132. Zhang, M.; Zhao, H. T.; Yang, X.; Dong, A. J.; Zhang, H.; Wang, J.; Liu, G. Y.; Zhai, X. C. *Sens. Actuators B: Chem.* **2016**, 229, 190-199.

133. Fernandes, C.; Encarnacao, I.; Gaspar, A.; Garrido, J.; Borges, F.; Garrido, E. M. *Int. J. Photoenergy* **2014**, 2014, 489873.

134. Xu, Q.; Liu, Z.; Yan, C.; Lu, R.; Zhou, W. *Food Addit. Contam. Part A Chem. Anal. Control Expo*

Risk Assess. **2021**, 38, 1743-1754.

135. Tu, X.; Gao, F.; Ma, X.; Zou, J.; Yu, Y.; Li, M.; Qu, F.; Huang, X.; Lu, L. *J. Hazard. Mater.* **2020**, 396, 122776.

136. Farooq, S.; Nie, J. Y.; Cheng, Y.; Bacha, S. A. S.; Chang, W. X. *J. Sep. Sci.* **2020**, 43, 1145-1153.

137. Mi, Y. D.; Jia, C. D.; Lin, X. W.; Liu, X. Y.; Zhang, S. B.; Zhou, W. F.; Gao, H. X.; Lu, R. H. *Microchem. J.* **2019**, 150, 104164.

138. Ding, Y.; Song, X.; Chen, J. *J. Food Sci.* **2019**, 84, 1651-1659.

139. Li, S. H.; Wu, X. J.; Zhang, Q.; Li, P. P. *Microchim. Acta* **2016**, 183, 1433-1439.

140. Yadav, M.; Das, M.; Bhatt, S.; Shah, P.; Jadeja, R.; Thakore, S. *Microchem. J.* **2021**, 169, 106630.

141. Dong, J. T.; Chen, W.; Qin, D. Z.; Chen, Y. X.; Li, J.; Wang, C.; Yu, Y. Q.; Feng, J. G.; Du, X. Z. *J. Hazard. Mater.* **2021**, 419, 126404.

142. Gao, S.; Liu, Y. Y.; Jiang, J. Y.; Li, X. M.; Ye, F.; Fu, Y.; Zhao, L. X. *Colloid Surface B* **2021**, 201, 111625.

143. Yang, L. P.; Kaziem, A. E.; Lin, Y. G.; Li, C.; Tan, Y. T.; Huang, S. Q.; Cheng, D. M.; Xu, H. H.; Zhang, Z. X. *Carbohyd. Polym.* **2021**, 266, 118150.

144. Wang, M. L.; Li, G. X.; Xia, C. L.; Jing, X. D.; Wang, R. B.; Liu, Q. Q.; Cai, X. Y. *Chem. Eng. J.* **2021**, 411, 128489.

145. Majd, M.; Nojavan, S. *Microchim. Acta* **2021**, 188, 380.

146. Zhang, T.; Shuang, Y.; Zhong, H.; Li, L.; Li, L. *Anal. Sci.* **2021**, 37, 1095-1103.

147. Zhang, Z.-J.; Shang, X.-F.; Yang, L.; Shi, Y.-B.; Liu, Y.-Q.; Li, J.-C.; Yang, G.-Z.; Yang, C.-J. *Front. Chem.* **2020**, 7, article 922.

148. Senosy, I. A.; Lu, Z.-H.; Abdelrahman, T. M.; Yang, M.-N. O.; Guo, H.-M.; Yang, Z.-H.; Li, J.-H. *Environ. Sci. Nano* **2020**, 7, 2087-2101.

149. Liu, C.; Huang, X.; Meng, Z.; Qian, H.; Liu, X.; Lu, R.; Zhou, W.; Gao, H.; Xu, D. *RSC Adv.* **2020**, 10, 28664-28673.

150. Shuang, Y.; Zhang, T.; Li, L. *J Chromatogr. A* **2020**, 1614, 460702.

151. Champagne, P.-L.; Kumar, R.; Ling, C.-C. *Sens. Actuators B: Chem.* **2019**, 281, 229-238.

152. Campos, E. V. R.; Proenca, P. L. F.; Oliveira, J. L.; Melville, C. C.; Della Vechia, J. F.; de Andrade, D. J.; Fraceto, L. F. *Sci. Rep.* **2018**, 8, 2067.

153. Kaziem, A. E.; Gao, Y.; Zhang, Y.; Qin, X.; Xiao, Y.; Zhang, Y.; You, H.; Li, J.; He, S. *J. Hazard. Mater.* **2018**, 359, 213-221.

154. Gharib, R.; Jemâa, J. M. B.; Charcosset, C.; Fourmentin, S.; Greige-Gerges, H. *Eur. J. Lipid Sci. Technol.* **2020**, 122, 1900402.

155. Menestrina, F.; Ronco, N. R.; Romero, L. M.; Castells, C. B. *Microchem. J.* **2018**, 140, 52-59.

156. He, C.; Lay, S.; Yu, H.; Shen, S. *J. Sci. Food Agric.* **2018**, 98, 2089-2097.

157. Lannoy, A.; Bleta, R.; Machut-Binkowski, C.; Addad, A.; Monflier, E.; Ponchel, A. *ACS Sustain. Chem. Eng.* **2017**, 5, 3623-3630.

158. Zhang, P.; Cui, X.; Yang, X.; Zhang, S.; Zhou, W.; Gao, H.; Lu, R. *J. Sep. Sci.* **2016**, 39, 412-418.

159. Zolfaghari, G. *Chem. Eng. J.* **2016**, 283, 1424-1434.

160. Yang, M.; Wu, X.; Xi, X.; Zhang, P.; Yang, X.; Lu, R.; Zhou, W.; Zhang, S.; Gao, H.; Li, J. *Food Chem.* **2016**, 197, 1064-1072.

161. Serio, N.; Roque, J.; Badwal, A.; Levine, M. *Analyst* **2015**, 140, 7503-7507.

162. Fu, X.-C.; Zhang, J.; Tao, Y.-Y.; Wu, J.; Xie, C.-G.; Kong, L.-T. *Electrochim. Acta* **2015**, 153, 12-18.

163. Gurarslan, A.; Shen, J.; Caydamli, Y.; Tonelli, A. E. *J. Incl. Phenom. Macrocycl. Chem.* **2015**, 82, 489-496.

164. Shen, C.; Yang, X.; Wang, Y.; Zhou, J.; Chen, C. *J. Incl. Phenom. Macrocycl. Chem.* **2011**, 72, 263-274.

165. Ferencz. L.; Adalbert. B. *Fresenius Environ. Bull*. **2010**, 19, 172-179.

Progress in host-guest macrocycle/pesticide research: recognition, detection, release and application

Pei hui Shan,[a] Jian hang Hu,[a] Ming Liu, [a] Zhu Tao,[a] Xin Xiao[a]* and Carl Redshaw[b]*